

ABSTRACT

Title: Controlled Electrochemical Synthesis of Conductive Polymer Nanostructures and Electrochromism Property Study

Rui Xiao, Doctor of Philosophy, 2007

Directed By: Professor Sang Bok Lee
Department of Chemistry and Biochemistry

Conductive polymers have attracted the attention of many scientists in the whole world since Australians DE Weiss and coworkers reported high conductivity in oxidized iodine-doped polypyrrole, a polyacetylene derivative. In recent years, conductive polymers have served as the basis for many different new technologies such as electrochemical power sources, electrochromic display devices, photovoltaic devices and biosensors. For all of these applications, it is necessary to maintain ultra-fast charge and discharge rates in the conductive polymer layers in order to obtain high energy capacity, fast sensing speed or color change rate. For conductive polymer films there is always a problem for the slow charge/discharge ratio due to the diffusion of counter-ions into and out of the conductive polymer layers. To solve this problem, one-dimensional conductive polymers are ideal choices.

We have investigated the electrochemical synthetic mechanism for conductive polymer nanotubes in a porous alumina template using poly(3,4-ethylenedioxythiophene) (PEDOT) as a model compound. As a function of monomer concentration and potential, electropolymerization leads either to solid nanowires or hollow nanotubes and it is the purpose of these investigations to uncover the detailed mechanism underlying this

morphological transition between nanowire and nanotube. Electrochemically-synthesized PEDOT nanostructures were characterized using transmission electron microscopy to measure the extent of nanotubular portion in the PEDOT nanostructure. The study on potential dependency of nanotubular portion shows that nanotubes are grown at a low oxidation potential ($< 1.2 \text{ V vs. Ag/AgCl}$) regardless of monomer concentration. This phenomenon is explained by the annular base electrode shape at the pore bottom of a template and further supported by an electrochemical study on a flat-top electrode. We investigate the mechanism by taking into account the effect of electrolyte concentration, temperature, and template pore diameter on PEDOT nanostructures. This mechanism is additionally used to control the nanotube dimensions of other conductive polymers such as polypyrrole and poly(3-hexylthiophene). The electrochromic properties and applications of PEDOT nanostructures are also addressed.

Controlled Electrochemical Synthesis of Conductive Polymer
Nanostructures and Electrochromism Property Study

by

Rui Xiao

Dissertation submitted to the Faculty of the Graduate School of the
University of Maryland, College Park, in partial fulfillment
of the requirements for the degree of
Doctor of Philosophy
2007

Advisory Committee:
Professor Sang Bok Lee, Chair
Professor Ellen Williams
Professor Michael Fuhrer
Professor Michael Coplan
Professor Bryan Eichhorn

© Copyright by
Rui Xiao
2007

Dedication

This work is dedicated in great love to
my parents, my wife, my son and my teachers

Table of Contents

List of Tables	vi
List of Figures	vii
Synopsis	xi
Chapter 1: Conductive Polymer	1
1.1 Introduction	1
1.2 Synthesis of Conductive Polymer	4
1.2.1 Chemical Synthesis	4
1.2.2 Electrochemical Synthesis	7
1.3 Structures and Properties of Conductive Polymers and Their Derivatives	7
1.3.1 Polypyrrole	8
1.3.2 Polythiophene	10
1.3.3 Poly (3, 4-ethylenedioxythiophene)	13
1.3.3.1 Chemical polymerization of the EDOT based monomers	14
1.3.3.2 Electrochemical polymerization of the EDOT derivatives	15
1.3.3.3 Properties of neutral PEDOT and its derivatives	16
1.4 Applications of Conductive Polymer	17
1.4.1 Electrochromic Devices	18
1.4.2 Electronics and Photovoltaics	21
1.4.3 Chemical Sensors and Biosensors	22
1.5 Summary	24
Chapter 2: One-dimensional Nanostructures	26
2.1 Introduction	26
2.2 Synthesis Methods	27
2.2.1 Vapor-Liquid-Solid Process	28
2.2.2 Self-Assembly	29
2.2.3 Template Synthesis	30
2.2.3.1 Hard Template Method	31
2.2.3.1.1 Porous Materials with Cylindrical Pores	32
2.2.3.1.2 Templating against Features on Solid Substrates	35
2.2.3.2 Surfactant Template	37
2.2.3.3 Template Based Upon Existing Nanostructures	39
2.3 One-dimensional Conductive Polymer Nanostructures	41
2.3.1 Introduction	41
2.3.2 Background	41
2.3.3 Methods of Electrochemical Synthesis	43
2.3.4 Characterization of Conductive Polymer Nanostructures	44
2.3.5 Various Conductive Polymer Nanostructures	45
2.3.5.1 Polypyrroles	45
2.3.5.1.1 Nanotubes of Polypyrroles	45

2.3.5.1.2 Nanowires and Nanofibers of Polypyrroles	46
2.3.5.2 Polyanilines	47
2.3.5.2.1 Nanotubes of Polyanilines	47
2.3.5.2.2 Nanowires and Nanofibers of Polyanilines	48
2.3.5.3 Polythiophenes	49
2.3.5.3.1 Nanotubes of Polythiophenes	49
2.3.5.3.2 Nanowires and Nanofibers of Polythiophenes	50
2.4 Summary	51
Chapter 3: Experiment Setup and Techniques	52
3.1 Introduction	52
3.2 Template Synthesis	52
3.2.1 Home-Made Alumina Template Synthesis	53
3.2.1.1 Alumina Oxide Barrier Film	55
3.2.1.2 Porous Alumina Template Synthesis	57
3.2.2 Alumina Template synthesis on ITO Glass	81
3.3 The Sample Preparation	89
3.4 The Equipment Hardware	91
3.5 The Software	93
3.6 Summary	93
Chapter 4: Conductive Polymer Nanotube Synthesis Mechanism	95
4.1 Introduction	95
4.2 Practical Procedures for Conductive Polymer Electropolymerization	97
4.2.1 PEDOT Electropolymerization Synthesis	97
4.2.2 Polypyrrole Electropolymerization Synthesis	98
4.2.3 Poly(3-hexylthiophene) (P3HT) Electropolymerization	98
4.3 Characterization of PEDOT Nanostructures	99
4.3.1 Morphology of PEDOT Nanostructures	99
4.3.2 Control of Nanotube Length	102
4.3.3 Rigidity of PEDOT Nanotubes	104
4.4 Effects of applied potential and monomer concentration	105
4.4.1 General Concern	105
4.4.2 Synthesis Mechanism above 1.4 V	109
4.4.3 Synthesis Mechanism below 1.4 V	111
4.5 Influences of Electrolyte Concentration and Temperature	117
4.6 Synthesis of PEDOT Nanotubes in the Smaller Pores	120
4.7 Synthesis Mechanism for Polypyrrole	122
4.8 Synthesis Mechanism poly(3-hexylthiophene) (P3HT) Nanostructures	125
4.9 Summary	127
Chapter 5: Electrochromic Properties of PEDOT nanostructures	128
5.1 Introduction	128
5.2 Effect of Nanotube Wall Thickness on Redox Rates	129

5.2.1	Control of PEDOT Nanotube Wall Thickness	129
5.2.2	Relationship between Redox Rates and Nanotube Wall Thickness	130
5.3	Electrochemical Response and Optical Response of PEDOT Nanotubes	132
5.4	Summary	134
Chapter 6: Electrochemical Synthesis of PEDOT nanostructures for Application of Electrochromic Window Device		135
6.1	Introduction	135
6.2	Template Fabrication and PEDOT Nanostructure Synthesis	137
6.2.1	Fabrication of Alumina Template on ITO Glass	137
6.2.2	Electrochemical Synthesis of PEDOT in Template	140
6.3	Study for Window-Type Electrochromic Device	142
6.4	Summary	145
Chapter 7: Conclusions		146
References		148

List of Tables

Table 4.1 Dependence of PEDOT tubular ratio on the electrolyte concentration	104
--	-----

List of Figures

1.1 Definition of L, R form and soliton.	2
1.2 The bipolaron hopping mechanism for poly(acetylene)	2
1.3 Applications of conductive polymer	3
1.4 Chemical polymerization of pyrrole	5
1.5 Possible chemical structure for polypyrrole chains	6
1.6 Proposed chain structure of neutral polypyrrole	10
1.7 General structure of polythiophene	12
1.8 α, α' -coupling of poly-2,5-thiophene	12
1.9 Schematic demonstration of poly-2,4-thiophene	13
1.10 Schematic demonstration of the molecular structure of PEDOT	13
1.11 SEM images for electrochemically synthesized PEDOT film	15
1.12 PEDOT nanotubular structure for electrochromic display device	21
2.1 Growth of silicon crystal by VLS	28
2.2 Schematic illustration of porous templates	32
2.3 SEM images of polycarbonate membrane and alumina membrane	33
2.4 Cross section view of anodic alumina template	34
2.5 Different hard templates based on micropatterns on solid substrates	36
2.6 Schematic illustration of various soft templates based upon surfactants	38
2.7 Scheme for the fabrication of nanostructures by using surfactant soft templates	38
2.8 Schematic illustration of templating against existing nanostructures	39
2.9 Epitaxial growth of bilayer nanotape structures	40

2.10 Demonstration of chemical and electrochemical template synthesis methods	43
3.1 SEM image for micropores on aluminum surface after anodization process	53
3.2 Schematic illustration of ion transport in the oxide film	56
3.3 Illustration of hexagonally patterned pores of an anodized alumina template.	57
3.4 Field emission SEM images of anodized alumina template	59
3.5 Demonstration of current density vs. time for alumina template pore formation	60
3.6 Schematic demonstration of alumina template pore bottom with scallop shape	61
3.7 Demonstration of relationship between interpore distance and applied voltage	63
3.8 Schematic demonstration of two-step anodization process	65
3.9 Schematic demonstration for the electropolishing experiment set-up	67
3.10 Schematic diagram for the experiment set-up for anodization	69
3.11 SEM images for alumina template under various pore widening durations	71
3.12 Tilted and cross sectional view of anodic alumina template	73
3.13 Synthesis process of a porous alumina template and metal nanowires	76
3.14 Pore widening of an alumina template without protection	78
3.15 Experiment set-up for removal of aluminum oxide barrier layer	79
3.16 SEM images for the barrier layer side and the top side of alumina template	80
3.17 Thermolyne 79300 tube furnace and anodization set-up	82
3.18 Demonstration of fabrication process for the alumina template on ITO glass	84
3.19 SEM images of alumina template on ITO glass	85
3.20 Alumina templates on ITO glass under different pore widening conditions	86
3.21 Alumina template anodized at 80 V under different pore widening conditions	89
3.22 Schematic demonstration of sample preparation	90

3.23 Schematic demonstration of three electrode cell and potentiostat	92
3.24 Schematic demonstration of the software for CHI 660A	93
4.1 SEM and TEM images of PEDOT nanostructures	100
4.2 SEM images for PEDOT nanostructures synthesized in aqueous solution	102
4.3 PEDOT nanotube lengths vs. applied potential and monomer concentration	103
4.4 TEM images of PEDOT nanotubes	105
4.5 Growth mechanism of PEDOT nanostructures	107
4.6 TEM images of PEDOT nanostructures in various conditions	108
4.7 Plots of tubular portion for PEDOT nanotubes vs. applied potential	109
4.8 SEM and TEM images of gold annular bottom electrode	113
4.9 Demonstration of PEDOT nanotube synthesis on gold bottom electrode	114
4.10 Demonstration of PEDOT nanostructures on gold electrodes with flat top	115
4.11 Tubular portion or PEDOT nanostructures grown on the flat-top electrodes	116
4.12 Mechanism study for electrolyte concentration and temperature	119
4.13 Synthesis PEDOT nanotubes in small template pores	121
4.14 Plot of tubular portion for polypyrrole nanotubes vs. applied potential	123
4.15 Electron micrographs of polypyrrole nanostructures	124
4.16 SEM images for the gold bottom electrode after removal of alumina template	125
4.17 Synthesis mechanism study for P3HT	126
5.1 Color change process for PEDOT	128
5.2 Dependence of PEDOT nanotube wall thickness on monomer concentration	129
5.3 Plot of electrochromic response time vs. nanotube wall thickness	132
5.4 The electrochemical response versus optical response	133

6.1 Fabrication of PEDOT nanotubes in a porous AAO film	138
6.2 SEM images of porous AAO films fabricated on ITO glass	140
6.3 TEM images of PEDOT nanostructures synthesis in AAO on ITO glass	141
6.4 Electrochromic propertie study for PEDOT nanotubes	143
6.5 PEDOT nanostructures synthesized in an alumina template on ITO glass	145

Synopsis

Chapter 1:

The general background of conductive polymers including chemical and electrochemical synthesis methods, structures and properties of various conductive polymers such as polypyrrole, polythiophene and poly (3, 4-ethylenedioxythiophene) (PEDOT) and their applications is discussed.

Chapter 2:

The background of one-dimensional nanostructures is discussed. Several synthetic methods for one-dimensional nanostructures such as vapor-liquid-solid process, self-assembly and template method are introduced. The alumina template synthesis method is emphasized because of its versatility, high through-put and simplicity. The synthesis and characterization of many other conductive polymer nanostructures are discussed as well.

Chapter 3:

This chapter discuss the alumina template synthesis by the anodization technique, the sample preparation process and equipment setups.

Chapter 4:

This is the most important chapter for this thesis. Through study of various parameters like monomer concentration, applied potential, bottom gold electrode, electrolyte concentration and temperature, we proposed mechanisms which can guide the fabrication of various conductive polymer nanostructures. Two mechanisms are mainly controlling the morphologies of conductive polymer nanostructures. The first one is related to monomer diffusion flux rate and electropolymerization reaction rate. The second one is

the bottom gold electrodes which can guide the formation of nanotubular structures at low potentials.

Chapter 5:

In this chapter I will discuss the electrochromic properties of PEDOT nanostructures through the study of redox rate dependence on nanotube wall thickness.

Chapter 6:

This chapter will introduce a window type electrochromic display device based on PEDOT nanotubular arrays. By fabricating alumina template on ITO glass, PEDOT nanotubes will be electropolymerized into the template pores and switched between oxidized state and reduced state alternatively displaying different colors.

Chapter 7:

Conclusions.

Chapter 1: Conductive Polymer

1.1 Introduction

Since the discovery in 1973 by Walatka, Labes, and Perlstein that polymeric $(\text{SN})_x$ crystals, instead of being semiconducting as previously believed, actually had conductivity as high as metals, conductive polymers have stimulated a lot of interest from scientists all around the world.^{1, 2} From 1975 to 1977, although many efforts had been made to synthesize analogous compounds to $(\text{SN})_x$, no success had been achieved.^{3, 4} In the two years from 1975 to 1977, $(\text{SN})_x$ was still the only intrinsically available synthetic polymer which had metallic conductivity. However, significant progress was achieved in 1977. It was found that when a variety of halogens, such as bromine, was incorporated into the structure of the $(\text{SN})_x$ lattice. Conductivity at room temperature could be increased by an order of magnitude.⁵⁻⁷ Also in 1977, polyacetylene $(\text{CH})_x$ film was demonstrated to exhibit metallic and semiconducting properties through partial oxidation or reduction with electron acceptors or donors.^{8, 9} Polyacetylene is the simplest conjugated polymer. In its linear form it precipitates out of solution as a black, air sensitive, infusible powder that cannot be processed. Poly(acetylene) can be taken as an example to illustrate principles of conduction mechanisms in conducting polymers. Because of Peierls Distortion,¹⁰ the one-dimensional atomic chain of poly(acetylene) is distorted into a quasi-one-dimensional system which results in two inequivalent ground states "R" and "L" that have alternating bond lengths. The band gap between the two states is not zero which means that activation energy is required for interconversion between the two states. As a consequence of the asymmetry of the poly(acetylene) ground state, the two equivalent polyene chains R and L can be interconverted through

the intervention of a soliton. The soliton is a mobile charged or neutral defect, or a “kink” in the poly(acetylene) chain that propagates along the chain without attenuation and thus reduces the barrier for interconversion. Figure 1.1 shows the definition of L, R form and soliton.

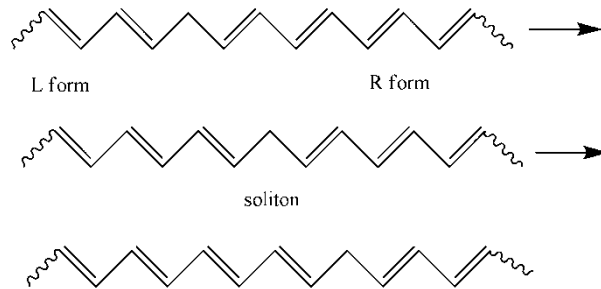


Figure 1.1. Definition of L, R form and soliton.

The charge carrier in negatively charged poly(acetylene) is a polyenyl anion of approximately thirty CH units in length which is stabilized by resonance. The defect is normally at the center of the chain. The bipolaron hopping mechanism can be used to explain how the soliton manages to travel from one end of a sample to the other.¹¹

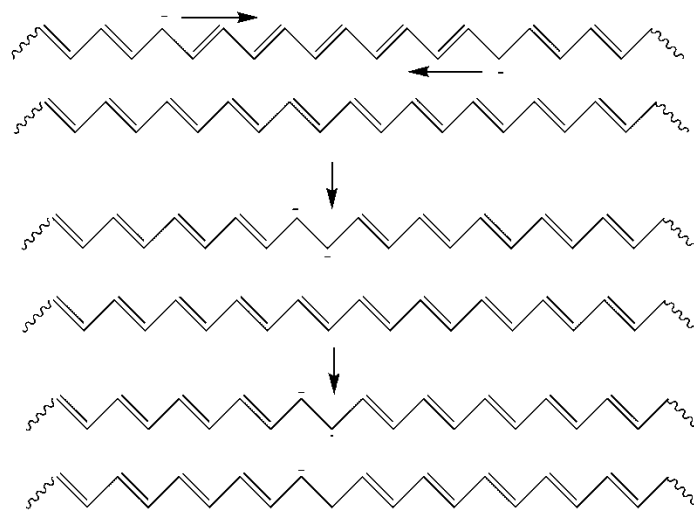


Figure 1.2 The bipolaron hopping mechanism for poly(acetylene)

It has been proven through many experiments that the interchain charge transport process is the rate-limiting step. For n-type solitons such as carbanions the conduction process includes transfer of an electron from the anion to a neutral soliton or a radical in a neighboring chain in an isoenergetic process. This kind of conduction process is also called interpolaron hopping.¹² If we only consider short chains, a mechanism for transfer of charge from one chain to another (e.g. intersoliton hopping) is needed to explain the conduction in poly(acetylene).

A lot of work has been devoted to the synthesis of conductive polymers.¹³⁻¹⁵ In the next section we will focus on two main methods: chemical oxidation and electrochemical polymerization. The advantages and disadvantages of these methods will be addressed in details. Conductive polymers have been used in applications such as chemical sensor and biosensor,¹⁶ transistor¹⁷ and switch, data storage,¹⁸ supercapacitor,¹⁹ photovoltaic cell,²⁰ electrochromic device,^{14, 15} actuator²¹ and surface protection²² as shown in Figure 1.3

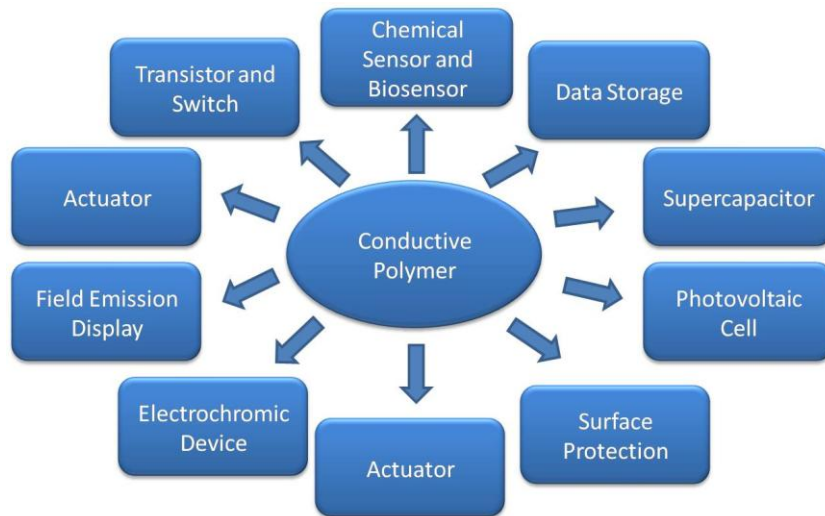


Figure 1.3 Applications of conductive polymer

1.2 Synthesis of Conductive Polymer

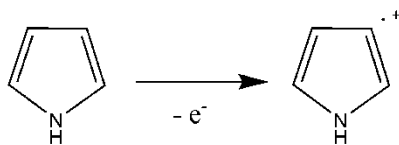
Generally, conductive polymers can be categorized into cationic and anionic salts of highly conjugated polymers. Through chemical oxidation or electrochemical polymerization, electrons are removed from the backbone of the conductive polymer resulting in the synthesis of cationic salts of conjugated polymers.²³ Chemical reduction is achieved with reagents such as sodium naphthalide or electrochemical reduction. Electrons are added to the backbone of the conductive polymer which results in the anionic salts of conjugated polymers. In general, there are two synthetic methods for conductive polymers: chemical polymerization²⁴ and electrochemical polymerization.²⁵ Both have been widely applied in industry and academic research. When mass production is needed, chemical polymerization is the best choice, but the introduction of reactant reagents and by products may sometimes affect the properties of the conductive polymers. Electrochemical polymerization is desirable for conductive polymer thin film and nanostructure fabrication. The fine control of conductive polymer film thickness and nanostructure morphology can be achieved by monitoring electropolymerization time, applied potential and total charge.²⁵ This thesis will mainly focus on the electrochemical synthesis of conductive polymer nanostructures.

1.2.1 Chemical Synthesis

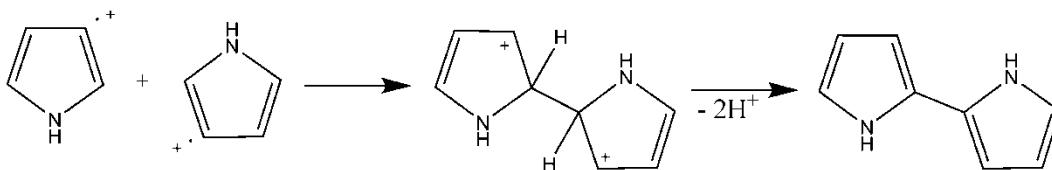
The typical chemical oxidation polymerization mechanism of pyrrole is illustrated in Figure 1.4. In the initial step, radical cations ($C_4NH_5^+$) are generated by oxidation of pyrrole monomer.²⁶ In the second step, through the radical-radical coupling and deprotonation between adjacent radical cations, dimers are generated leading to a

bipyrrole. Through the reoxidation and coupling with other radical cations bipyrroles are connected with each other and the propagation step is repeated consecutively. When the nucleophilic attack of water molecules or impurities in the polymer chain appear, the chemical polymerization of conductive polymer is stopped.

1. Oxidation of monomer



2. Radical coupling



3. Chain propagation

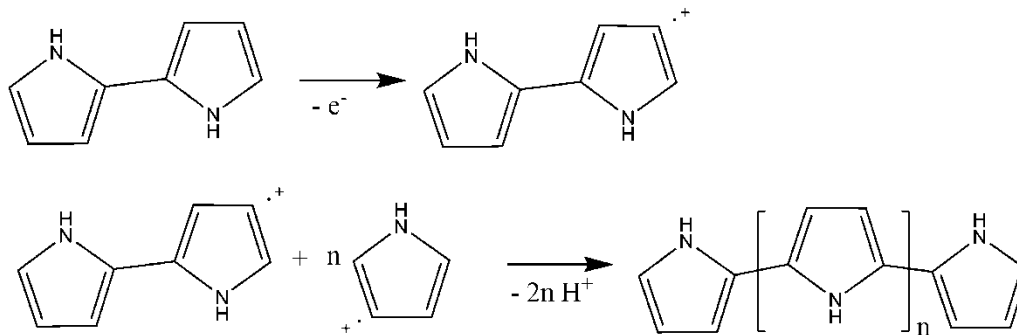


Figure 1.4 Chemical polymerization of pyrrole

The possible chemical structure of polypyrrole during chemical oxidation polymerization is shown in Figure 1.5. Compared with the protons at β - position, the protons at α - position of pyrrole are more readily removed from the pyrrole monomer. The coupling

reaction and linear molecular structure of polypyrrole are mainly attributed to the elimination of protons in the α -position of pyrrole monomer in the monomer-monomer coupling reaction. Although the coupling between adjacent pyrrole units through α - α coupling leads to a high degree of conjugation for the backbone of polypyrrole, cross linked polypyrrole chain also exists through the α - β coupling between adjacent pyrrole units. This will reduce the linearity and planarity of polypyrrole chains and explains the insolubility of polypyrrole in common solvents.

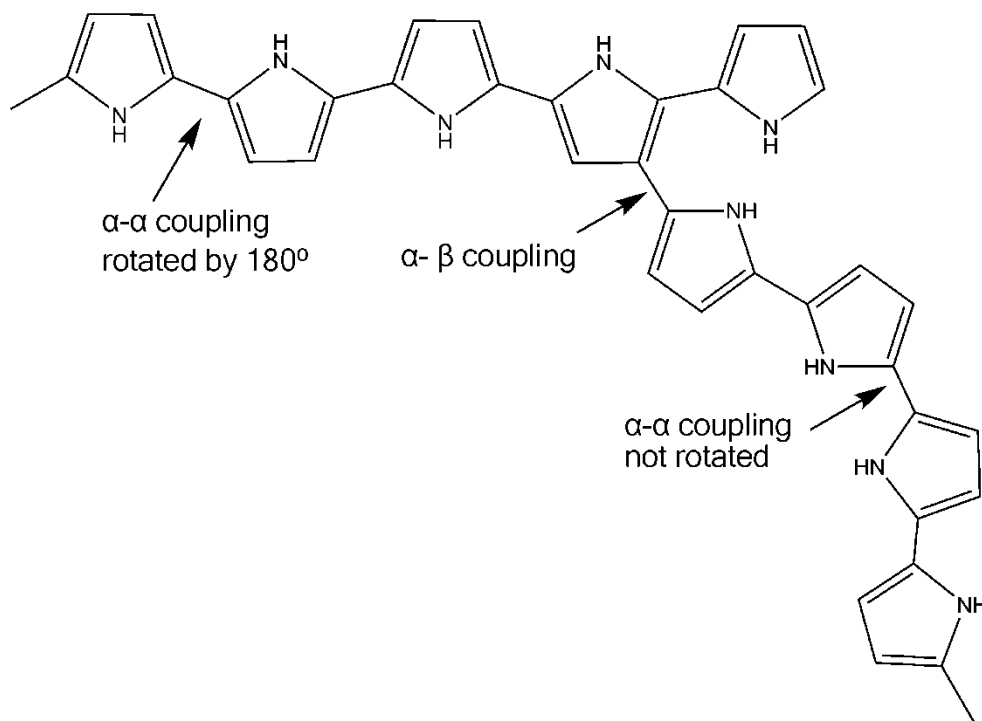


Figure 1.5 Possible chemical structure for polypyrrole chains

1.2.2 Electrochemical Synthesis

For the electropolymerization of thiophene and pyrrole, when a positive potential is applied at the electrode, the monomer is oxidized to a delocalized radical cation. The radical cations will induce the following radical-radical coupling which generates the dimerization of the monomer radicals through the deprotonation at the α -position. The neutral dimer is formed by removal of two H^+ ions. The following step is chain propagation through the oxidation of neutral dimers into dimer radicals. These dimer radicals will react with other monomers or dimers and result in the elongation of the polymer backbone. This electrochemical oxidation and radical coupling process is repeated continuously and finally results in a polymer film on anodic electrode.

In this thesis, an electrochemical synthetic method was selected for the fabrication of conductive polymer nanostructures such as nanowires, nanotubes and nanobelts because precise control of nanotube length, wall thickness and even the tubular portion ratio can be achieved through the adjustment of the electropolymerization potential, time, passed charge and monomer concentration.²⁵ The details will be discussed in the following chapters.

1.3 Structures and Properties of Conductive Polymers and Their Derivatives

Conductive polymers are conjugated polymers, namely organic compounds with an extended π -orbital system. This extended conjugation provides a route through which electrons can move from one end of the polymer backbone to the other end making them highly conductive. In general, conductive polymers are semiconductors with versatile properties and various applications. These characteristics have motivated the synthesis of many different conductive polymers with different synthetic methods.^{27, 28} A partial list of

conductive polymers that have been studied is given below: polyanilines (PAni),²⁹⁻³¹ polypyrroles (PPY),³²⁻³⁴ polythiophenes,³⁵⁻³⁷ polyphenylenes³⁸⁻⁴⁰ and poly(p-phenylene vinylene)s.⁴¹ In mid 1980s, one polythiophene derivative: Poly (3, 4-ethylenedioxythiophene) which is known as PEDOT was synthesized in the Bayer AG laboratories in Germany.⁴²⁻⁴⁴ Here we will only focus on the most important conductive polymers: polypyrrole, polythiophene and Poly (3,4-ethylenedioxythiophene). Although Poly (3,4-ethylenedioxythiophene) is a derivative of polythiophene, it will be discussed in a separate section due to its many unique properties.

1.3.1 Polypyrrole

The importance of the polypyrrole originated from several factors. Although initially the most important factor was the chemical and thermal stability of the polymer in severe environment conditions,⁴⁵ ease of synthesis is also an advantage. The possibility of modifying the electrical and physical properties with derivatives, copolymers, or specific counter anions in order to achieve the desired polymer properties is another advantages.⁴⁶ The electrochemical properties of various pyrrole systems have been studied.⁴⁷ When polypyrrole is fabricated it is in its oxidized conducting state. Through a simultaneous polymerization and oxidation of the π system of the final polymer, the polypyrrole film can be reduced, electrochemically or chemically, to give the neutral polypyrrole. The reduction is carried out in dry deoxygenated acetonitrile solution with tetraethyl- or tetrabutylammonium salts as the electrolyte. The neutral state of polypyrrole is highly insulating imposing a limit on the maximum polymer thickness that can be reduced. The neutral polymer is essential for the characterization of the polypyrrole system. The

neutral form of polypyrrole is very readily oxidized in air due to its low oxidation potential and must be handled with care in dry environments. Electrochemical switching between the oxidized and reduced state of polypyrrole is accompanied by a color change which makes polypyrrole a possible candidate for electrochromic display material.⁴⁸ Although the electrochemical switching process is reversible, EDX experiments demonstrate that there is a large and irreversible loss of original counter anions in the polypyrrole film. This results in the degradation of stability and cyclability of the polypyrrole electrochromic display devices. It seems that there is no change in the conductivity of the polymer film on cycling. This means that while the polymer film remains ionic, its neutrality is maintained by some anion other than the original one.

Polypyrrole has poor crystalline structures. In order to obtain knowledge of the structure of these systems, a variety of indirect measurements are needed. The pyrroles are primarily bonded via the α, α' - carbons. From this fact it can be concluded that if these α -positions are blocked, the electrochemical polymerization of pyrrole will not occur. From magic angle spinning ¹³C-NMR and IR data, for the polymers derived from unsubstituted pyrroles, the crosslinking of the polymer could occur due to the existence of β -carbons in the chain bonding. If the two β -positions are blocked with a methyl group, the possibility of other than α, α' -bonding can be eliminated. The result of this will lead to a much more ordered polymer chain and a significant increase in the crystallinity of the chain. Many techniques such as electron diffraction, XPS, UPS and NMR have been used to analyze the crystallographic structure of polypyrrole systems and have demonstrated the increased order due to the blocking of two β -positions. The XPS data and electron diffraction data of the two pyrrole polymers demonstrated similar properties.

This means that both polymers must have same chain structure although the unsubstituted pyrrole will clearly show the effects of disorder related to the partial involvement of the β -carbons in ring-ring bonding. It is believed that a linear, completely planar, exclusively α, α' -bonded chain in which the orientation of the pyrrole molecule alternate, is the ideal model for the structure of polypyrrole. This structure is illustrated in Figure 1.6.

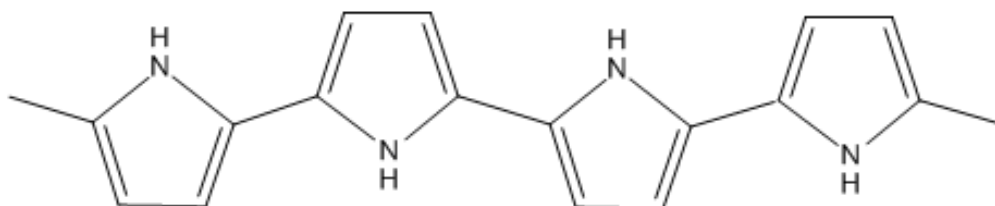


Figure 1.6. Proposed chain structure of neutral polypyrrole

In air, at room temperature, the electrochemical properties of polypyrrole are very stable.⁴⁹ For unprotected films, in one year the conductivity decreases by about 20%. Under appropriate protection, considerable improvement in the stability can be expected. When the temperature is elevated to 100-200 °C, polypyrrole remains very stable, depending on the nature of the anion. Polypyrrole is also quite stable in acid conditions, but basic conditions can cause temporarily reversible loss of conductivity. Polypyrrole may have some potential applications in battery materials.⁵⁰ It has a lower open circuit voltage than polyacetylene, but its nonfibrous structure is a disadvantage.

1.3.2 Polythiophene

Polythiophene and its derivatives can be chemically and electrochemically synthesized. Through chemical or electrochemical doping and dedoping (oxidation or reduction of the polymer), the electrical conductivity of polythiophene films can be varied over 12 orders

of magnitude, with properties ranging from insulator ($\sim 10^{-10}$ s/cm) to semiconductor to metal ($\sim 10^2$ s/cm).

The application of the conductive polymer has been impeded by high reactivity toward oxygen and moisture. Therefore, experiment conditions such as argon controlled atmosphere and a highly purified medium is required to prevent conductive polymers from reacting with oxygen and moisture. It is necessary to synthesize a stable conductive polymer which can be reversibly doped and undoped under severe environment conditions. Based on these criteria, the doping level, the regularity, and the homogeneity of the chain structure have been shown to be critical. It is found that polythiophene and its derivatives are good candidates for conductive polymers that are stable under various environment conditions, exhibiting the following distinguished properties:

1. High chemical and electrochemical stability in both doped and undoped states.
2. Reversible doping level (the percentage of counter ions which are doped in the polymer) in the range 25-50% instead of 6-20% for polyacetylene.
3. A highly regular polymeric backbone obtained by varying the nature of the dopant and the structure of the monomer.

Thiophene, furan and selenophene can be polymerized with a variety of initiators: sulfuric acid, iron (III) chloride and Ziegler catalysts. The electrochemical synthesis of polythiophene does not require oxidizing or reducing reagents and it is easy to control film thickness.⁵¹ In our research in conductive polymer nanostructure synthesis we chose to use the electrochemical polymerization method because of the above advantages. The working electrode on which polythiophene is deposited is placed in a three electrode cell with acetonitrile as solvent and 0.1 M LiClO₄ as supporting electrolyte. The counter and

reference electrode are platinum and Ag/AgCl electrode respectively. The concentration of thiophene can vary from 10 mM to 500 mM depending on the desired amount of polythiophene. It is found that the initial electropolymerization potential of thiophene starts at 1.2V and the electropolymerization rate increases with the increase of applied potential. The polythiophene film thickness can be controlled by monitoring the electropolymerization time and applied potential.

The general structure of polythiophene is related with the coupling of monomeric units in 2, 5-positions with preservation of the aromatic nucleus:

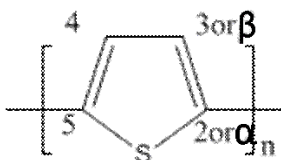


Figure 1.7. General structure of polythiophene

If we compare the infrared spectra of chemically or electrochemically synthesized polythiophene, we can find they are very similar and exhibit several characteristic bands such as (a) thiophene vibrations ($1500, 1400, 1230, 1200, 1080, 1050 \text{ cm}^{-1}$) and (b) polymer (788 cm^{-1}) for the α, α' -coupling of poly-2,5-thiophene which is demonstrated in the structure below:

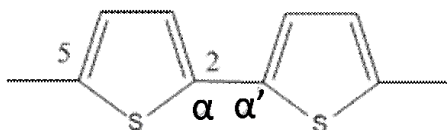


Figure 1.8. α, α' -coupling of poly-2,5-thiophene

For chemically synthesized poly-2,4-thiophene, the band at 788 cm^{-1} is replaced by two new ones at 820 and 730 cm^{-1} due to the α,β' -coupling as shown below:

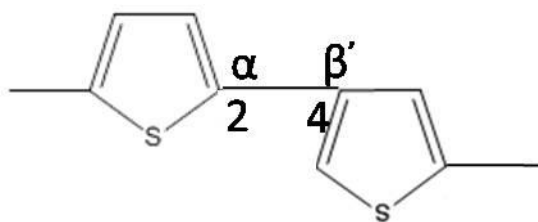


Figure 1.9. Schematic demonstration of poly-2,4-thiophene

The dominance of the $\alpha-\alpha'$ linkage in polythiophene and its derivatives has been confirmed by ^{13}C nuclear magnetic resonance spectrum analysis. For polythiophene there are two sharp absorption bands at 120 and 127 ppm while for poly(3-methylthiophene) there is only one absorption band at 117 ppm due to the $\text{C}_\beta\text{-H}$ bonding.

1.3.3 poly(3,4-ethylenedioxythiophene)

In the latter 1980s, scientists at the Bayer AG research laboratories in Germany synthesized a new polythiophene derivative, poly(3,4-ethylenedioxythiophene),⁵² which has the following backbone structure:

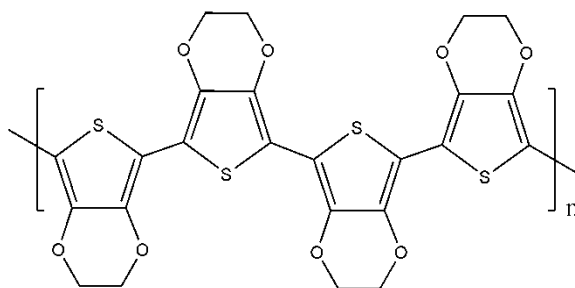


Figure 1.10 Schematic demonstration of the molecular structure of PEDOT

PEDOT can be synthesized chemically or electrochemically through standard oxidative chemical reagents or electrochemical polymerization methods.^{24, 25} When PEDOT is in its oxidized state, it is found that in addition to very high conductivity (ca. 300s/cm), PEDOT is almost transparent in its thin film state. If PEDOT is reduced by chemical reducing reagents or electrochemical methods, its color changes to a deep blue violet. This property of PEDOT is called electrochromism.¹⁴ Many electrochromic devices based on this exclusive property have been fabricated. The detailed electrochromic application of PEDOT will be discussed in the next section. Here we will mainly focus on the synthesis, characterization and electrical, optical and electrochemical properties of PEDOT and its derivatives.

The synthesis of PEDOT and its derivatives can be divided into two different types of polymerization reactions:

- Oxidative chemical polymerization of the EDOT based monomers
- Electrochemical polymerization of the EDOT based monomers

1.3.3.1 Chemical polymerization of the EDOT based monomers

There are several methods which can be used to chemically polymerize EDOT monomers. The classical method employs oxidizing agents such as FeCl_3 .²⁴ The chemically polymerized PEDOT is a black, insoluble and infusible compound. Reynolds and Kumar reported that by increasing the ratio of $[\text{FeCl}_3]/[\text{monomer}]$ above two in the chemical polymerization of EDOT, a fraction of the as-polymerized PEDOT becomes insoluble in organic solution which is the result of crosslinking during the polymerization.⁵³ If the $[\text{FeCl}_3]/[\text{monomer}]$ ratio is above five, an insoluble polymer is obtained.

The second polymerization method reported by de Leeuw is utilizing $\text{Fe}(\text{OTs})_3$ by using imidazole as a base. The polymerized PEDOT film is black, insoluble and infusible. The conductivity is up to 550 S/cm after rinsing with water and n-butanol.⁵³

1.3.3.2 Electrochemical polymerization of the EDOT derivatives

Compared with chemical polymerization, electrochemical polymerization has many advantages such as absence of oxidizing or reducing reagents, control of polymer film thickness through monitoring passed charge, applied voltage and polymerization time, and short polymerization time.⁵⁴

Electrochemical polymerization results in the formation of a highly transparent, deep blue-violet, doped PEDOT at the anode. The electrochemically synthesized PEDOT has good stability in both acidic and basic environments and has good conductivity as high as 300 S/cm. The electrochemically synthesized PEDOT film has a rough and porous morphology which is shown in Figure 1.11.

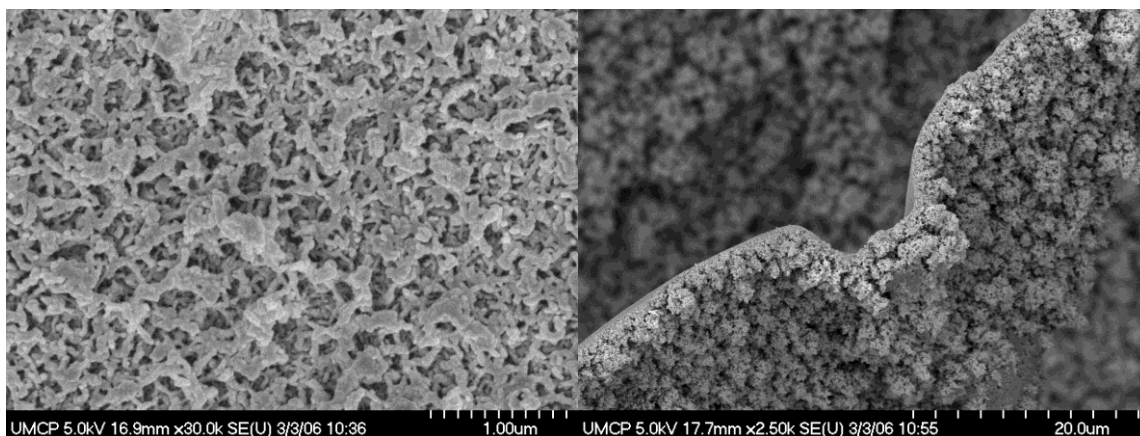


Figure 1.11. SEM images for electrochemically synthesized PEDOT film

1.3.3.3 Properties of neutral PEDOT and its derivatives

The electronic bandgap, defined as the onset of the π - π^* absorption, is 1.6-1.7 eV and demonstrated a λ_{max} of 610 nm which makes the color of PEDOT a deep blue-violet. Because of the low PEDOT oxidation potential, care must be taken in the handling of PEDOT neutral film in air or it will be oxidized quickly.

The flexible synthesis of EDOT, has made it a prominent component for conjugated polymers with variable bandgaps. In general, the electronic bandgap of a conjugated polymer chain can be controlled by changing the degree of π -overlap along the backbone via steric interactions, and by controlling the electronic character of the conjugated π -system with electron-donating or accepting substituents.⁵² The controlling of the electronic character can be achieved by using substituents and co-repeat units that can adjust the highest occupied molecular orbital (HOMO) and lowest unoccupied molecular orbital (LUMO) energy levels of the π -system.

A variety of EDOT-based polymers have been fabricated with higher energy gaps than the original PEDOT. Using a series of oxidatively polymerizable bis-EDOT-arylenes, PEDOT with bandgaps ranging from 1.4-2.5 eV have been obtained.⁵² Corresponding to these bandgaps, neutral polymers with colors ranging from blue through purple, red, orange, green, and yellow have been synthesized. Various spacers such as vinylene ($E_g = 1.4$ eV), 2,5-dialkoxyphenylene ($E_g = 1.75$ to 2.0 eV), biphenyl ($E_g = 2.3$ eV), dialkylfluorene ($E_g = 2.3$ eV), and carbazole ($E_g = 2.5$ eV) have been used for the bandgap control of PEDOT.

By controlling monomer concentration, applied potentials, temperature and electrode materials, free-standing PEDOT film or nanostructures can be obtained by using various

dopant anions. The conductivity of PEDOT film is between 1- 100 S/cm depending on the nature of various dopant anions. For example, by using PF_6^- as counterion, conductivity as high as 300 S/cm at room temperature can be obtained. PEDOT films doped with sulfated poly(β -hydroxyether) (PEDOT/S-PSE) exhibit outstanding mechanical properties imparted by the polyelectrolyte dopant with concurrent high conductivities in the range of 150-180 S/cm. Conductivity as high as 400 S/cm can be obtained by using a bis-trifluoromethyl-functionalized sulfated poly(β -hydroxyether). These results, show the variability of PEDOT film conductivity that can be obtained through the choice of suitable counterion dopants.

Because of the low oxidation potential and relatively low bandgap, PEDOT and its derivatives have exhibited excellent electrochemical and spectroscopic properties which not found in other polymers. Because the bandgap of PEDOT is near the transition between near IR and visible region of the spectrum, PEDOT is strongly cathodically colored and has high transmissivity to visible light in its oxidized doped state.⁵² The color of PEDOT film is almost sky-blue transparent in its conducting state and deep blue violet in the reduced insulating state.

1.4 Applications of Conductive Polymer

Recent advances in optimization of conductivity, ease of processing and functionalization have motivated studies of conductive polymers.

1.4.1 Electrochromic Devices

Electrochromism is a reversible optical process for materials that occur when materials have redox states (reduced and oxidized forms) which have different UV-Visible absorption spectra. When an electric potential is applied to materials, they are showing the redox states described above and displaying different colors for the oxidized and reduced states. These materials can be called electrochromic devices. Because of the unique electrochromic property, electrochromic devices have numerous applications both in academia and industry. They have been used to make rear-view mirrors in cars. The rear-view mirror can automatically become darkened to prevent temporary blinding of the driver. This particular characteristic of electrochromic devices is also applied to make “smart windows” which can be darkened with the flick of a switch to provide privacy. Alternatively, electrochromic devices have applications in dynamic flat-panel displays, computer screens and electronic paper.⁵⁵

Electronic paper can offer all the advantages of old-fashioned newsprint: excellent resolution, high contrast that can be read in strong or dim light, no need for external power to maintain an image. It is light and flexible enough to be carried easily on a morning commute. But unlike newsprint, electronic paper can spare trees and will not leave any messy newsprint on your fingers. Nowadays a lot of research and improvements have been carried out worldwide to achieve enormous developments in electronic paper technology. All of these efforts are for the aim to find robust, light-weight, low-power consuming and fast responsive materials which can be manufactured on a thin flexible carrier. In the area of electrochromic displays, a lot of research work has been performed to obtain good color contrast ratio and fast color switching rate by

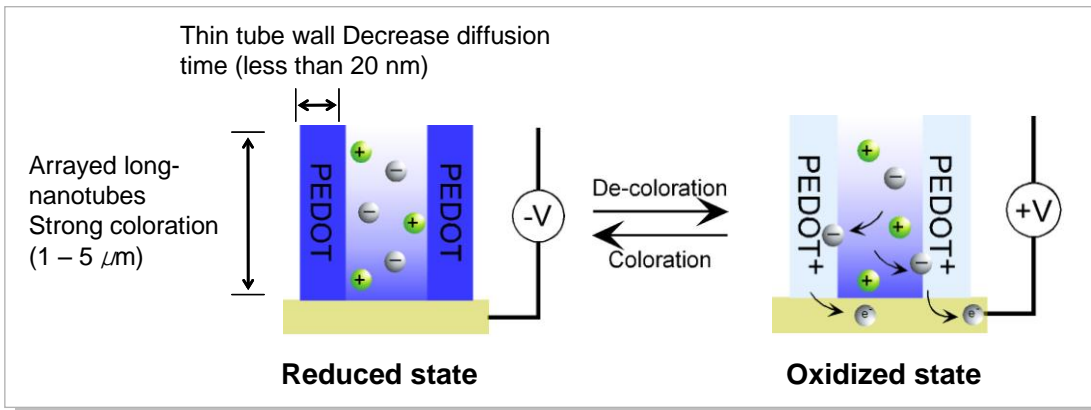
various means of synthetic methods. However, little success has been reported in obtaining color switching rates faster than 40ms which is the requirement for moving images. This is the reason why electrochromic materials are not widely used in the domain of electrochromic display.

As one of the most important conductive polymers, PEDOT has many excellent properties, such as good mechanical stability, prominent color contrast, high conductivity (200s/cm) at doped state, low oxidation potential and facile fabrication. It has become one of the most promising conductive polymers in the world and attracted attention of many researchers in this area. PEDOT proved itself an excellent candidate for electronic paper. But the color switching rate of PEDOT is not sufficiently fast for display technology because the color switching rate of PEDOT is limited by the diffusion rate of counter-ions into the polymer film in the redox process.¹⁴ The faster the diffusion of counter-ions the faster the color switching rate. The diffusion time t (the time which is needed for the counter-ions to reach a saturation concentration in the polymer layer) can be expressed as the following formula:

$$t \propto x^2/D$$

where t is the time (ms) needed for the counter ions to diffuse through the polymer film; x is the thickness (μm) of the polymer film; D is the diffusion coefficient (cm^2/s) of counter ions. The thicker the counter-ions diffusion distance the longer the color switching time needed. So the most efficient way to improve the color switching rate is to decrease the thickness of PEDOT polymer film in order to decrease the counter ions diffusion distance in the polymer layer. To achieve this goal, there are several options. One is to make the PEDOT film as thin as possible. But this method has its own

limitations. The thickness of the polymer film can only reach the magnitude of hundreds of nanometers. This implies that the color switching rate is about 2.2 seconds for a 300 nm thick PEDOT film.⁵⁶ But the color switching rate in the magnitude of seconds is far from the extent for PEDOT film to be used to make commercially available displays. Another method to decrease the polymer layer thickness is to make nanofibers. Charles R. Martin and Van Dyke reported that the charge transport rate can be increased by a factor of five for the fibrillar polypyrrole structures compared with conventional polypyrrole films (1 μ m in thickness).⁵⁷ However, the charge transport rate was still in the range of second due to the nanofiber structures whose diameter is around 200nm. This response time is not sufficient to meet the requirement of electrochromic display technology. The color switching rate can be around 10 ms if the counter-ions diffusion distance is as thin as 20 nm.¹⁴ This kind of color switching rate is sufficient for display technology, however there is another problem, poor coloration contrast due to the ultra thin polymer film. How is it possible to get both fast color switching rate and good coloration contrast at the same time? A well-defined nanotubular array structure can achieve this goal.^{14, 15} By synthesizing PEDOT nanotubes, which have ultra thin wall thickness at around 10-20nm, a color switching rate of approximate 10 ms can be obtained. At the same time due to the length of PEDOT nanotubes which is in micrometer magnitude, strong coloration contrast is also possible. Figure 1.12 shows the PEDOT nanotubular structure for electrochromic display device.



Cho et al. *Advanced Mater.* (2005), **17**,171

Figure 1.12 PEDOT nanotubular structure for electrochromic display device.

1.4.2 Electronics and photovoltaics

Because of the high conductivity and controllable morphologies of conductive polymer nanostructures, conductive polymers have been used in electronic logic devices such as field-effect transistors and photoswitching devices.⁵⁸ A typical organic field-effect transistor contains a source, drain, gate and dielectric layer. With a voltage between gate and source electrodes, the current between the drain and source electrodes can be easily varied. When there is no voltage between the gate and source electrodes, there will be no current flow between the gate and source electrodes. This state is called “off” state of the field-effect transistor. When a voltage is applied on the gate electrode, the flow of charge will be introduced through the interface between the conductive polymer layer and dielectric layer. At this state, the field-effect transistor is turned on.

Due to the low cost, easy synthesis and high mechanical flexibility, conductive polymers have been applied as a promising alternative of inorganic semiconductors and optical

devices. Polythiophene has been applied in the fabrication of solar cells and photovoltaic devices as a pure polymer or polymer-inorganic hybrids.²⁰ Because the performance of hybrid solar cell devices depends on the morphologies of each working layer, it is very important to improve the homogeneity of the active layers. Conductive polymer can act as an electron donor phase in the active layers. At the same time, there must be an electron acceptor phase in the active layers such as the nanocrystals and nanowires of CdSe and fullerene. Alivisatos and co-workers have reported over 54% quantum efficiency and a monochromatic power efficiency of 6.9% by using a hybrid solar cell which is constituted with regioregular P3HT and CdSe nanostructures.²⁰ By controlling the CdSe nanorod length, the distance through which electrons are transported in the thin film device can be controlled. The band gap can be tuned by altering the CdSe nanorod radius to optimize the overlap between the absorption spectrum of the cell and the solar emission spectrum.

1.4.3 Chemical Sensors and Biosensors

Because the oxidation level of conductive polymers can be controlled by their inherent doping-dedoping process which causes the variations in conductivity, color, mass, volume, and so forth, they have been widely used in a variety of chemical and biological sensing applications.⁵⁹ Upon contacting specific chemical and biological species, conductive polymers can exhibit sensitive responses which can be utilized as sensing signals. The sensing abilities of conductive polymers can also be tailored through the modification of functional groups on the polymer chain or incorporating appropriate counter-ions during the polymerization process. Because of these characteristics, much

effort has been devoted to the fabrication of sensor devices based on conductive polymers.^{16, 60} It is noteworthy that the nanostructures including nanorods, nanofibers, and nanotubes not only provide a high surface-to-volume ratio but also allow rapid diffusion of analytes into and out of the material.

Polypyrrole is the most widely used conductive polymer for chemical and biological sensors such as toxic gas sensors, non-toxic gas sensors, aroma sensors, humidity sensors, and microbial sensors.⁶¹ A carbon nanotube-polypyrrole sensor was fabricated by coating polypyrrole on the single wall of a carbon nanotube to increase the specific surface area. Carbon nanotube-polypyrrole sensors showed an *n*-type behavior owing to the anion doping in polypyrrole during the chemical polymerization. Upon exposure to NO₂ gas, the sensitivity of the nanocomposites was about ten times higher than that of pristine polypyrrole.

PEDOT has also been applied in the applications for sensor systems in recent years because of its outstanding stability in severe environment and low bandgap. It was reported that PEDOT nanorod (diameter: ca. 40 nm, length:ca. 200 nm) was used in order to detect HCl and NH₃ vapor.⁶² For NH₃ detection, when PEDOT nanorod contacts the NH₃ vapor, the NH₃ vapor will diffuse into the PEDOT nanorod resulting in a rapid dedoping process of PEDOT nanorod. The dedoping process which is related to the interaction between the PEDOT backbone and NH₃ vapor will generate a sharp increase in PEDOT nanorod resistance. Through monitoring the change of PEDOT nanorod resistance the concentration of NH₃ can be easily obtained. On the other hand, the interaction between PEDOT nanorod and HCl vapor will result in the decrease of

PEDOT nanorod resistance by the doping mechanism. Therefore the PEDOT nanorod can be used as a sensor for HCl vapor concentration detection.

1.5 Summary

In this chapter we have introduced the general background of conductive polymers and various synthesis methods including chemical oxidative polymerization and electrochemical polymerization. We also discussed the structures and properties of various conductive polymers such as polypyrrole, polythiophene and poly(3,4-ethylenedioxythiophene) (PEDOT). At the last section many important applications of conductive polymer was introduced.

For applications of thin film structures of conductive polymers to electronic, optical and electrochromic devices, film morphology is a limiting factor. Energy storage and electrochromic devices require very fast charge-discharge rates in order to get high efficiency and fast color switching rate. Although fast charge and discharge rates can be achieved for very thin conductive polymer films, the amount of conductive polymer will be very low due to the thin film thickness. This will result in low energy density for the energy storage devices and poor color contrast for the electrochromic devices. Photovoltaic devices require undisturbed charge conduction paths which are essential to reduce the recombination rate. But thin film structure apparently can't meet this requirement due to a high charge-hole recombination rate. Well-defined conductive polymer nanostructures can be the best solution.

Compared with thin film structures, well-defined conductive polymer nanostructures have many advantages such as fast charge-discharge rate, high surface area and

feasibility of inner-outer surface modification as well as undisturbed charge conduction paths. All of these have made one-dimensional conductive polymers a prominent candidate for electronic, optical, sensor and electrochromic device applications. In the next chapter we will discuss the importance of one-dimensional nanostructures in detail.

Chapter 2: One-dimensional Nanostructures

2.1 Introduction

Nanostructured materials can provide intrinsically high surface area leading to high charge/discharge capacity and short diffusion distance for ion transport. These properties of nanostructured materials can result in a fast charge/discharge rate.^{13, 63} Nanostructures are defined as structures which have at least one dimension in the range of 1-100 nm.⁶⁴ Nanotechnologies to synthesize and characterize such nanomaterials are essential to fabricate highly-integrated, tiny, and lightweight electronic devices with high performance. Nanostructures can be categorized into nanoparticle, nanofiber, nanobelt, core-shell nanostructure, hollow nanosphere, nanotube, nanocomposite and so on. The reason why nanostructures are attracting a lot of research interest from many scientists is that compared with bulk structures they have many unique properties such as ultra high surface area, prominent electronic and optical properties, excellent mechanical and chemical performance.

In the first chapter we discussed the synthetic methods for many conductive polymers and the applications of these conductive polymers. The limitations of thin film structures of conductive polymers for electronic, optical and electrochromic devices were also addressed. The best solution for all these problems of film structures can be readily solved using one-dimensional conductive polymer nanostructures. Charles Martin and co-workers have extensively investigated the applications of one-dimensional nanostructures for battery use.⁶⁵⁻⁶⁸ Our group also conducted research work into the electrochromic applications of conductive polymer nanostructures.^{14, 15} In this chapter I will discuss many synthesis methods of one-dimensional nanostructures such as vapor-liquid-solid

method, self assembly and template method. The synthetic strategies, background and importance of many one-dimensional conductive polymer nanostructures will be addressed in detail. Because of broad applications of one-dimensional conductive polymer nanostructures in both academia and industry areas, it is very important to understand the synthesis mechanism which can control the morphologies of conductive polymer nanostructures. In chapter 4 we will focus on this mechanism study in detail.

2.2 Synthesis Method

Desired nanostructures have been prepared by various methods, such as vapor-liquid-solid process,⁶⁹ self-assembly,⁷⁰ and template synthesis,^{64, 71-73} *etc.* The template synthesis method has particularly fascinated scientists due to its simplicity and diverse applicabilities. The Martin group pioneered and extensively studied this method^{13, 71, 72, 74, 75} since it was first reported by Possin et al.⁷⁶ A variety of materials including metals, conductive polymers, and semiconductors can be chemically or electrochemically deposited within the cylindrical pores of a membrane. The deposition process produces nearly monodispersed nanotubes, nanowires, or nanorods. Furthermore, dimensions of the deposited nanostructures can be easily controlled by regulating the template pores and deposition conditions. In the following sections the three most important synthesis methods: vapor-liquid-solid process, self-assembly, and template synthesis will be discussed in detail.

2.2.1 Vapor-Liquid-Solid Process

The VLS mechanism has been known for more than 40 years and been widely applied in fabrication of a variety of single crystal one-dimensional nanowire structures such as silicon, CdS, GaAs, GaN etc. In 1964, Wagner and co-workers proposed the concept of a vapor-liquid-solid process for the fabrication of silicon whiskers.⁷⁷

They found that there must be some impurities which served as seeds for the VLS process. The importance of these impurities is to form liquid alloy droplets which have relatively low freezing temperature. It is believed that the liquid alloy droplet is a preferred site for the deposition of desired materials from vapor. In the process of VLS, the liquid will first be saturated with silicon. Then the silicon whisker will grow by the precipitation of silicon from the droplet. The growth of silicon whiskers is described as the following process. First, a small particle of Au is placed on a (111) surface of silicon wafer at a temperature of 900 °C. At this high temperature, a small droplet of Au-Si alloy will be generated as shown in Figure 2.1.

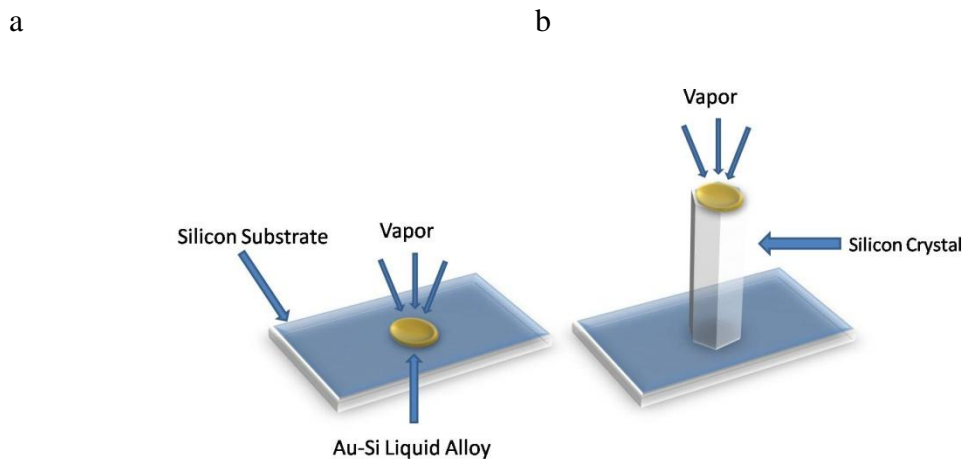


Figure 2.1. Growth of silicon crystal by VLS. a. Initial stage with liquid droplet on silicon substrate. b. The silicon whisker growth with liquid droplet on top.

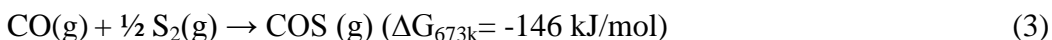
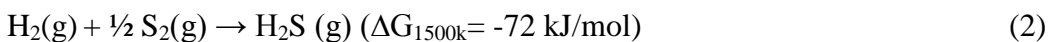
2.2.2 Self-Assembly

Except the vapor-liquid-solid method, self-assembly is also widely applied in the synthesis of a variety of nanostructures. Long-Wei Yin and co-workers reported the synthesis of wurtzite-type single crystalline nanotubes with hexagonal cross-sections.⁷⁰ In the synthesis, no H₂S, H₂ or sulfur was applied. Commercial ZnS powder was used as a precursor and H₂O gas was fed into the graphite crucible by argon gas to form reductive CO and H₂. The ZnS nanotubes are single-crystalline with hexagonal cross-sections and without any impurities inside. In the whole fabrication process, no template or metal catalysts were used. The synthesis of ZnS nanotubes is a totally self-assisted growth process or actually self-assembly process.

For the synthesized ZnS nanotubes, both ends are open. It was also noticed that there were no metallic particles at the tip or among the ZnS nanotubes. The fabrication process can be described as follows. Under high temperature, the water vapor was fed into the reaction chamber using argon gas. When the water gas reacted with C in the graphite crucible, reducing reagents CO and H₂ were produced as described in reaction (1).



Under high temperature in the reaction chamber, the ZnS powders evaporated into ZnS vapor and decomposed into Zn and S vapors respectively. The S vapor reacted with the CO and H₂ which were synthesized in the previous process and generated H₂S and COS gas. This process is described in reactions (2) and (3) :



In the next process, H₂S, COS and Zn vapor gases were transferred to a low temperature region and the Zn vapor reacted with H₂S and COS vapor to synthesize the ZnS vapor as describes in reaction (4) and (5) respectively.



The ZnS vapor aggregated and crystallized due to the condensation of ZnS clusters. It is believed that temperature and water vapor partial pressure are the most important factors influencing the fabrication of faceted ZnS nanotubes. In the initial growth stage, the nucleation of ZnS crystals is essential for the subsequent growth of the hexagonally faceted ZnS nanotubes. If the temperature is decreased or water vapor partial pressure is changed from the optimum value, no ZnS nanotubes could be obtained.

2.2.3 Template Synthesis

The template synthesis method represents an easy and straightforward strategy for fabricating various one-dimensional nanostructures.^{14, 15, 25, 71} In the template synthesis method, the template is acting as a mold around which the desired material is formed and conserves its morphology along the contour of the template. Many research groups have studied a variety of template synthesis methods. Templates include step edges present on the surfaces of a solid substrate;⁷⁸ channels of porous materials;⁷¹ mesoscale structures self-assembled from organic surfactants or block copolymers;^{79, 80} Sometimes, in order to obtain the synthesized nanomaterials, post-treatment such as chemical etching or calcinations have to be applied. In some chemical processes, the template will be consumed as the reaction proceeds and the final pure nanomaterials can be obtained.

Template synthesis methods provide a simple, low-cost and high-throughput strategy for the fabrication of varieties of nanomaterials.

In this chapter, we will discuss several template synthesis methods and their capabilities and extensions.

2.2.3.1 Hard Template Method

The template synthesis technique, developed by the Martin group in the mid 80's, has particularly fascinated scientists due to its simplicity and diverse applicabilities.⁷¹ The importance of template synthesis method lies in the simplicity and easy morphology control through the adjustment of template thickness, pore diameter and density. Varieties of materials including metals, conductive polymers, and semiconductors can be fabricated within the pores of a membrane in the forms of nanotubes or nanowires.^{25, 81, 82}

This is also the reason template synthesis method is applied for the fabrication of all nanostructures in our research work. The dense and uniform pores in templates can guide the high yield synthesis of monodisperse nanomaterials. At the same time, the length and diameter of nanomaterials can be easily controlled using the template synthesis method. Figure 2.2 shows the template synthesis strategy for nanotubes and nanorods through complete filling or partial filling of the template pores.

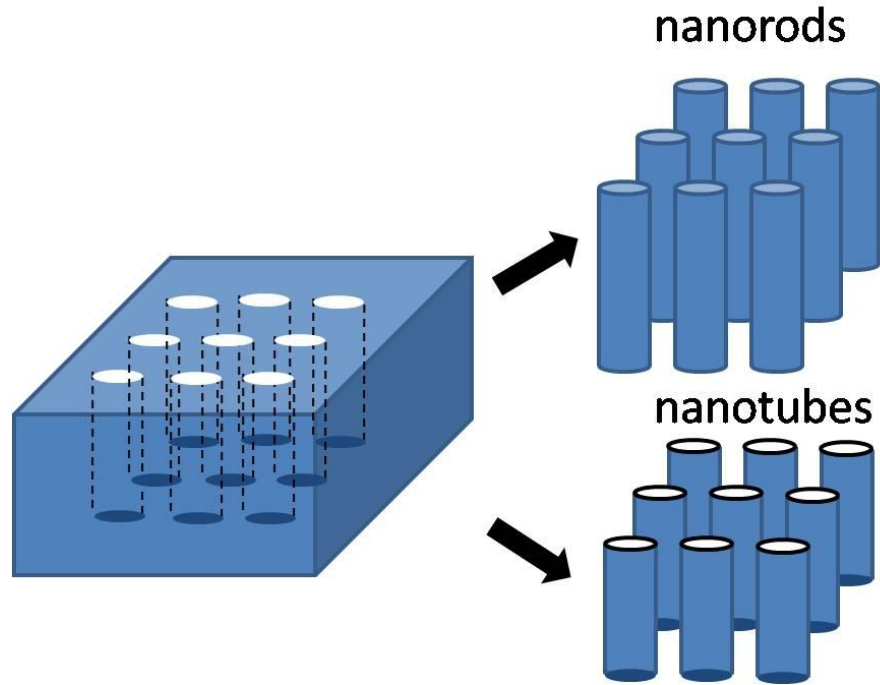


Figure 2.2 Scheme illustrating the fabrication strategy for nanorods and nanotubes of desired materials through complete filling or partial filling of template cylindrical pores respectively.

2.2.3.1.1 Porous Materials with Cylindrical Pores

Various materials can be used as templates for nanomaterial fabrication. In general, glass, nanoporous solids, mica, zeolites and block copolymer films are used as templates. Ion-track-etched membranes and anodic aluminum oxide templates are the most important and widely used materials.⁷¹ These two templates are commercially available from companies such as Nuclepore, Poretics and Whatman. Figure 2.3 shows ion-track-etched polycarbonate membrane and anodic alumina membrane.

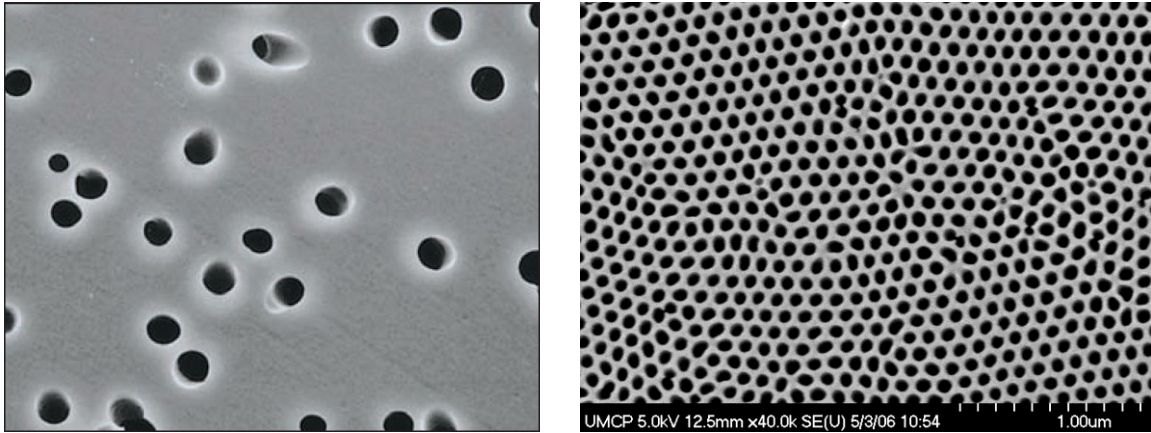


Figure 2.3 SEM images of ion-track-etched polycarbonete membrane (left) and anodic alumina membrane (right).

The ion-track-etched polycarbonete membrane is fabricated by bombarding the polymer film (6-20 μm thick) with heavy ions which are generated through nuclear fission. The irradiated heavy ions will generate randomly scattered spots all through the whole polymer film. After that, chemical etching is applied in order to generate uniform and cylindrical pores in the polymer membrane. The pores generated by ion-track etched method are not generally vertical to the template. The orientation of these pores is usually tilted by as much as 34° with respect to the surface normal. The anodic alumina membrane is usually fabricated by anodizing aluminum foil in an acid electrolyte such as oxalic acid, sulfuric acid and phosphoric acid.⁸³ The template thickness can be controlled by monitoring the anodization time. The pore diameter and density depend on several parameters such as selection of acid electrolyte, applied potential and temperature. Different combinations of these variables can generate hexagonally patterned pores with different diameters and densities throughout the alumina template.⁸⁴ Figure 2.4 shows cross sectional view of an anodic alumina template.

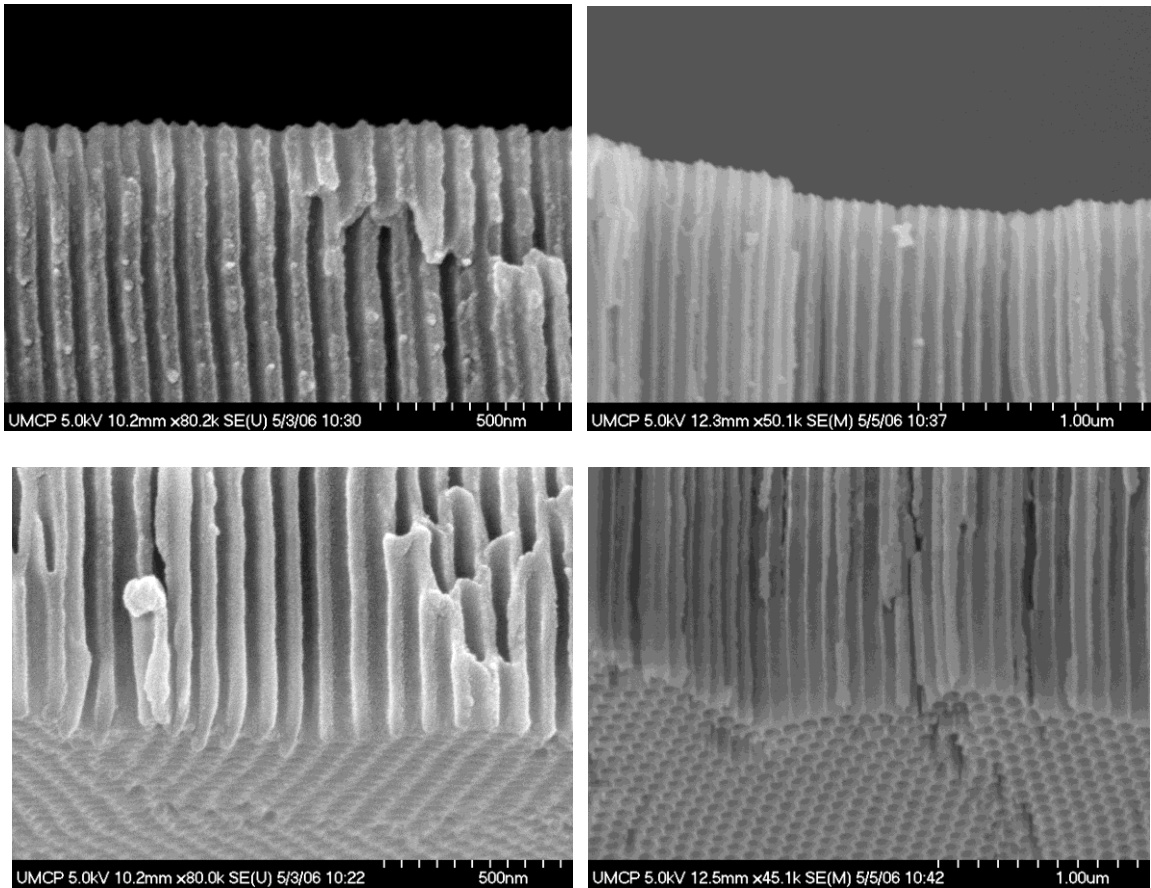


Figure 2.4. Cross sectional view of anodic alumina template. The top two images show the top of the template. The lower two images are for the bottom of the alumina template.

From Figure 2.4 it can be seen that the pores have a well-ordered hexagonal pattern on the surface of the alumina membrane and have a cylindrical morphology all through the template. The home-made alumina template which is synthesized by anodizing aluminum foil in acidic electrolytes will have a thin barrier layer at the bottom of the pores. In images above the barrier layer was removed using acid etching. The detailed anodization synthesis process of alumina templates will be discussed in the next chapter.

2.2.3.1.2 Templating against Features on Solid Substrates

Microstructures present on the surface of a solid substrate can be applied as another kind of hard template for fabrication of various nanomaterials. Lithography and etching of solid substrates can be used to synthesize these micropatterns for the fabrication of nanowires of many materials. Jorritsma and co-workers reported a strategy for the synthesis of metal nanowires with diameter as small as 15 nm by shadow sputtering a metal source on an array of V grooves which were etched on a Si(100) wafer as shown in Figure 2.5 (a).⁷⁸ Another procedure which also applies the V shape of these etched grooves is to deposit metal or semiconductor at the bottom of V grooves using vapor-phase deposition such as MBE or liquid-phase electrochemical plating. This method is shown in Figure 2.5 (b).⁸⁵ The advantage of this simple method is that nanowires with more than one hundred micrometer length can be synthesized at the bottom of V grooves as parallel arrays. These arrays of nanowires can be easily released from the underlying substrate as free-standing forms or transferred to another substrate. Many scientists have conducted research based on this method. Muller and co-workers have fabricated Ge nanowire arrays along the V grooves of an etched Si(100) substrate.⁸⁶

Various metal and semiconductor nanostructures have been fabricated by using the cross section of multilayer films generated by MBE as templates.⁸⁷ This hard template method is generally referred to as cleave-edge overgrowth (CEO). The CEO method takes the advantage of MBE to obtain high accuracy in layer thickness.

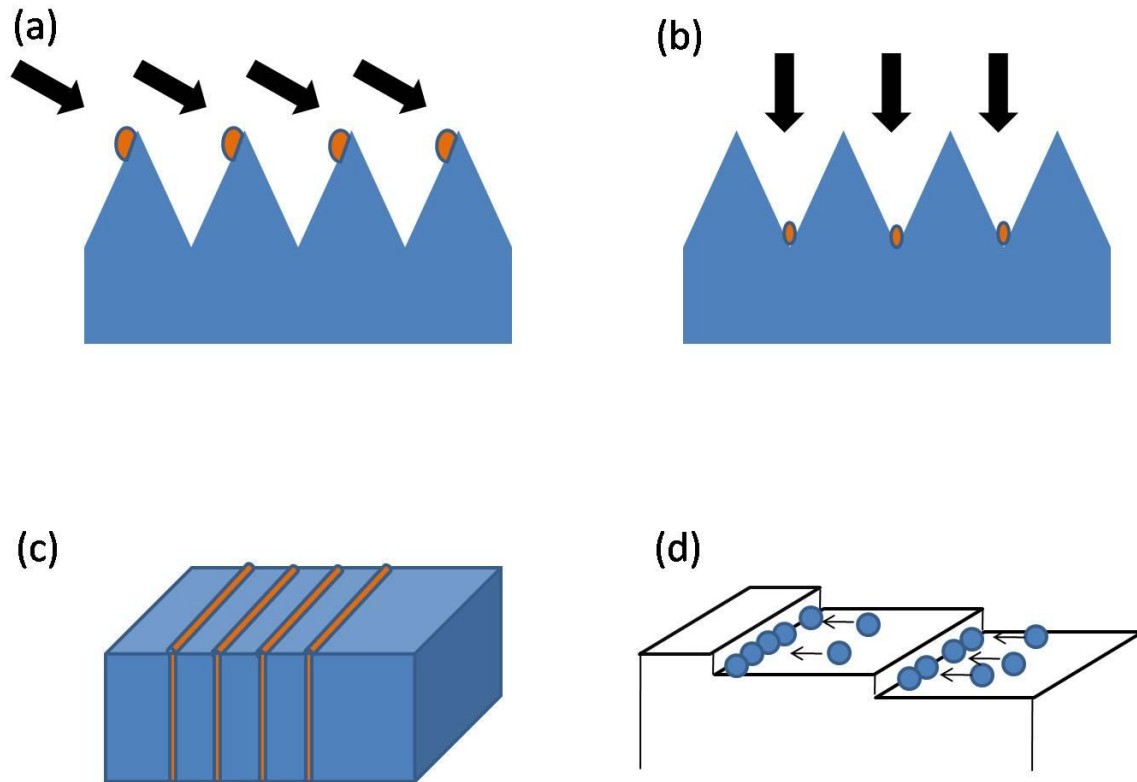


Figure 2.5 Different hard templates based on micropatterns on solid substrates. (a) shadow evaporation (b) deposition of nanowires at the bottom of V grooves etched on a Si wafer (c) cleaved-edge overgrowth on the cross section of multilayer films (d) templating along the step edges of a solid substrate

In this method, first MBE is applied to fabricate alternating multilayers of a superlattice such as AlGaAs and GaAs. The second step is to cleave the whole superlattice through its thickness and expose a clean surface for further nanomaterial deposition. Compared with other synthesis techniques such as e-beam or optical lithography, the nanomaterials fabricated by CEO provide more uniform morphologies and structures due to the precise structure control of MBE. There are also many limitations for CEO techniques. For example, nanostructures can only be fabricated along the natural cleavage directions of a

substrate and along MBE preferred growth planes. Figure 2.5 c shows the CEO process for nanostructure synthesis.

It has been reported by Penner and co-workers that the steps of a highly oriented graphite can be applied as a hard template for the synthesis of nanowire structures by electrochemical deposition method.⁸⁸ They claimed that except for the synthesis of many noble metal nanowires (e.g. Au, Ag, Pd and Cu) along this template, many electronically conductive metal oxides such as MnO_x , MnO_2 , Cu_2O and Fe_2O_3 can also be reduced into their corresponding metals (Mn, Cu and Fe) by hydrogen gas at high temperature along these sharp steps. It was found that the nanowires nucleated preferentially along these step edges and grew into parallel nanowire arrays. For the synthesis of metal nanowires through their oxide precursors, the morphologies and dimensions of the original metal oxide nanowires could be retained in the hydrogen reduction process.

2.2.3.2 Surfactant Template

Many surfactants can self-assemble into mesophase structures which can serve as another kind of template for the synthesis of various one-dimensional nanomaterials.^{30, 44} When the concentration reaches a critical value, many surfactants will spontaneously self-assemble into spherical micelles, cylindrical micelles or lamellar micelles as shown in Figure 2.6. These micelles with various structures can be directly applied as soft templates for the fabrication of nanospheres, nanorods or films of many materials.

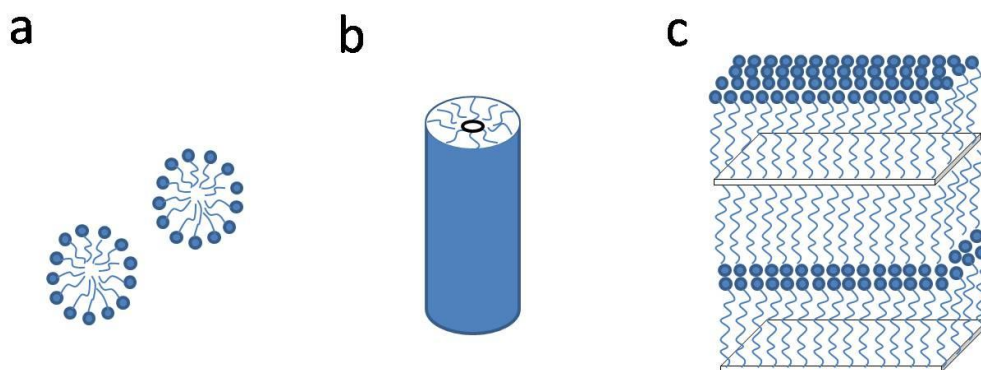


Figure 2.6 Schematic illustration of various soft templates based upon surfactants. a. sphere micelle. b. cylindrical micelle. c. lamellar phase

In addition to nanorods, nanospheres or layered nanomaterials can also be synthesized using spherical micelles or lamellar phases as soft templates as shown in Figure 2.7 below.

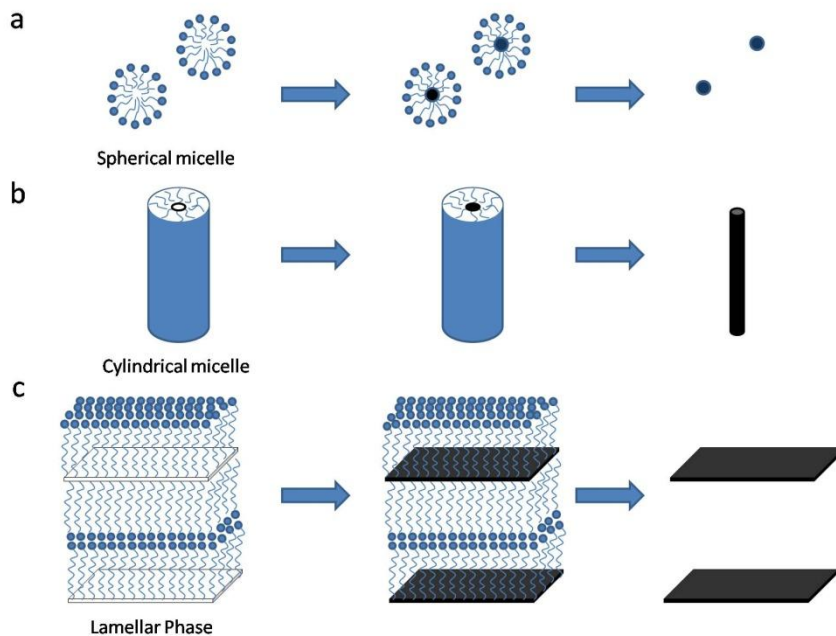


Figure 2.7. Schematic illustration for the fabrication of various nanostructures using surfactant soft templates. a. Surfactants self-assembled into spherical micelles, with the

desired material synthesized in the center of this spherical micelle. After removal of the surfactant micelle the nanosphere of desired material was obtained. b. Surfactant self-assembled into cylindrical micelles. The desired material was synthesized in the center pore of the micelle. After removal of surfactant micelle the nanorod of the desired material was obtained. c. Surfactant self-assembled into lamellar phases. The desired material was synthesized between the layers of lamellar phases. After removal of surfactants, nanofilms of the desired material were obtained.

2.2.3.3 Templates Based Upon Existing Nanostructures

Nanostructures which have already been synthesized could be applied directly as templates for the fabrication of various other nanomaterials. The basic idea is to coat the existing nanowires by a sheath of other material to generate a core-shell nanostructure. After removal of inner core material, nanotubular structures of outer material can be obtained. As discussed in the beginning of this chapter, the vapor-liquid-solid method takes advantage of the existing nanostructures as templates for the synthesis of outer shell nanostructures. Figure 2.8 shows this method.

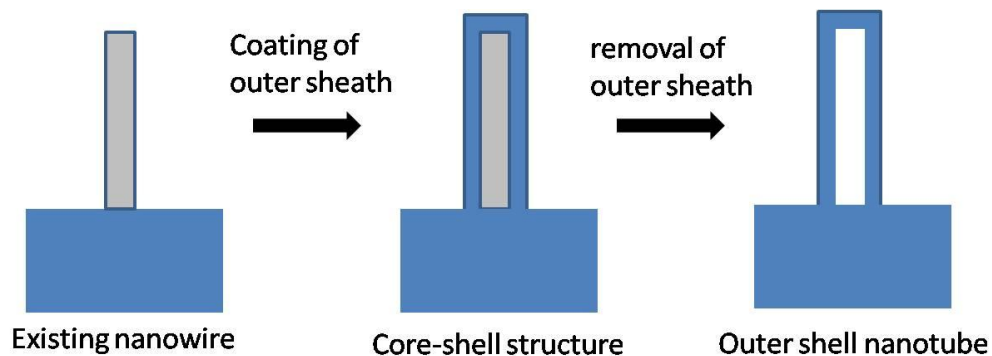


Figure 2.8. Schematic illustration of templating against existing nanostructures.

Recently, Yang and co-worker found that some single crystalline nanowires which were synthesized by thermal evaporation and laser ablation can serve as direct substrates for the epitaxial fabrication of nanostructures with other morphologies such as coaxial and bilayer structures.⁸⁹ In this synthesis method, single crystalline SnO₂ nanoribbons with high aspect ratio (i.e., 100-2000) were first synthesized. These SnO₂ nanoribbons have growth direction along <101> and well-faceted, nearly rectangular cross-sections. The single crystalline property and well faceted surfaces of these SnO₂ nanoribbons are ideal substrates for the epitaxial growth of other crystalline nanostructures.

In the next process, pulsed laser ablation was used to deposit TiO₂, Co_{0.05}Ti_{0.95}O₂ and BaTiO₃ onto SnO₂ nanoribbons for the formation of bilayer nanotapes as shown in Figure 2.9.



Figure 2.9. Epitaxial growth of bilayer nanotape structures using SnO₂ nano-ribbon as template.

Some disadvantages for this method are difficulties for precise control of composition and crystallinity of final products. At the same time the nanostructures synthesized by this method are mostly polycrystalline and few have single crystalline structures.

Although understanding of this method is still limited, it provides a promising strategy for the synthesis of various nanostructures.

2.3 One-dimensional Conductive Polymer Nanostructures

2.3.1 Introduction

Compared with other one-dimensional nanostructures, conductive polymer nanostructures are indispensable building blocks for the development of organic electronic device, energy storage devices, light-emitting diodes, and electrochromic displays. The nanowire or nanotube morphology of conductive polymers can enhance their performance significantly by improving charge transport rate, energy storage density, and surface areas. However, the detailed understanding of electrochemically synthesized conductive polymer nanostructures is very limited. In the next sections, we will discuss the general background of one-dimensional conductive polymer nanostructures, methods of electrochemical synthesis, their properties and applications.

2.3.2 Background

The electric, electrochemical, optical and electrochromic properties of conductive polymers such as polypyrrole, polyaniline and polythiophene have been used in various organic electronic, photovoltaic and display devices.^{14, 15, 20, 90} In general, conductive polymers have three main forms: thin film, nanofibrillar form and nanotube form. The thin film is the most widely used morphology of conductive polymers as building blocks for organic electronic devices such as electroluminescence device and electrochromic display devices.⁹⁰⁻⁹² For the fabrication of defect-free homogeneous thin films by spin-

coating on a conductive or insulating substrate, oxidative chemical polymerization method is frequently used. For sensor or battery applications, nanofibrils or nanotubes are usually selected due to high sensitivity and surface area requirements.^{71, 93, 94} The template synthesis method is one of the most popular strategies for the fabrication of conductive polymer nanostructures since Martin and Penner pioneered the electrochemical synthesis of polypyrrole nanofibrils using a polycarbonate membrane in 1986.^{71, 74, 95} Alumina template and polycarbonate membrane have many unique advantages such as low cost, high throughput and simplicity compared with other conventional synthesis methods. Because the morphologies of desired nanomaterials are confined by the template pore channels, precise control of template pore diameter can give nanostructures different dimensions. Chemical polymerization, due to its simplicity, is usually applied as the synthesis method for many nanostructures.^{71, 96, 97} By monitoring polymerization time and controlling monomer concentrations, nanofibrils or nanotubes can be obtained.

Electrochemical polymerization is also widely applied for the fabrication of various conductive polymer nanomaterials. Compared with chemical polymerization method, electrochemical polymerization method has many advantages as discussed in the previous chapter.^{74, 95} Figure 2.10 shows the chemical and electrochemical template synthesis methods.

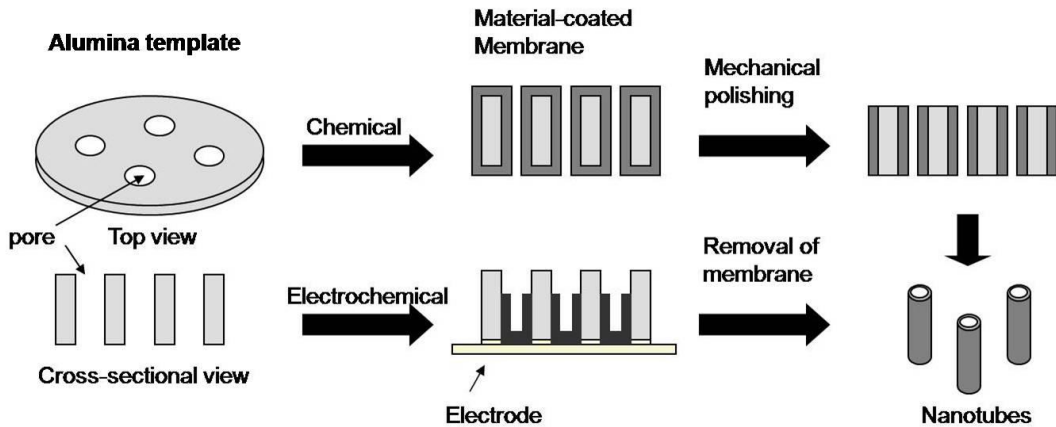


Figure 2.10. Schematic demonstration of chemical and electrochemical template synthesis methods for conductive polymer nanostructures

For the application of electrochromic display devices, nanotubular structures of conductive polymers are attracting attention due to ultra-fast charge and discharge rate for the counter ions to diffuse into and out of the thin tube walls. This property makes conductive polymer nanotubes much more superior than nanofilm structure for electrochromic display applications. It is essential to control the morphologies of one-dimensional conductive polymer nanostructures such as tube length, diameter, wall thickness and even tubular ratio. Unfortunately, detailed research in this area is very limited. But our research on the controlled synthesis of conductive polymer nanostructures has filled this vacancy.²⁵ The detailed mechanism study will be introduced in chapter 4.

2.3.3 Methods of Electrochemical Synthesis

Electrochemical polymerization of conductive polymer is conducted in a three-electrode cell which contains a solution of monomer and supporting electrolyte. The first step of

electrochemical synthesis is to deposit a thin layer of metal such as gold or indium-doped tin oxide by sputtering on one side of the alumina template. This conductive layer serves as a working electrode in the electrochemical polymerization process and is connected to a working electrode of a potentiostat. In the three-electrode cell, counter electrode is generally a platinum plate while reference electrode is a Ag/AgCl electrode. The detailed experiment setups will be discussed in Chapter 3.

Compared with chemical polymerization method, electrochemical polymerization for the synthesis of one-dimensional conductive polymer nanostructures has many distinguished advantages.^{14, 15, 25} Through controlling applied potential, electropolymerization time and monomer concentrations we can tune the morphologies of conductive polymer nanostructures. The nanostructure length, nanotube wall thickness and even tubular ratio can all be controlled. In Chapter 4 we will discuss this synthesis strategy in details.

2.3.4 Characterization of Conductive Polymer Nanostructures

Transmission electron microscopes (TEMs) and scanning electron microscopes (SEMs) have been widely applied to characterize the conductive polymer nanostructures. The SEM can be used to observe detailed morphologies of outer surface of conductive polymer nanostructures. But it has limitations. If we want to determine whether a conductive polymer nanostructure is a hollow nanotube or a filled nanowire, SEM can give false result because we can't see the inner structure using SEM. For example, Duvail and co-workers reported that through SEM image of the top ends of the poly (3,4-ethylenedioxythiophene) (PEDOT) nanomaterials, the outer structures were shown to have thick walls. From TEM image it is clear that the structure is an almost filled

concave shape with an open end.⁹⁸ Both SEM and TEM were applied to analyze the morphologies of conductive polymer nanostructures in our experiments. For TEM observation, the alumina template must be dissolved by phosphoric acid to release the confined nanostructures. The detailed sample preparation process will be introduced in the next chapter.

2.3.5 Various Conductive Polymer Nanostructures

2.3.5.1 Polypyrroles

Polypyrrole has many prominent properties such as good environmental stability, good mechanical properties, high conductivity, and easy synthesis. These properties are promising for applications such as gas sensors,⁹⁹ biosensors¹⁰⁰, actuators²¹, and electroluminescent devices.¹⁰¹ In the following we will discuss the nanotube and nanowire structures of polypyrrole respectively.

2.3.5.1.1 Nanotubes of Polypyrroles

Martin and co-workers first reported the electrochemical synthesis of the tubular structures of conductive polymer with N-methylpyrrole in a nuclepore membrane with 1.0 μm pores.⁹⁷ They proposed a mechanism to explain the formation of polypyrrole nanotubes along the template pore wall. The key in the whole process is adsorption of nascent polyheterocyclic chain to the template pore wall. In the electrochemical polymerization process, cationic radicals are obtained through the oxidation of monomers, while the pore walls in the nuclepore membrane are anionic. Thus the

electrostatic interaction between the template pore wall and the polyheterocyclic chain contributes to the formation of polypyrrole nanotubes. Demoustier-champagne and co-workers also studied the electrochemical synthesis of polypyrrole nanotubes in a track-etched polycarbonate membrane with 35-200 nm pore diameter.^{102, 103} The electrochemical polymerization was carried out at +0.8 V SCE in 0.05-0.1 M pyrrole aqueous solution. In order to understand influences of limited monomer diffusion to the formation of polypyrrole nanotubes inside the template pores, they used chronoamperometry technique. But they claimed that the diffusion of monomers inside the template pores is not the determinant parameter for the formation of polypyrrole nanotubes. The proof for this conclusion is that there was no change of polypyrrole nanotube wall thickness when the monomer concentration was changed from 0.05-0.35M.

2.3.5.1.2 Nanowires and nanofibers of Polypyrroles

The nanowire and nanofiber structure of polypyrrole have also been widely studied due to their high conductivity and good stability in severe environments. Martin's group observed high conductivity of polypyrrole nanowires which were synthesized in a nucleopore template at a high monomer concentration. They also claimed that alignment of the polymer chain by stretching could enhance the conductivities of the polymers.⁹⁶ Bulk synthesis of polypyrrole nanofibers with diameter of 60-90 nm was conducted using V₂O₅ nanofiber (diameter: 15 nm) seeds as templates. The V₂O₅ nanofibers were chemically treated with pyrrole monomers and used as a reactive seed template. Pre-polymerization reaction on the surface of a fibrillar template results in a bulk fibrillar

morphology with subsequent addition of an oxidizing agent.³³ Liu and co-workers reported a simple method for the synthesis of polypyrrole nanowires or ribbon-like structures.¹⁰⁴ In the synthesis process, lamellar inorganic/organic mesostructures were applied as templates which were formed during polymerization between surfactant cations and oxidizing anions. These templates were removed after polymerization. The diameter of synthesized polypyrrole nanowires was in the range of 20-65 nm and with length up to several micrometers.

2.3.5.2 Polyanilines

Mesostructural polyaniline has its controllable chemical and physical properties, which is according to its oxidation and protonation state, and the fact that it can act as an organic semiconductor.

2.3.5.2.1 Nanotubes of Polyanilines

Demoustier-Champagne and co-workers synthesized polyaniline nanotube structures chemically and electrochemically using the template method. They used track-etched porous polycarbonate membranes with pore diameters ranging from 20 to 220 nm.¹⁰⁵ They found that the pore diameter of the template is one of the most important parameters to control growth rate of the polyaniline nanotubes. When the pore diameter was reduced, the polyaniline growth rate along the template pore wall decreased due to the limited diffusion of monomers into the smaller pores. They also claimed that the polyaniline nanotubes with smaller diameters exhibited higher values of conductivity, due to more ordered structures in the smaller-diameter nanotubes. Shi and his group members reported a novel method for the synthesis of polyaniline nanotubes using a

reactive template of manganese oxide.¹⁰⁶ The templates used were nanowires and nanotubes of oxidative manganese oxide. They were used not only to shape the synthesized polyaniline nanotubes but also to act as a chemical oxidative initiator for aniline polymerization. The advantage of this method is that in the synthesis process, the manganese template was spontaneously removed after the reaction leaving only polyaniline nanotubes. This process can be explained by reduction of manganese oxide into soluble Mn^{2+} ions. This strategy demonstrated strong potential for morphology and structure control using manganese oxide templates and varied reaction conditions.

2.3.5.2.2 Nanowires and Nanofibers of Polyanilines

Kaner and co-workers synthesized polyaniline nanofibers using interfacial polymerization without involvement of templates or functional dopants.¹⁰⁷ An aqueous/organic biphasic system is required for the interfacial polymerization of polyaniline nanofibers. So nanofibers can be synthesized in a large scale. In order to control the morphologies of polyaniline nanofibers such as diameter, it is essential to choose suitable solvents, doping agents, monomer concentrations and reaction temperatures. For example, when hydrochloric acid is used, the average diameter of the nanofiber could be controlled at 30 nm. For perchloric acid the diameter could be as large as 120 nm.

Manohar and co-workers reported a nanofiber seeding method for the fabrication of polyaniline nanofiber without organic dopants, surfactants and insoluble templates.¹⁰⁸ With this novel method, even very small amounts of inorganic or organic nanofibers could dramatically change from nonfibrillar (particulate) morphology to almost

exclusively nanofibers. This result may be very promising for applications in morphological control in all precipitation polymerization reactions.

2.3.5.3 Polythiophenes

As one of the most important conductive polymers, polythiophene has attracted considerable interest all around the world. Because of its environmentally and thermally stable properties, polythiophene has been applied as building blocks of many electronic devices, optical devices, energy storage devices and electrochromic displays.

2.3.5.3.1 Nanotubes of Polythiophenes

Duvail and co-workers synthesized PEDOT nanotubes using cyclic voltammetry or chronoamperometry techniques.⁹⁸ They claimed that unlike polypyrrole and polyaniline PEDOT was likely to be electrochemically synthesized as nanowires instead of hollow nanotubes in a porous template. They believed that the preferential growth along the template pore wall for PEDOT is much less important compared to other conductive polymers.

From our recent research for electrochemical synthesis of poly(3,4 ethylenedioxythiophene) (PEDOT) using alumina template method, we found that the synthesis of PEDOT nanotubular or nanowire structures can be controlled by several experiment parameters such as monomer concentration, applied potential, bottom electrode shape, electropolymerization time, electrolyte concentration and temperature. All of these parameters influence the final morphologies of PEDOT nanostructures in different ways. Thus it is very important to understand the detailed synthesis mechanism

for PEDOT nanostructures. We found that the monomer concentration and applied potential are the most important parameters for the synthesis of PEDOT nanostructures. Their influence can be understood in terms of the monomer diffusion flux rate and electropolymerization reaction rate respectively. We have conducted electropolymerization under different monomer concentrations (10 to 500 mM EDOT) and applied potentials (1.2 to 1.8 V). It was found that competition between the monomer diffusion flux rate and electropolymerization reaction rate determined the tubular ratio (ratio of a tubular part of a nanostructure over the total length of the whole nanostructure) of PEDOT nanostructures. At the same time, we also found that gold bottom electrode shape was controlling the formation of PEDOT nanotubes at low potentials. The detailed mechanism study will be discussed in Chapter 4.

2.3.5.3.2 Nanowires and Nanofibers of Polythiophenes

Various polymerization strategies have been applied for the synthesis of polythiophene nanofiber and nanowires. Duvail and co-workers synthesized PEDOT nanowires by electrochemical polymerization in a track-etched polycarbonate membrane with diameters ranging from 35 to 200 nm.¹⁰⁹ The electropolymerization was conducted in a three-electrode cell with an aqueous electrolyte solution which contains 0.07 M sodium dodecyl sulfate (SDS). They found that at room temperature the estimated conductivity of PEDOT nanowires was independent on the nanowire diameter. Electrical transport measurements have been performed to 1.5 K for nanowires and films. Unexpectedly, a reinforcement of the insulating character is evidenced when the diameter of PEDOT nanowires decreases. Duvail claimed that a competitive effect induced by the confined

synthesis is involved. This research work demonstrated that the confined electrochemical synthesis of PEDOT within template pores can generate a range of electrical properties as well as the improvement of molecular and supermolecular structures such as increase in conjugation length.

2.4 Summary

In this chapter we have discussed the general background of one-dimensional nanostructures from many aspects. The most important three synthesis methods have been introduced especially the template synthesis method which is widely applied for the fabrication of various one-dimensional nanostructures. We have discussed in details the conductive polymer nanostructures which include polypyrrole, polyaniline and polythiophene as well as their synthesis methods and unique properties. Compared with nanowire structures, nanotubular structures of conductive polymers have many useful properties such as ultra-fast charge and discharge rate due to thin tube wall thickness and feasibility for the inner and outer surface modification. For electrochromic display applications, PEDOT nanotubes are ideal structures to achieve ultra-fast color changing rate and good color contrast. Thus it is very important to understand the synthesis mechanism for conductive polymer nanostructures and this is exactly what has been done in our research work. In chapter 4 we will discuss in details about the controlled synthesis of one-dimensional conductive polymer nanostructures.

Chapter 3: Experiment Setup and Techniques

3.1 Introduction

The template synthesis method has been intensively studied for the preparation of one-dimensional nanomaterials in recent years for applications to electrochemical sensors, energy storage devices and photovoltaic devices. This method has advantages of simplicity, versatility and easy control of final morphologies.

We have discussed hard template synthesis methods including alumina templates and polycarbonate templates, surfactant soft templates and templates based upon existing nanostructures. The alumina template and polycarbonate template synthesis methods have been extensively studied in our group for fabrication of various polymer, metal, metal oxide and semiconductor nanostructures. In this chapter we will discuss the mechanism and fabrication of the alumina template and its application in preparation of various nanomaterials.

3.2 Template Synthesis

In this section, we will discuss the mechanism, procedure and experiment setup of alumina template synthesis. Two kinds of alumina template will be introduced. The first one is home-made alumina template fabricated through anodizing commercially available aluminum foil. The second alumina template is based upon conductive ITO glass. This template is prepared by anodizing evaporated aluminum thin film on ITO glass.

3.2.1 Home-Made Alumina Template Synthesis

Many metals such as aluminum, niobium, tantalum, titanium, tungsten and zirconium have a layer of oxide film deposited on their surfaces by an electrochemical process called anodization.^{83, 110-112} The process conditions that promote growth of a thin, dense and uniform barrier oxide layer of each of these metals are different. The thickness, density and other properties of these oxide barrier layers depend upon many parameters. Aluminum is unique among all of these metals because the anodization process produces a thin oxide barrier layer and a thick aluminum oxide coating which contains many patterned microscopic pores with high density. Figure 3.1 shows the SEM image of the hexagonally patterned micropores after anodization.

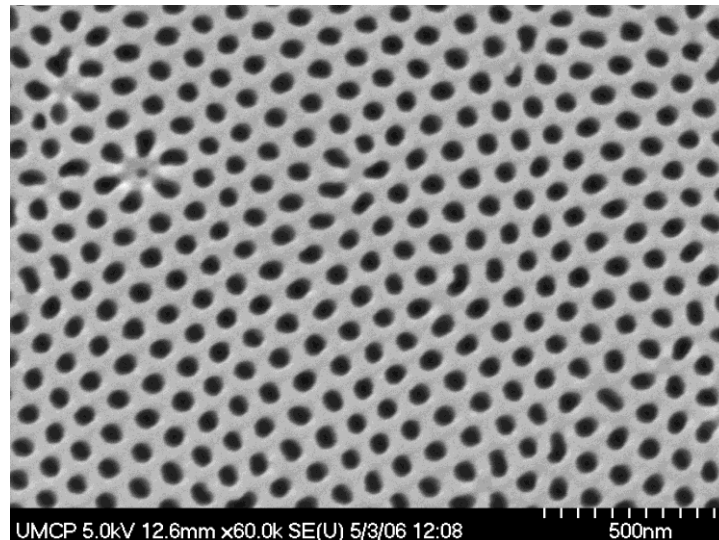


Figure 3.1. SEM image for micropores on aluminum surface after anodization process.

The porous oxide coating of the anodized aluminum has applications such as architectural finishes, corrosion protection in automobile and aerospace industry, and electrical

insulation. In the electrochemical cell of an anodization system, the aluminum workpiece is applied as an anode by connecting it to a positive terminal of a DC power supply. The cathode is generally a plate or rod made of an electric conductor such as carbon, lead, nickel or stainless steel and is inserted in the anodization electrolyte solution. When anodization starts, electrons are withdrawn from the metal at the interface between the metal and the electrolyte at the positive terminal. Anodizing allows the metal ions to react with water to form an aluminum oxide layer on the aluminum surface. At the same time, electrons return to the cathode where they react with hydrogen ions to generate hydrogen gas.

The anodization electrolyte should allow the oxide layer to be insoluble or dissolve at a slower rate than it deposits. Under this condition, the aluminum oxide layer will grow continuously. The selection of suitable electrolyte is essential in determining the morphologies of final product.¹¹³ Some baths can generate oxide barrier layers while others can form porous aluminum oxide structures. If the anodization bath is a neutral solution, barrier oxide will be obtained because the aluminum oxide is hardly soluble in these solutions. They are most commonly ammonium borate, phosphate or tartrate compositions. Aluminum oxide with porous structures can be used by using acidic electrolyte solutions in which there exists an equilibrium between the deposition and the dissolution of the oxide. The most widely used bath is dilute sulfuric acid, oxalic acid and phosphoric acid.¹¹³

In air, metals can be readily oxidized by oxygen. Therefore under ambient conditions the surface of metal is always covered by a thin layer of oxide film. The morphology of the film structure and composition are determined by the condition of ambient atmosphere in

which the metal is exposed. On the surface of aluminum, there is always an aluminum oxide barrier layer which is about 2-3 nm thick and stabilizes the aluminum surface against further reaction. In a borate electrolyte anodization solution, due to electronic insulating property of the barrier layer, there is no apparent current flow until the voltage is raised to between 1 and 2 V. Electric field in the oxide barrier layer is of the order of 1 V/nm. Under this electric field, water is oxidized to evolve oxygen. But the generation of oxygen is not observed. The reason is that electron movement from electrolyte to metal is blocked by the oxide barrier layer. The voltage across the oxide barrier layer can be increased without initiating current flow. When the electric field across the oxide is large enough to drive aluminum and oxygen ions through the oxide layer, these ions will react with each other to form the oxide barrier layer.

3.2.1.1 Alumina Oxide Barrier Film

High-field ionic conduction is essential for an anodization. At the interface between metal and oxide, the oxide anions move toward the metal and react with aluminum to form aluminum oxide. While at the interface between the oxide and anodization electrolyte the aluminum cations are moving outward to react with water to form aluminum oxide. These processes are occurring at the anode. At the cathode, hydrogen gas is generated by reduction of hydrogen ions. The new aluminum oxide is formed at both interfaces of the oxide as shown in Figure 3.2.

The thickness of the oxide barrier layer is proportional to the current density. The value of electric field in the oxide film does not depend on the oxide thickness and barely depends on the current density and temperature.

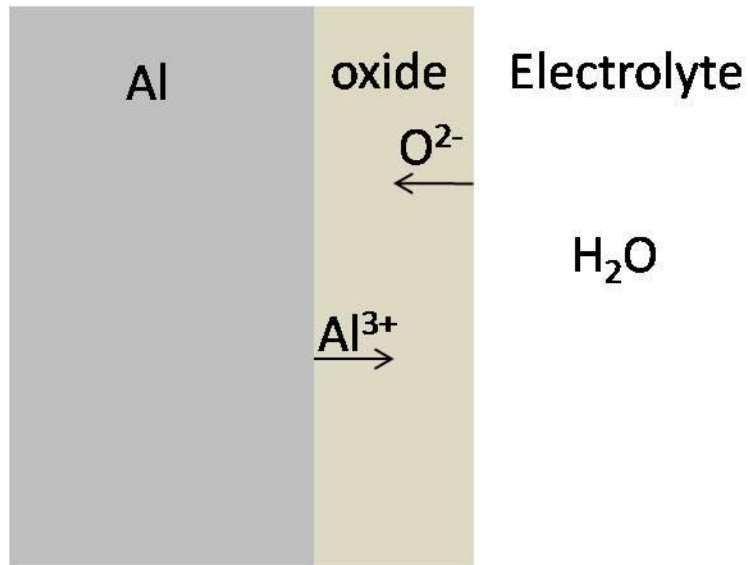


Figure 3.2. Schematic illustration of ion transport in the oxide film.

At a given temperature and electrolyte bath composition, there is a maximum voltage at which breakdown occurs. The generation of oxygen, oxidation of solute or sparking due to electron avalanche will occur when the voltage reaches the value of breakdown. The breakdown voltage is inversely proportional to the concentration of electrolyte. The lower the electrolyte concentration, the higher the breakdown voltage.

3.2.1.2 Porous Alumina Template Synthesis

The anodized alumina template has morphologies of hexagonally patterned pores with aspect ratios commonly higher than 1000:1 (channel length vs. pore diameter). This high aspect ratio is very difficult to obtain with conventional electron beam lithographic techniques. The cost of fabrication of nanoporous structures with lithography is too high for industry.

The anodizing bath should retain a relatively high concentration of aluminum in the electrolyte solution. This is necessary, because a large portion of the anodized aluminum is transported into the solution rather than returned to the film. For instance, anodization of aluminum in sulfuric acid retains about 60 % of the oxidized aluminum in the film with the remaining 40 % in electrolyte solution. The thickness of the anodized aluminum can be as large as 100 μm , much higher than that of the oxide barrier film. Figure 3.3 shows an idealized alumina template with hexagonally patterned pores.

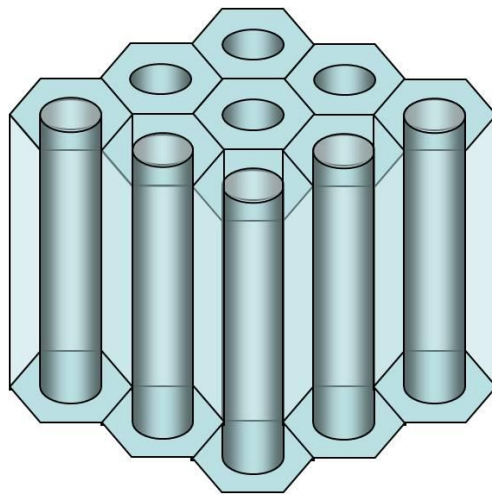


Figure 3.3. Schematic illustration of hexagonally patterned pores of an anodized alumina template.

Figure 3.3 shows the anodized alumina oxide with a uniform hexagonally patterned cellular structure and a central cylindrical pore in each cell. Most anodization conditions generate films with disordered pore structures. The cell size and pore diameter are distributed in a range of sizes. The diameter of the cell and pore depend on several parameters such as electrolyte composition, temperature and applied potential. For a fixed electrolyte bath and temperature the cell diameter, pore diameter and barrier layer thickness depend on the applied potential.¹¹³ The following three formulas show this.

$$\text{Pore diameter} = 1.29 \text{ nm} \times \text{applied voltage} \quad (1)$$

$$\text{Cell diameter} = 2.77 \text{ nm} \times \text{applied voltage} \quad (2)$$

$$\text{Barrier layer thickness} = 1.35 \text{ nm} \times \text{voltage} \quad (3)$$

The magnitude of applied voltage is between 20 V and 200 V.

From the above three empirical formulas, it is easy to predict the dimensions of anodized alumina template when the electrolyte and temperature are fixed. The cell density is from approximately 10 to more than 100 per μm^2 . Figure 3.4 shows field emission SEM images of an alumina template which was anodized in 0.3 M oxalic acid at 10 °C with the applied voltage at 40 V.

(a)

(b)

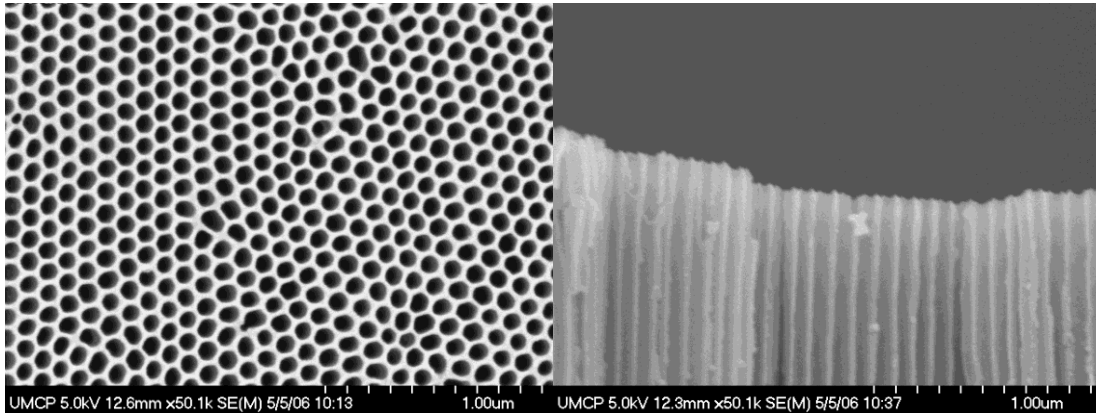


Figure 3.4. Field emission SEM images of anodized alumina template. The anodization condition is in 0.3 M oxalic acid, 10 °C with 40 V applied voltage. The left one showed the hexagonally patterned pores on top the alumina template. The right one illustrated the cross-sectional view of the cylindrical channels of the pores.

Figure 3.5 shows stages of alumina template pore formation. We can see that when an anodic potential is applied a barrier layer of aluminum oxide is formed on the surface of an aluminum substrate, stage I. With time small cracks appear at the interface between the aluminum oxide and the electrolyte. These cracks are widened to form pores on the aluminum surface, stage II.

The initiation of the cracks originates from the morphology of the aluminum metal surface. The surface of aluminum foil has a degree of roughness related to the metal fabrication process. Even electropolishing which is widely applied in the anodization pretreatment in order to make the aluminum sheet surface smooth and flat can create a scalloped surface texture with shallow cells of the order of 100 nm diameter.

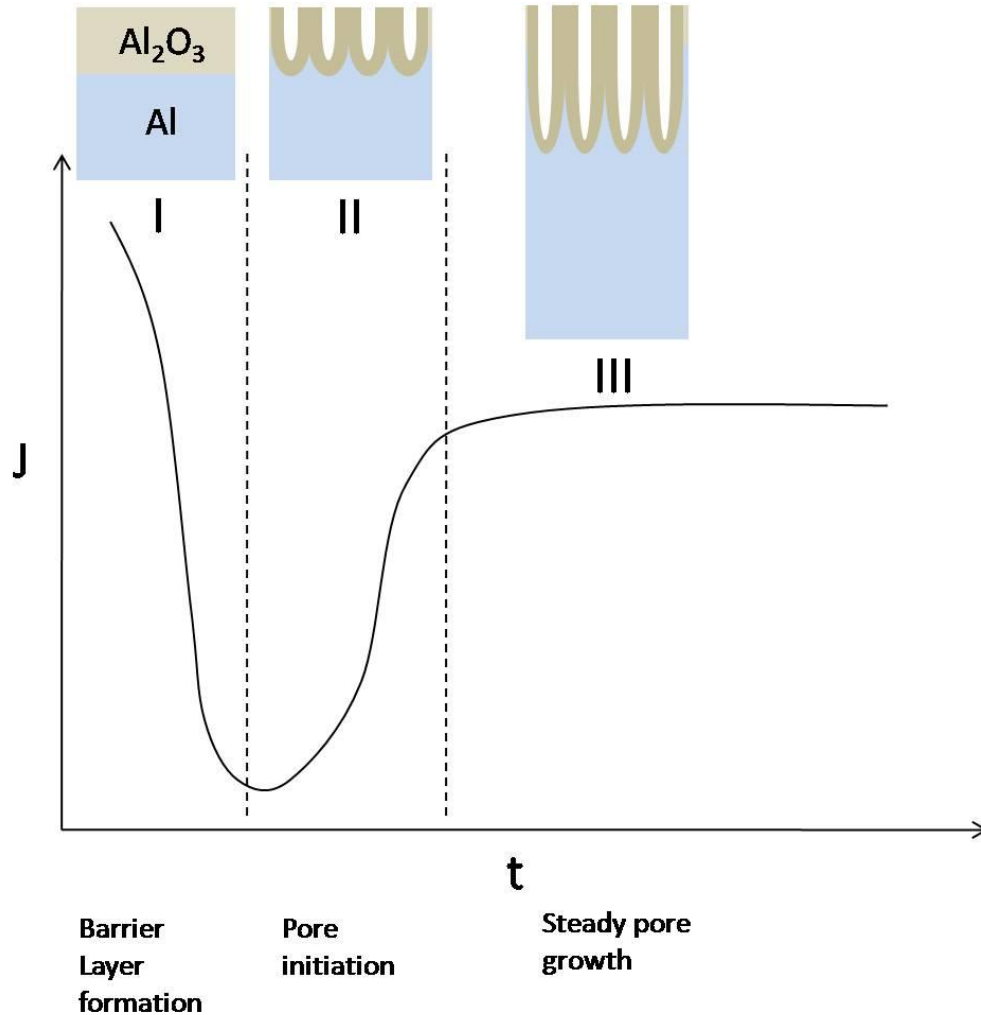


Figure 3.5. Schematic diagram of current density vs. time for different alumina template pore formation stages at a constant voltage for the anodization of aluminum in an acid electrolyte.

In the early growth stage, the oxide film on ridges and protuberances becomes thicker than in the depressions. It seems that ions move through the oxide more easily at these locations. This may be due to high film stress, impurities, or oxide flaws which can concentrate current at these locations. As the oxide become more uniform, the current is

concentrated towards the thinner oxide in depressions. The concave geometry that develops on the surface of alumina barrier layer results in a slightly higher electric field in depressions. Field-assisted dissolution promotes local oxide thinning and current concentration. Further anodization causes the pores to attain a constant dissolution speed as shown in stage III of Figure 3.4. This initiates pores, and the pore size, density, and distribution adjust until an equilibrium between the dissolution of aluminum and deposition of aluminum oxide is reached. For commercial processes most of the adjustment typically occurs within the first minute.

In the initial growth stage, the current density reaches a very high value and drops to the minimum quickly. In stage I, a thin layer of aluminum oxide barrier layer has been formed. In stage II, the shallow pores with scallop bottom shape which is demonstrated in Figure 3.6 have been initiated on the barrier layer and the current density starts to increase due to the local accumulation of current. In stage III, at steady state, the template pores grow continuously and the current density is stable.

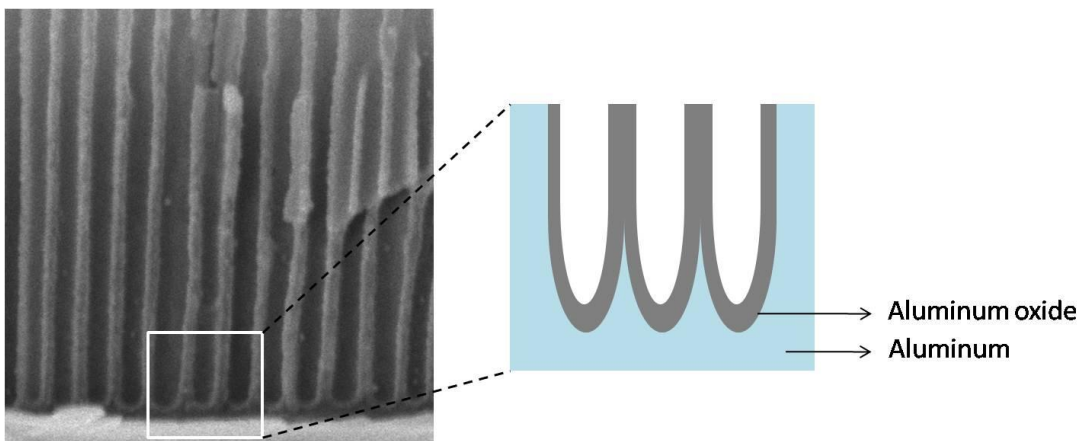


Figure 3.6. Schematic illustration of alumina template pore bottom with scallop shape.

The square part in the left SEM image is enlarged to the scheme at the right.

The well-developed pore structure consists of closely packed hexagonal cells each containing a long pore separated from the aluminum metal by a layer of scalloped oxide as shown in Figure 3.6.

Many scientists have studied the growth process of alumina template pores. Parkhutik assumed that in the steady state the alumina template pores have a hemispherical bottom.¹¹⁴ From study of kinetics of the oxide formation, they obtained the electric field at the oxide/electrolyte interface tip and found that the pore grows at the maximum possible speed. Hence, they concluded that this geometry yielded the desired linear relationship between the pore diameter and applied voltage.

The reaction occurring at the interface between the oxide and electrolyte is chemical dissolution enhanced by the electric field. The dissolution of metal at the metal/oxide interface is due to charge transfer or electrochemical reactions. The local electric field is the essential variable that determines the reaction rate and the speed of the propagation of the interface.

In order to obtain different pore diameters, it is very important to choose a suitable acidic electrolyte and corresponding potential for the anodization process.

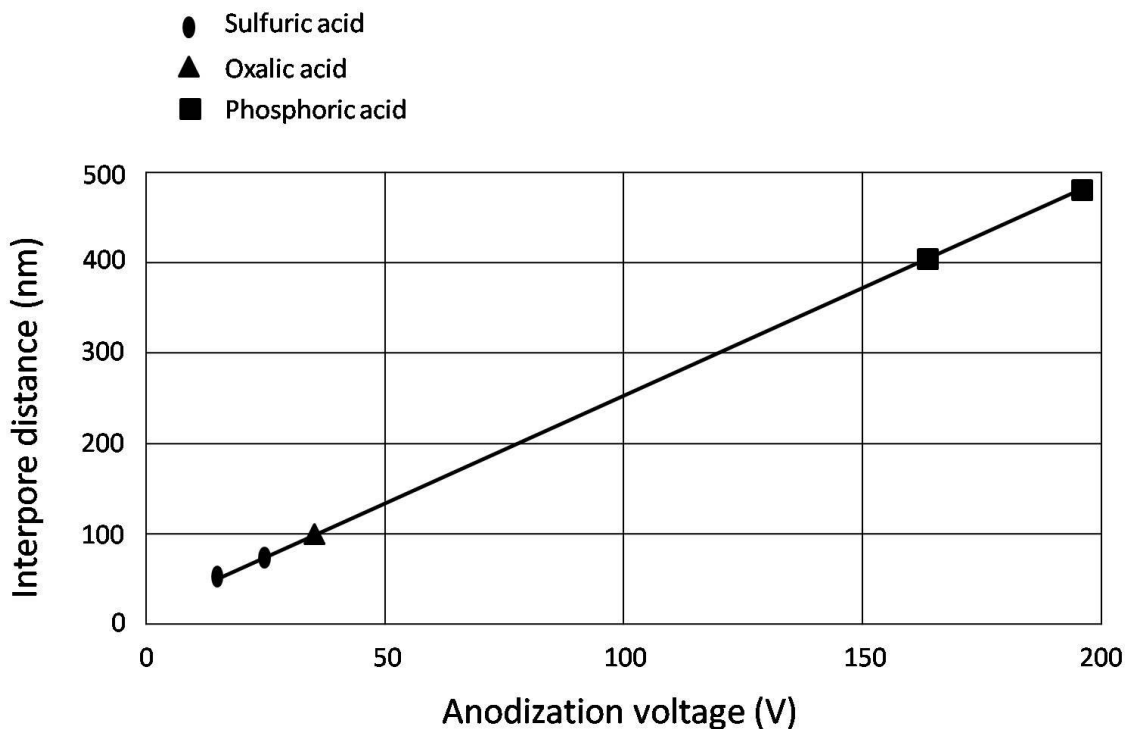


Figure 3.7. Schematic demonstration of the relationship between interpore distance and applied voltage for various acidic anodization electrolytes. The concentrations of phosphoric acid, oxalic acid and sulfuric acid are 10% (vol), 3% (wt) and 10% (vol) respectively.

Figure 3.7 shows relationship between interpore distance and applied voltages for various acidic anodization electrolytes. It can be seen that sulfuric acid and oxalic acid are suitable for the formation of template pores with small diameters at low potentials. While for the synthesis of alumina template with bigger pore diameters, phosphoric acid is a better choice. It can also be seen from this plot that no matter what acidic electrolyte is applied for the anodization process, the interpore distance has a linear relationship with the applied potential. The higher the voltage, the bigger the interpore distance. This result is consistent with the prediction of formula (2) which has been discussed previously.

The following section will discuss the detailed anodization of alumina template in oxalic acid. Oxalic acid is chosen as the anodization electrolyte because it yields well-ordered hexagonal pattern of pores which is more homogeneous than that obtained in other acidic electrolyte solutions.

If only one anodization process is conducted, it is impossible to get an ordered hexagonal pattern of pores on anodized aluminum foil. This is related to the poor top surface morphologies attributed to higher film stress, impurities, or oxide flaws for commercially available aluminum foil. In order to get a good hexagonal pattern for the final synthesized pores, a first anodization of long duration is necessary to produce better morphologies at the bottom of pores. When the first anodization step is finished, a chemical etching step is applied to remove the top alumina layer and leave good hexagonally patterned concaves of alumina barrier layer on the underlying aluminum substrate. This pre-patterned alumina barrier layer serves as a mold that can guide the subsequent growth of template pores. After the second anodization, well-ordered alumina template with a hexagonal pattern is obtained. Figure 3.8 shows this two-step anodization process for the synthesis of an alumina template. The following is the procedure for two-step anodization of commercially available aluminum foil.

1. Pretreatments of aluminum sheet

- Material: 0.5 mm thick, annealed, 99.99% purity aluminum sheet purchased from Alfa Aesar (sock # 40531). The aluminum foil is cut into small pieces with size of 20 cm² for the fitting of anodization jacket.
- Annealing (when necessary)

conditions: 400 °C in argon atmosphere for 2 hours

purpose: increases the grain size of aluminum sheet and provides the sheet homogeneous conditions for pore growth over large area.

- Degreasing

condition: ultrasonicate the sample in acetone for 1 hour

purpose: remove organic impurities which may decrease the final product quality.

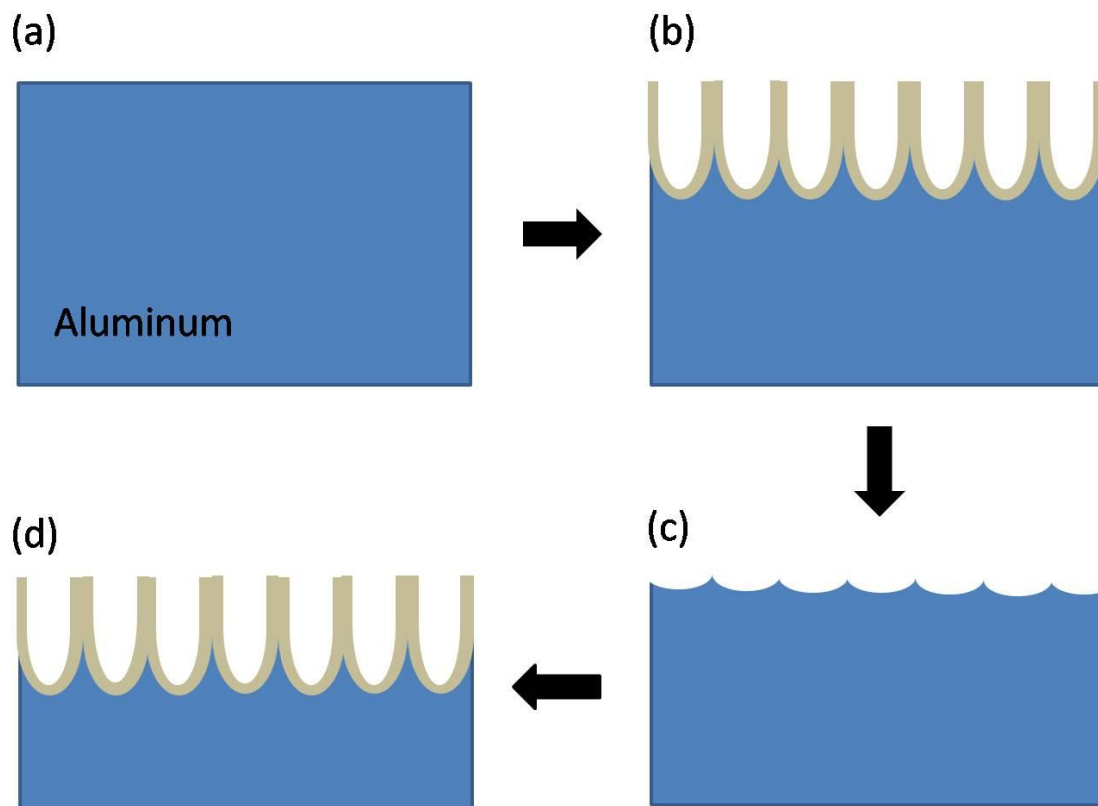


Figure 3.8. Schematic illustration of two-step anodization process for the synthesis of alumina template. (a) electropolished aluminum sheet (b) first anodization generates pre-patterned pores (c) chemical etching to remove the layer of anodized aluminum oxide (d)

based on the concaves of the barrier layer, second anodization forms well-patterned template pores with a hexagonal pattern.

2. Electropolishing

- Conditions: 1 to 5 mixture of perchloric acid and ethanol at 5 °C for 10 min under a constant voltage of 15 V.
- Makes the surface of aluminum sheet smooth and homogeneous. Surface roughness may influence accumulation of local heat, and disrupt highly ordered pore formation.
- Caution: It should be noted that there must be a small part of the aluminum foil exposed outside the electropolishing solution. This part is attached to the anode of a Sorensen DHP series programmable high power supply. At the interface between the air and electropolishing solution, the aluminum foil is wrapped with a layer of insulating tape 1.5 cm wide to avoid the accumulation of charges at the interface. Without this insulating tape, the aluminum foil is damaged by the high density of charge at the air-solution interface and quickly breaks. The electropolishing solution cannot be reused. A mirror-like surface is obtained on the aluminum sheet by electropolishing. The glass jacket is connected with a circulator to control the whole system temperature.

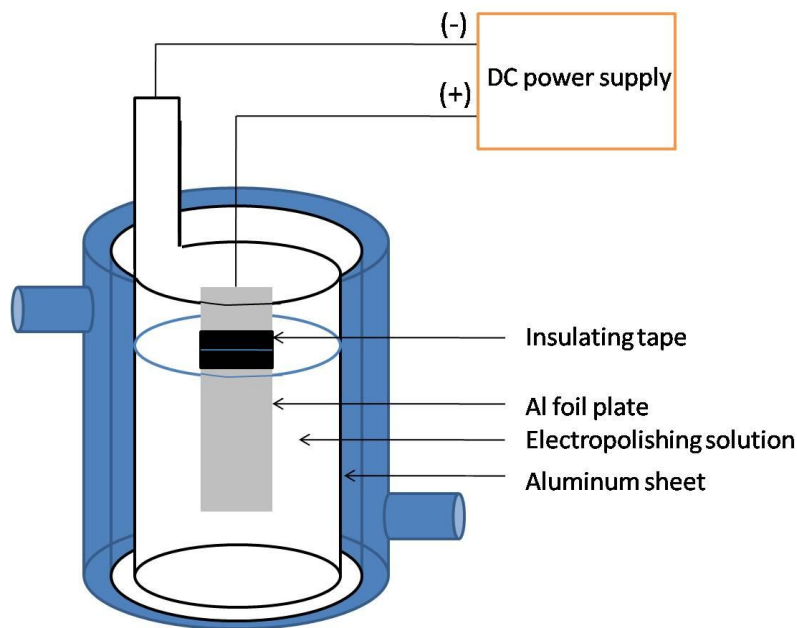


Figure 3.9. Electropolishing experiment set-up. An aluminum sheet is placed in the electropolishing solution and connected to the cathode of a DC power supply. A 20 cm² aluminum sheet is clipped to the anode of the DC power supply and immersed in the electropolishing solution (EtOH: HClO₄ = 5: 1). The air/solution interface is protected by a layer of insulating tape. The temperature is controlled by a circulator which is connected with the glass jacket.

3. First Anodization

- Before the first anodization, pretreat the aluminum sheet in 0.25 M H₂CO₃ solution at 80 °C for 1-3 min to remove the natural aluminum oxide monolayer on the surface.
- Condition: 0.3 M oxalic solution at 10 °C for at least 5 hours under a constant voltage of 40 V.

- The first anodization improves regularity of the pore arrangement, and supplies a large defect-free region. At the beginning of the first anodization, the pore pattern is irregular. As anodization proceeds, pore regularity improves. The longer the anodization, the more uniform the pore pattern. At least 5 hours are required to get an ordered anodic alumina template with well-ordered hexagonally patterned pores.
- At the interface between the air and oxalic acid, the aluminum sheet is protected by a layer of insulating tape. Epoxy is used to seal the voids between the insulating tape and underlying aluminum sheet. This prevents charges from concentrating at this junction and the aluminum sheet from breaking. The oxalic acid solution is stirred continuously to keep local concentration of protons; remove reaction products; and maintain temperature homogeneity.

Figure 3.10 shows the experiment set-up for the anodization of aluminum sheet in oxalic acid. The experiment set-up is similar to that for electropolishing process except that the solution is oxalic acid and the applied voltage is 40 V.

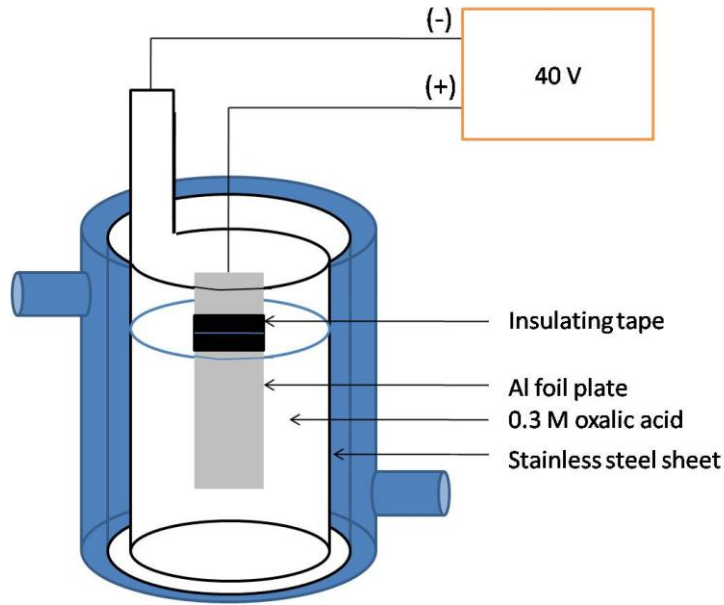


Figure 3.10. Schematic diagram for the experiment set-up for anodization

4. Etching

- Condition: an aqueous mixture of phosphoric acid (6 wt%), chromic acid (1.8 wt%) at 60 °C for about $\frac{2}{3}$ of the first anodization time with stirring.
- With one step of anodization, it will be difficult to get well-ordered alumina template with a hexagonally patterned pore structure. Through etching, the first layer of aluminum oxide is removed and a well-ordered alumina barrier layer with hexagonally patterned scallop shape is left. This barrier layer serves as a mold to guide the formation of well-ordered pores for the second anodization.
- If the first layer of alumina is over-etched, the well-ordered alumina barrier layer will be removed. This will result in loss of regularity for the second anodization.

5. Second anodization

- Condition: The second anodization is conducted under the same conditions as for the first step. Only anodization time is changed.
- Purpose: During the second anodization, barrier layer thickness, pore diameter, pore length, interpore distance, etc. can be controlled by varying the anodization conditions. Pore length depends on the second anodization time. As a rule of thumb, it was estimated that the rate is about 100 nm per min.
- The second anodization solution can't be reused but it may be used for first anodizations. Contact of the solution surface with the aluminum sheet above the insulating tape should be avoided because high density of charges at this interface may damage the aluminum sheet.

6. Pore Widening

- Condition: 0.1 M phosphoric acid at 38 °C with stirring for 10 – 40 min.
- Purpose: The main purpose of chemical pore widening is to increase the pore diameter through the reaction between phosphoric acid and aluminum oxide. By controlling acid concentration, temperature and time the pore diameter can be controlled.
- It is important to keep a constant temperature and continuous stirring of the phosphoric acid. Through convection, new phosphoric acid can be supplied to the template pores and reaction debris can be removed. Precise control of pore widening time is critical for obtaining well-ordered pores with desired diameter. If the pore widening time is too long, the pores will

be over-etched and connected with each other. Figure 3.10 shows the field emission SEM images of alumina templates for various pore widening times.

It can be seen from Figure 3.11.a that after the second anodization the pores of the alumina template have a diameter of about 20 nm. The hexagonal pattern for these pores is barely visible. After 50 min in 0.1 M phosphoric acid at 38 °C, the diameter of the template pores has been enlarged to about 80 nm and shows a well-ordered hexagonal pattern as shown in Figure 3.11.b. If the treatment time is too long, the template pores will be over-etched and connected with each other. Figure 3.11.c shows this condition.

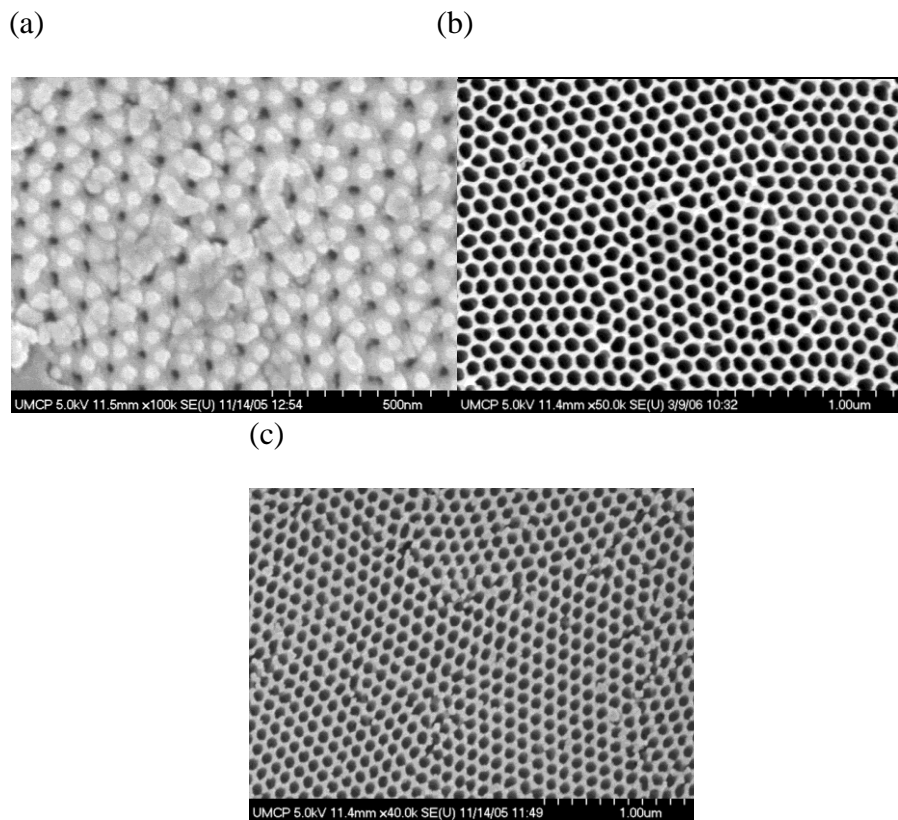


Figure 3.11. SEM images for alumina templates under various pore widening durations.

(a) no pore widening (b) 50 min pore widening (c) 60 min pore widening (over-etched)

7. Barrier Layer Removal (optional)

- Condition: Saturated mercury chloride solution is applied to remove the un-anodized aluminum substrate for applications when both ends of the template channel need to be open. The aluminum oxide barrier layer at the bottom of template pores is removed by chemical etching with 5 % phosphoric acid at 30 °C for 50 to 90 min depending on pore size.
- Purpose: For some applications such as sol-gel method, it is not necessary to remove the underlying un-anodized aluminum substrate because precursors for nano-fabrication can diffuse into the template pores from the bulk solution. But for electrochemical synthesis method, it is necessary to deposit a layer of metal which serves as a working electrode at the bottom of the template pores for electrochemical deposition. The aluminum oxide barrier layer blocks flow of electrons for this electrochemical synthesis. Therefore acidic solution should be applied to remove the barrier layer and expose the bottom of the template pores.
- Caution: Because dissolution of the aluminum substrate requires a large amount of mercury chloride, it is very important to keep the saturation of mercury chloride solution. Heat is released from the solution and drops of mercury can be observed on the surface of aluminum substrate. When the aluminum is completely dissolved a transparent alumina template can be obtained.

Figure 3.12 shows the tilted view of a hexagonally patterned alumina template and its cross sectional view.

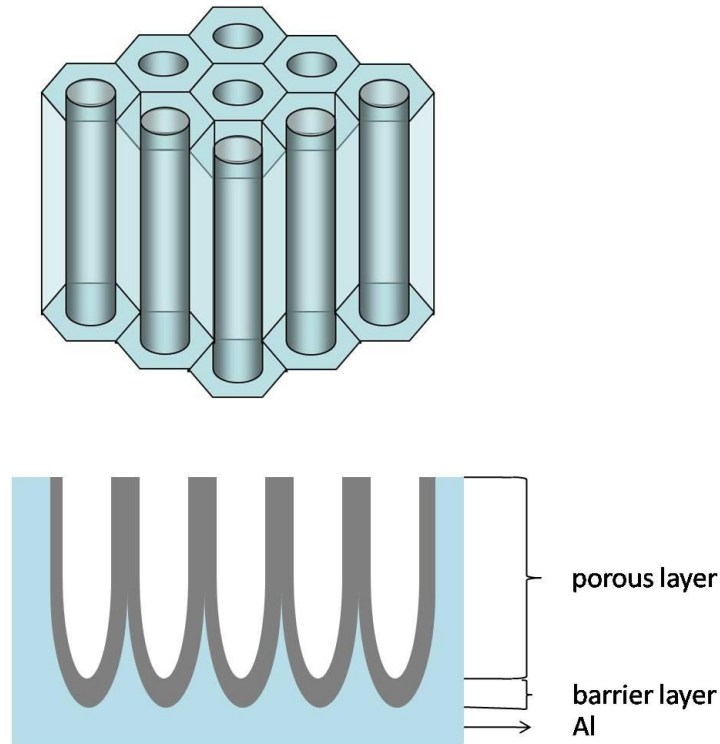


Figure 3.12. Perspective and cross sectional view of anodic alumina template.

From Figure 3.12 it can be seen that there is always an alumina barrier layer between the bottom of the pores and the unanodized base aluminum which acts as the electrochemical anode. The thickness of the alumina barrier layer is generally between 10 and 100 nm. The existence of this alumina barrier layer has two major disadvantages. First, it will block direct contact of chemical agents or electrical conduction between the materials in the pore channels and the base conducting substrate. This will prevent electrodeposition of nanowires or nanotubes inside the cylindrical channels of the pores. Second, the alumina template is sticking firmly to the underlying unanodized aluminum substrate.

This will make it difficult to obtain free-standing alumina templates for other applications.

Several methods have been developed to remove the alumina barrier layer and expose the bottom of the cylindrical channels of the pores. The most widely used method is to etch the underlying aluminum substrate by using a saturated solution of HgCl_2 and then remove the alumina barrier layer by chemical etching. When the anodized alumina template is put into a saturated solution of HgCl_2 , bubbles are generated and heat is released. The aluminum is oxidized by HgCl_2 and small mercury drops appear on the surface of the aluminum substrate and fall to the bottom of the reaction container. The whole process depends on the size of the aluminum substrate that remains after anodization.

Generally there are two methods for the electrodeposition of various nanomaterials in the pores of alumina templates. The first method uses direct current for the deposition of various metal, metal oxide and polymer materials in the cylindrical pores of alumina templates.^{14, 115} In order to achieve this, the anodized alumina template must be detached from the underlying aluminum substrate and the alumina barrier layer at the bottom of the template pores has to be removed by chemical etching. A thin layer of metal should be sputtered on the side of barrier layer which is removed by chemical etching and serves as a working electrode in the three electrode system. If the insulating barrier layer is not removed, the flow of current through the pores is stopped and no electrochemical deposition can occur. Removal of alumina barrier layer needs a free-standing alumina template with thickness of at least 20 μm . For most applications, the thickness of porous alumina template should be hundreds of micrometers.

Another method for the removal of the alumina barrier layer is a combination of chemical etching and limited anodization. Ulrich Gosel and co-workers reported uniform nickel deposition into ordered alumina template pores by pulsed electrodeposition.¹¹⁶ In this method, the porous alumina template remained on the underlying aluminum substrate and the desired metal was deposited on the tips of alumina barrier layer at the bottom of template pores through an alternating deposition potential. With this method, the synthesis of ordered metal nanostructure arrays is not limited by the thickness and size of alumina barrier layer. Figure 3.13 shows the synthesis of a highly ordered porous alumina template and the preparative steps for the subsequent filling of nanostructures. The alumina template was synthesized by the two-step anodization process. A first long duration anodization formed an ordered hexagonally patterned cylindrical pore array with a high aspect ratio and regular pore arrangement.

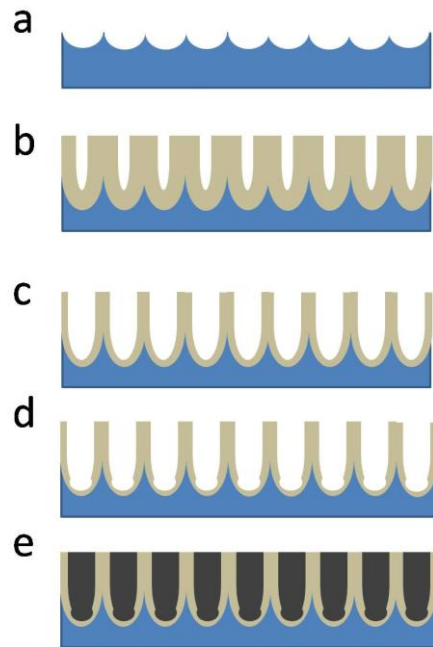


Figure 3.13. The synthesis process of a highly ordered porous alumina template and the preparative steps for the subsequent filling of the nanostructures. a. After long duration first anodization, the first layer of alumina was removed and the patterned hexagonal structures were left on the aluminum substrate. b. highly ordered alumina template structures were obtained after the second anodization step. c. The pore diameter and alumina barrier layer were further thinned by isotropic chemical etching. d. The alumina barrier layer was continually thinned by two current-limited anodization steps and dentrite pore formation occurred on the alumina barrier layer. e. nickel nanowires were deposited in the template pores by pulsed electrodeposition.

When the first anodization process was finished, this layer of alumina template was dissolved and the tips of the original template pores left a well-ordered hexagonal pattern on the surface of underlying unanodized aluminum substrate. This pattern can serve as a

mask for the second anodization process which generates hexagonal pores with uniform diameters and patterned arrangement as shown in Figure 3.13.b. The quality and homogeneity of the subsequent deposition process is improved by further thinning the barrier layer. The thinning of the barrier layer significantly decreases the barrier for the electrons to tunnel through it and the metal was electrochemically deposited at the tip of the pore bottom. The direct result of thinning is to lower the required potential for the filling of the template pores.

The first step for barrier layer thinning is to widen the pores by chemical etching. Oxalic acid was heated to 30 °C to decrease the barrier layer thickness as shown in Figure 3.13.c. Then the template was anodized twice under constant current conditions. The thickness of the barrier layer and applied potential both decreased. Finally, the anodization potential was reduced to 6-7 V which is corresponding to a barrier layer with less than 10 nm thickness. Further thinning of the barrier layer will cause the alumina template to peel off from the underlying aluminum substrate.

Here we will discuss the details of barrier layer removal. If the alumina template is put in phosphoric acid directly the barrier layer cannot be removed without over-etching the top of the alumina template. When the alumina template is immersed in the phosphoric acid directly the acid solution will diffuse into the pores from the top and starts to etch the pore wall. Because there is always a gradient of acid concentration all along the pore channel due to the limitation of diffusion, at the bottom of the template pore which is also the barrier layer part the local acid concentration is relatively lower compared with that on the top. The etching of pore wall is conducted from both sides and the etching rates from the two sides are same. While for the barrier layer side, the etching rates for both

sides are different because of the relative low acid concentration above the barrier layer at the pore bottom. This will result in a faster etching speed for the top compared with that for barrier layer. Figure 3.14 demonstrated the SEM images for the pore widening of an alumina template which is directly immersed in phosphoric acid.

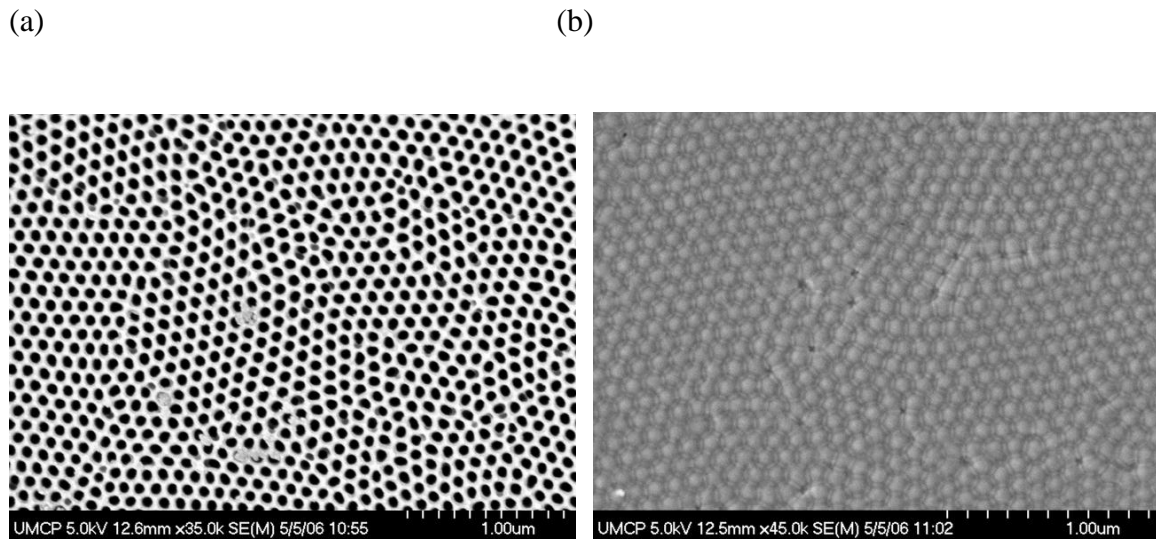


Figure 3.14. SEM images for the pore widening of an alumina template which is directly immersed in phosphoric acid. (a) Top side (b) Barrier layer side. The condition is 5 % phosphoric acid at 30 °C for 90 min etching.

Form Figure 3.14 it can be seen that if there is no protection of the top side of the alumina template, after 90 min etching the top part approaches the limit for pore widening while the barrier layer is still not removed as can be seen in b. Figure 3.14.b shows that the pores remain closed due to the slower etching rate of the barrier layer compared with that for the top part of the template. In order to remove the barrier layer without over-etching the top of the alumina template, the top side should be protected from the attack of

phosphoric acid. The following scheme shows the experiment set-up we used to protect the top side of the alumina template.

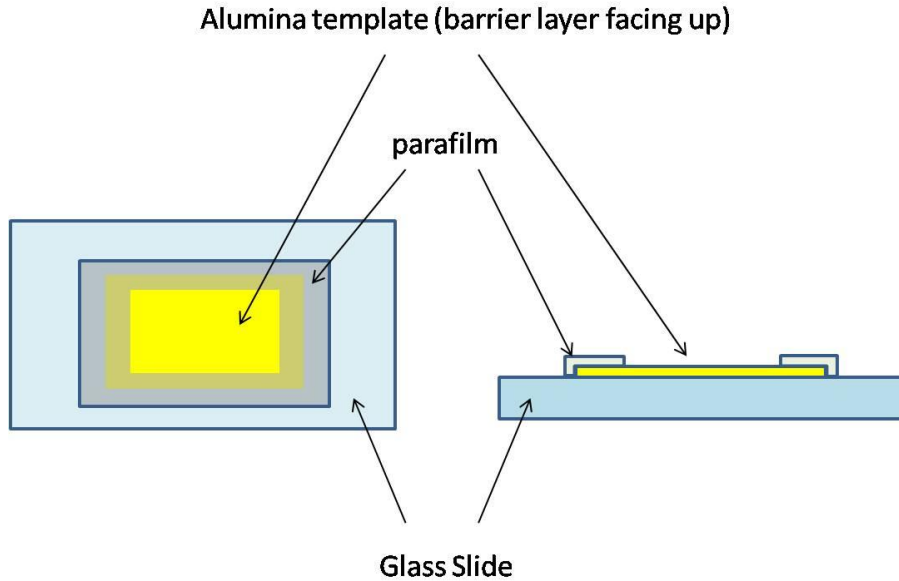
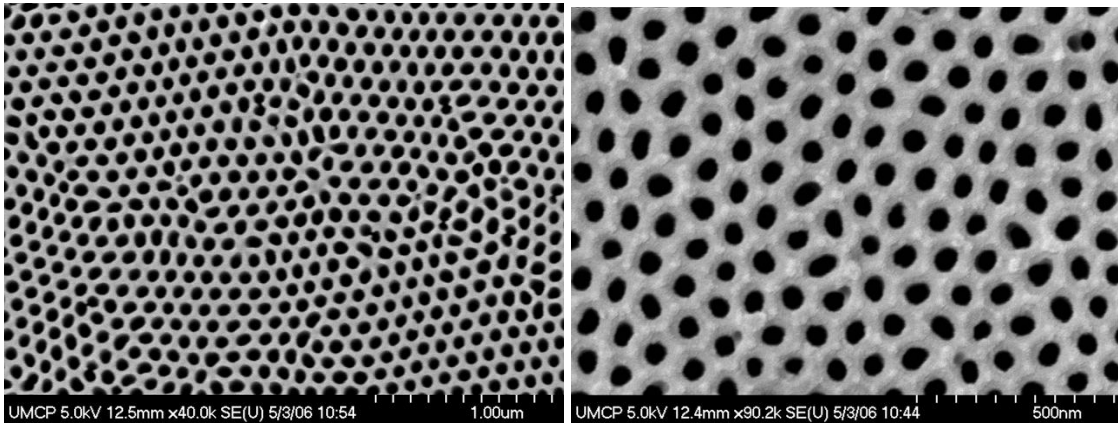


Figure 3.15. Experiment set-up for removal of aluminum oxide barrier layer

It can be seen that with the top side of the alumina template facing down and the sides sealed by parafilm, only the barrier layer will be attacked by phosphoric acid. Experiments showed that the barrier layer started to be open at around 40 min in 5 % phosphoric acid at 30 °C. Once the pore is exposed, acid solution will diffuse into the channels and starts to widen the pores. Figure 3.16 shows SEM images of the barrier layer side and the top side of an alumina template after removal of the barrier layer.

(a)

(b)



(c)

(d)

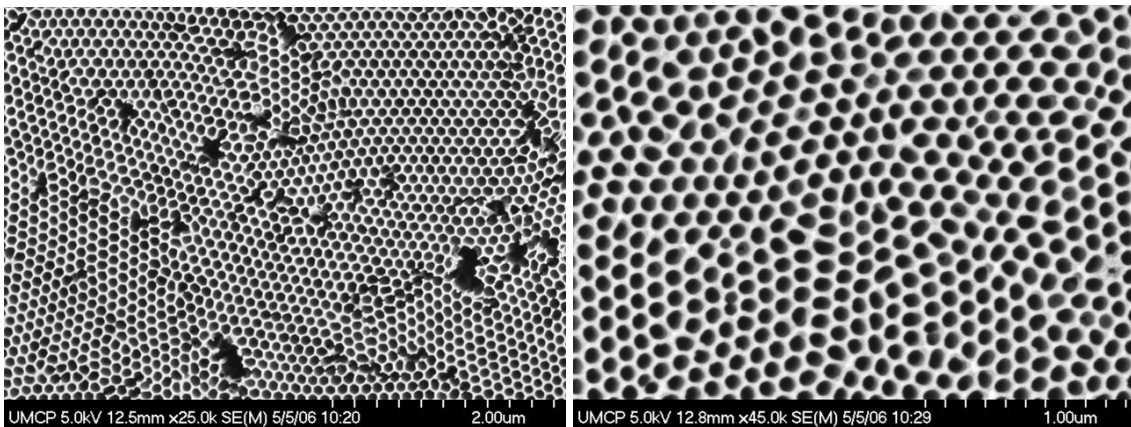


Figure 3.16. SEM images of the barrier layer side and the top side of an alumina template after removal of the barrier layer with top side protection. (a) 85 min etching, barrier layer side (b) 85 min etching, top side (c) 90 min etching, barrier layer side (d) 90 min etching, top side

From Figure 3.16 it can be seen that precise control of etching time is essential for the removal of barrier layer. For 85 min etching, the barrier layer has been removed and the pore diameter at barrier layer side has reached the maximum value of about 90 nm. For the top side of alumina template, the pore size is smaller compared with that of barrier layer side due to the protection of top side as shown in Figure 3.16. a and b respectively. If the etching time is too long, although the top side keeps well-ordered pore structures, the barrier layer side will be over-etched and the patterned pore structures will be damaged. This condition is shown in Figure 3.16.c and d respectively.

3.2.2 Alumina Template synthesis on ITO Glass

Compared with the alumina template which is fabricated by anodizing commercial aluminum foil, anodic alumina template which is synthesized on ITO-covered glass substrate has many advantages such as thin alumina template thickness, good mechanical property and optical transparency.^{113, 115, 117} For home-made alumina templates, a thickness of 50 – 60 μm is required to hold it without breaking. For anodic alumina template fabricated on ITO glass, it is possible to control the thickness of the alumina template to less than 500 nm because of the glass substrate support. The glass substrate provides the anodic alumina template with good mechanical strength. The most important property of anodic alumina templates on glass substrates is optical transparency after anodization. This makes it a candidate for photovoltaic and electrochromic applications.

The anodic alumina template on ITO glass is also fabricated by anodizing aluminum in an acid electrolyte solution. First, indium tin oxide (ITO) coated glass was cleaned by sonication in ethanol for 10 minutes and rinsed thoroughly with de-ionized water. It was then air dried with nitrogen gas and a thin layer of aluminum 500 nm to 1.5 μm is coated on the conductive ITO glass by electron beam evaporation or sputtering. After coating, a mirror-like aluminum layer on the ITO glass can be obtained. In the next step the aluminum coated ITO glass is put into a Thermolyne 79300 tube furnace for annealing at 450 $^{\circ}\text{C}$ in an argon atmosphere for 2.5 hours. Annealing increases the grain size of aluminum coating and provides a homogeneous condition for pore growth. When annealing is complete, the aluminum coated ITO glass is cut into 3.2 cm^2 pieces and put into the anodization jacket. Figure 3.17 shows the images for the Thermolyne 79300 tube furnace and anodization experiment.

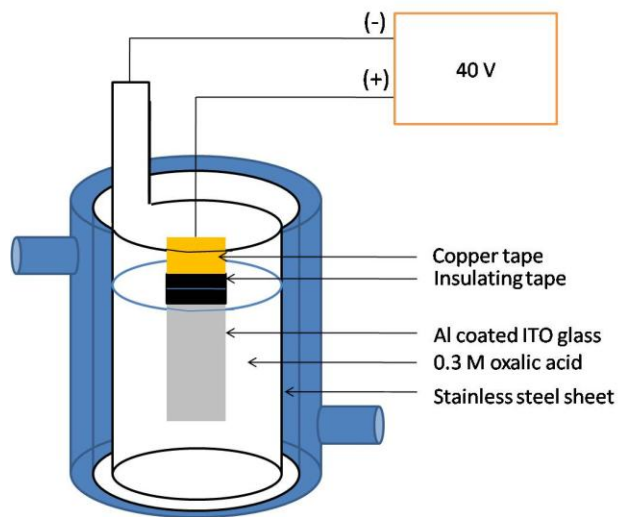


Figure 3.17. Anodization set-up for aluminum coated ITO glass.

The anodization set-up for aluminum coated ITO glass is same to that for the anodization of aluminum foil. At the interface between oxalic acid solution and air the sample is protected by insulating tape. Without the insulating tape the aluminum coating at the solution/air interface will be damaged very quickly by accumulation of high charge density. It should be noted that for the fabrication of anodic alumina template on ITO glass the electropolishing step is omitted and only one anodization process is used because the thickness of the aluminum coating is generally less than 1.5 μm . In an electropolishing solution this thin layer of aluminum would be dissolved immediately.

Due to the thin thickness of aluminum coating on ITO glass it is impossible to conduct first anodization for long duration. Thus only one-step anodization with short duration is carried out for synthesis of this kind of template. The transparency of Al coated ITO glass is used to determine the end of anodization. Before anodization the sample is mirror-like, however when the pores reach the bottom of the Al layer and contact the ITO surface, the whole sample becomes transparent due to the transparency of the ITO film and the porous anodic alumina template. Anodization time is an important parameter. If the anodization is not complete the bottom of pores does not reach the ITO layer and the alumina barrier layer at pore bottom blocks electric conduction, making electrochemical deposition impossible. On the other hand if the anodization time is too long, the ITO film will be anodized eventually resulting in the degradation of the conductivity. Anodization must be stopped immediately once transparency is observed. Figure 3.18 shows the fabrication process for an anodic alumina template on ITO glass.

Fabrication Process

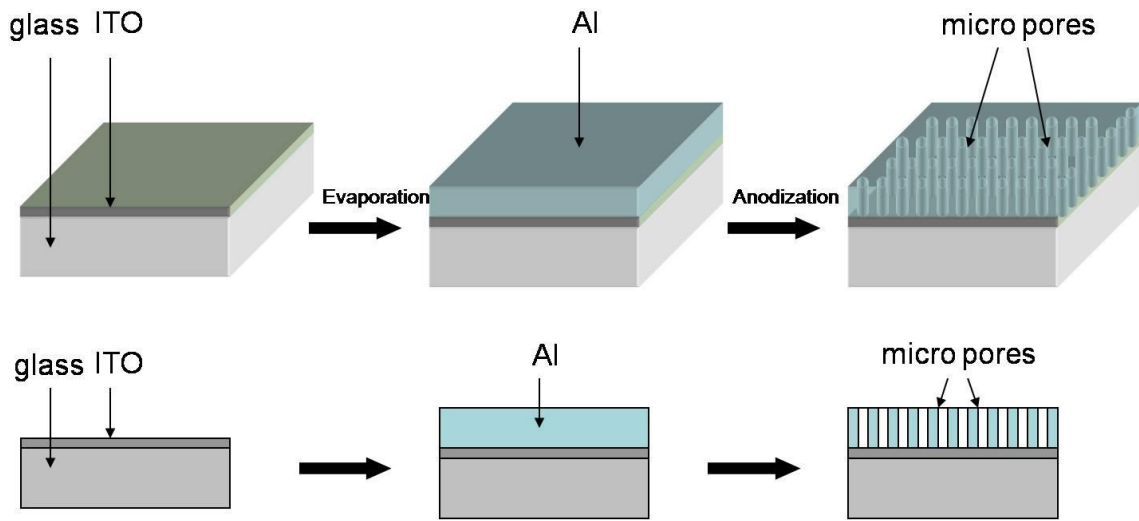


Figure 3.18. Schematic demonstration of the fabrication process for the alumina template on ITO glass.

The pore diameter in the anodic alumina template on ITO glass is about 10 to 20 nm when there is no pore widening. To widen the template pores 0.1 M phosphoric acid is applied for 40 – 50 min at 38 °C. Because of the thin aluminum coating and absence of long duration of first anodization, well-ordered hexagonally patterned pore structures can barely be observed. Figure 3.19 shows SEM images of an anodic alumina template on ITO glass before and after the pore widening.

(a)

(b)

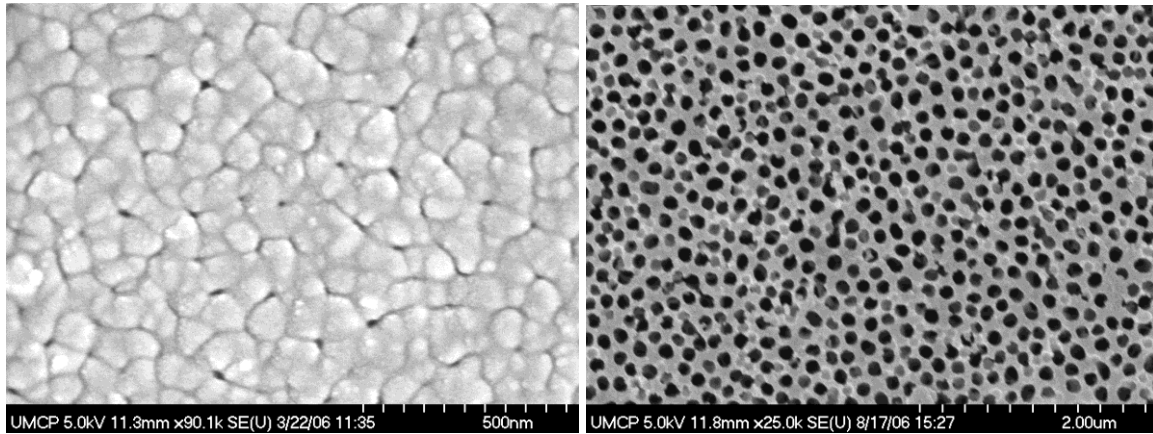


Figure 3.19. SEM images of anodic alumina template on ITO glass before (a) and after (b) pore widening by 0.1 M phosphoric acid at 38 °C for 40 min. The thickness of alumina template is 1.5 μm . Anodization potential is 40 V.

The removal of the aluminum oxide barrier layer is also a big challenge in the fabrication of anodic alumina templates on ITO glass. Due to the limited diffusion of acid solution into the template pores, the local acid concentration at the bottom of pores or top of barrier layer is lower than that at the top part of the channels. Thus the rate at which the template pore diameter increases is faster than the etching rate of the barrier layer. For this reason it is very important to choose a suitable template thickness to remove the barrier layer without over-etching the top part of alumina template. Experiment results showed that if the thickness of aluminum coating is higher than 2 μm , it is impossible to remove the barrier layer without over-etching the top part of the alumina template pore structures. Because the phosphoric acid can only diffuse into the pores from the top, the barrier layer can only be attacked from the top. If the template is too thick the local acid concentration at the template pore bottom will be lower than that on the top. This will

result in a slower etching rate for the barrier layer. Experiments showed that the ideal template thickness is around 1.5 μm . On the other hand, if the template is too thin the pore structure will be poor due to short duration of anodization. Figure 3.20 shows the anodic alumina templates under different pore widening conditions.

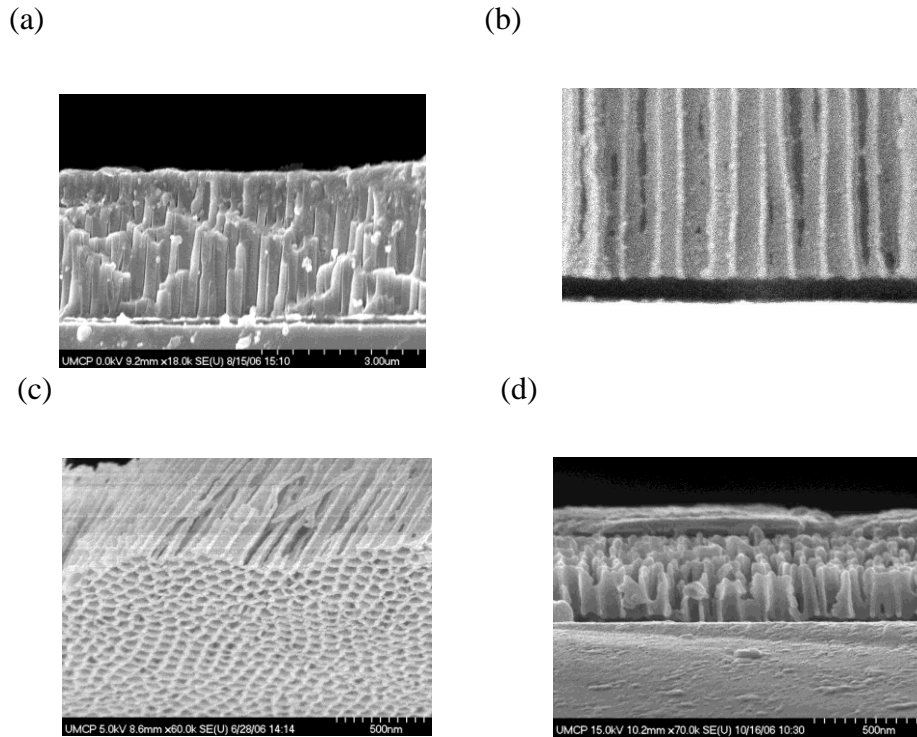


Figure 3.20. SEM images for anodic alumina templates on ITO glass under different pore widening conditions. (a) 2 μm alumina template after anodization, no pore widening. (b) cross sectional view for the bottom part of a 1.5 μm thick alumina template, after 40 min pore widening in 0.1 M phosphoric acid at 38 $^{\circ}\text{C}$. (c) perspective view for the bottom of the alumina template in (b) after the alumina template has been removed from the ITO glass substrate. (d) 500 nm thick alumina template after 32 min pore widening in 0.1 M phosphoric acid at 38 $^{\circ}\text{C}$.

From Figure 3.20.a it can be seen that anodization produced many vertical channels along the whole alumina template. Without anodization the diameter of the pores is as small as 10 nm. Figure 3.20.b shows the bottom part of an anodic alumina template on ITO glass for which the barrier layer has been removed. It is apparent that the bottom ends of these channels are open. This makes electrochemical deposition of various nanomaterials in the template pores possible. It should be noted that there is a gap between the template pore bottom and the ITO glass substrate as shown in Figure 3.20.b. This gap is produced by local pressure which originates from the generation of oxygen from the electrolyte solution in the anodization process. Figure 3.20.c shows the bottom view of an anodic alumina template with barrier layer removed. It can be seen that when the pore widening time is well controlled, the barrier layer can be removed without over-etching the template pore wall. Figure 3.20.d shows an anodic alumina template of 500 nm thickness. Due to the thinness of the template, well-ordered pore structure is hard to produce.

The diameter of the template pores is proportional to the applied anodization potential. This conclusion is also applicable to the anodization of aluminum coating on ITO glass. In order to study the dependence of pore diameter upon applied potential, we increased the anodization voltage from 40 V to 80 V. At this high potential, in 0.3 M oxalic acid the aluminum coating on ITO glass was quickly dissolved and a large amount of heat was generated. This is due to the high electric field on the anode: aluminum coating. To solve this problem, we reduced the concentration of oxalic acid and temperature until the reaction became stable. It is found that 0.04 M oxalic at 3 °C is a satisfactory anodization condition. When the anodization was complete, 0.1M phosphoric acid at 38 °C was applied to widen the pores and remove the barrier layer. We found that the ideal pore

widening time for alumina template anodized at 80 V is different from that for alumina template anodized at 40 V. For the latter, the maximum pore widening time is 40 min while for alumina template anodized at 80 V it can be as long as 58 min. The reason is according to bigger inter-pore distance due to high anodization potential. Figure 3.21 shows SEM images for anodic alumina templates anodized at 80 V under different pore widening conditions.

From Figure 3.21 it can be seen that pore diameter increases with pore widening time and reaches a maximum value (100 nm) in 58 min. Figure 3.19.d shows the cross sectional view of this alumina template. It can be seen that the barrier layer was removed and is ready for the electrochemical deposition of various nanomaterials.

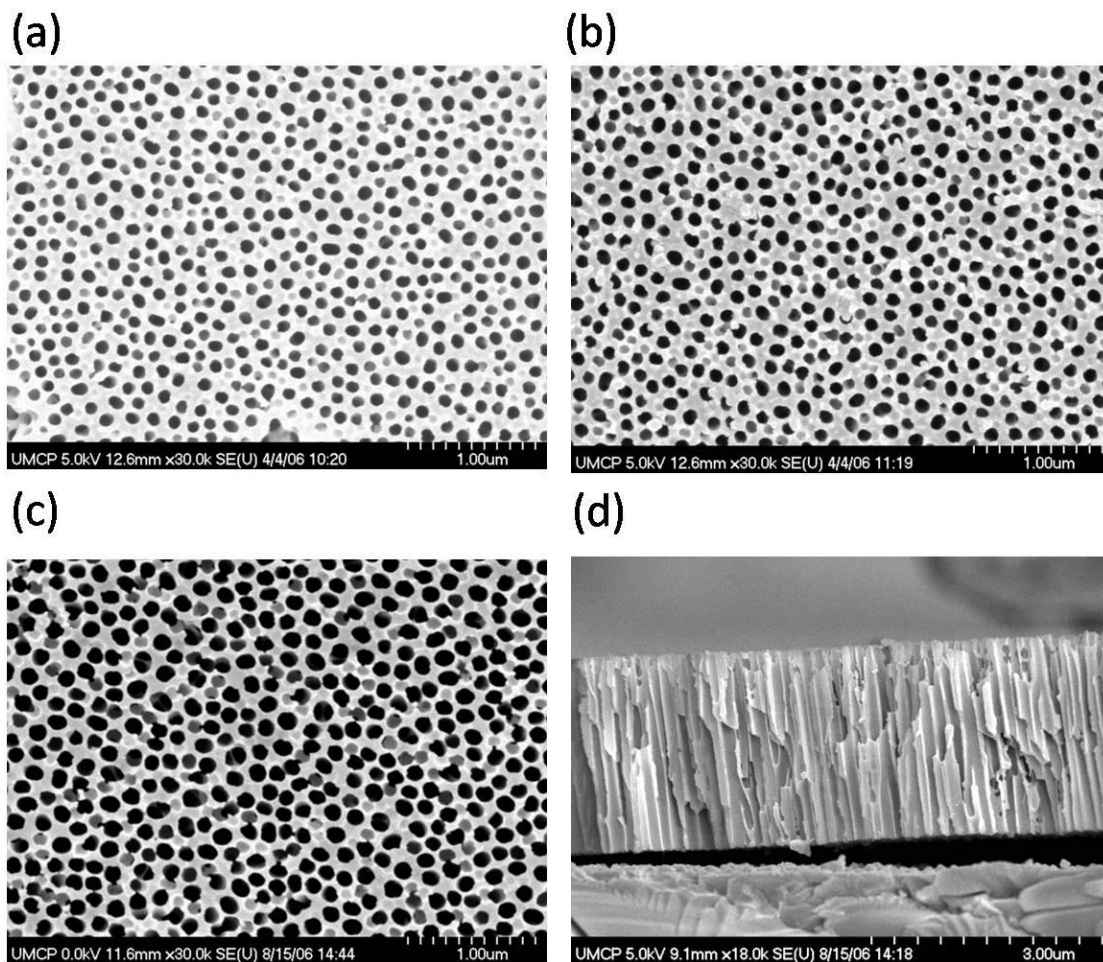


Figure 3.21. Anodic alumina template which is anodized at 80 V under different pore widening conditions. (a), (b), (c) are for 52, 56 and 58 min pore widening in 0.1 M phosphoric acid at 38 °C respectively. (d) Cross sectional view for alumina template in (c)

3.3 The Sample Preparation

Various nanomaterials have been synthesized with commercially available alumina templates that can be purchased from Whatman (Clifton, NJ) with a pore diameter of 200

nm and thickness of 60 μm . For electrochemical deposition, one side of the alumina membrane was coated with a thin layer of gold (ca. 300 nm thick) as a working electrode by using an ATC 1800 3-target S-gun sputtering system (AJA international, North Scituate, MA). After gold sputtering, the sample was clamped between two pieces of parafilm and mounted on a glass slide. The gold coated side contacts a copper tape which is connected to the working electrode of a potentiostat. The whole sample was then put into an acetonitrile solution for electrochemical deposition of various conductive polymer nanomaterials such as PEDOT, polypyrrole or P3HT.

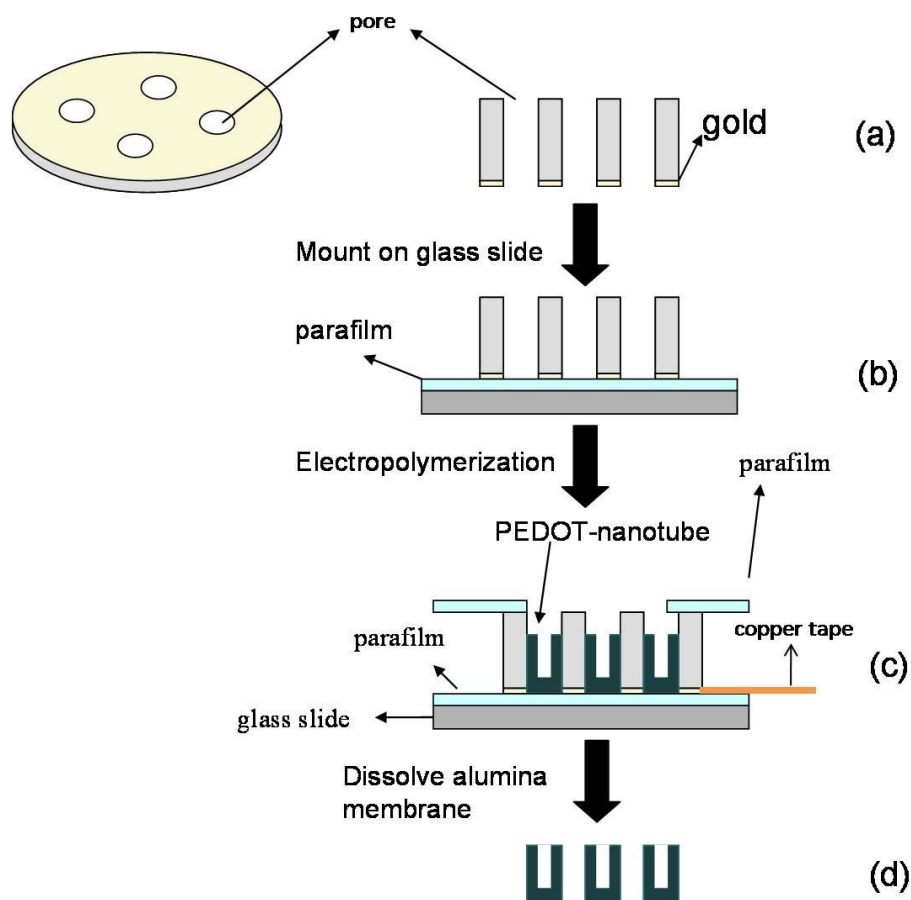


Figure 3.22. Schematic demonstration of sample preparation. (a) gold sputtering (b) mount on glass side (c) electrochemical deposition (d) removal of alumina template

PEDOT grows along the alumina template pore walls and resulted in the formation of nanotubes. PEDOT, polypyrrole, and P3HT nanostructures were investigated using a field-emission scanning electron microscope (SEM; Hitachi S-4700, operated at an acceleration voltage of 5 keV) and a transmission electron microscope (TEM; Zeiss EM10CA, operated at 80 keV). The sampling methods for SEM and TEM analysis were described in detail previously.¹⁴ Briefly, the gold-coated side of a small piece of alumina template was tightly attached onto a SEM specimen holder with a carbon tape. The template was dissolved to expose the nanomaterials by using phosphoric acid (25 wt%). The sample was rinsed with de-ionized water (ca. 18 M Ω /cm resistivity) obtained by using a Milli-Q water purification system (Millipore, Dubuque, IA). The sample was dried in air before observation. For TEM sampling, the gold layer was removed by using an aqua regia solution after growing desired nanostructures in a gold coated alumina template. The alumina template was dissolved by using phosphoric acid (25 wt%). The released nanomaterials were repeatedly rinsed with de-ionized water and ethanol. 6 μ L of the nanomaterial solution was deposited and dried on a TEM grid.

3.4 The Equipment Hardware

The electrochemical deposition was conducted in a three electrode cell which is connected to a potentiostat (660A CH Instruments, Austin, TX). A U-tube was used as a container for the cell. The gold coating on the alumina template was connected to the working electrode of the potentiostat. A platinum plate was folded and put into the cell as a counter electrode. The reference electrode used is a Ag/AgCl electrode. Figure 3.23 demonstrated the set-up for the three electrode cell.

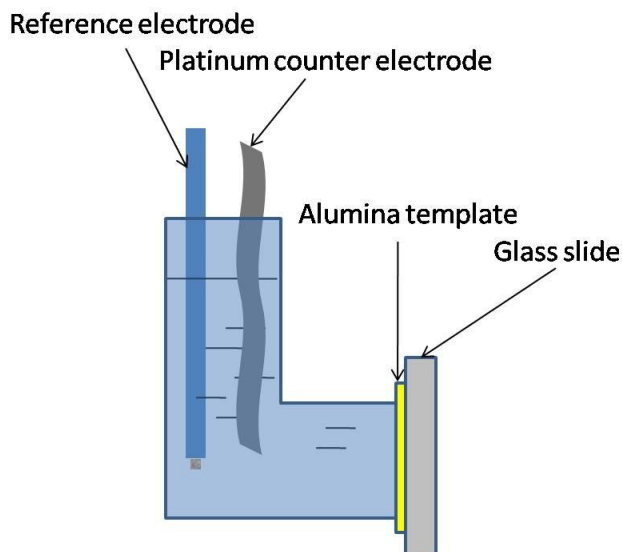


Figure 3.23. Schematic demonstration of three electrode cell.

CHI 660A is a computerized electrochemical instrument. The system contains a fast digital function generator, high speed data acquisition circuitry, a potentiostat and a galvanostat. The potential control range is ± 10 V and the current range is ± 250 mA. The instrument is capable of measuring current down to picoamperes. The instrument can automatically re-zero both potential and current to compensate for drift due to temperature and time. The instrument is controlled by an external PC under Windows environment. It also provides file handling, graphics, data analyses, and digital simulation. The next section will discuss the software for CHI 600A.

3.5 The Software

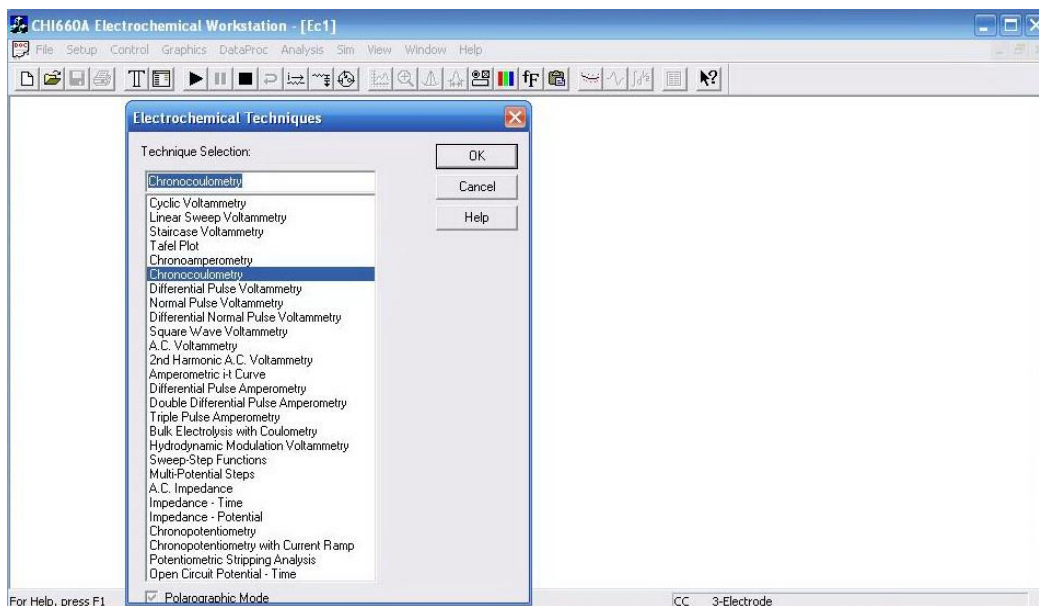


Figure 3.24. Schematic demonstration of the software for CHI 660A

Figure 3.24 shows the user interface of the software used for CHI 660A. In electrochemical techniques window there are many techniques can be chosen such as cyclic voltammetry, chronoamperometry, chronocoulometry, liner sweep voltammetry, etc. For our electrochemical deposition experiment, chronocoulometry was applied as a main method for the synthesis of conductive polymer nanostructures.

3.6 Summary

In this chapter we discussed the detailed fabrication processes for alumina template. Two types of alumina template have been introduced. The first one is synthesized by anodizing commercial aluminum foil. The second one is fabricated by anodizing

evaporated aluminum coating on ITO glass. Both of them are sharing many similarities in morphologies. But they have different applications due to differences in structure. The experiment set-ups, electrochemical experiment hardware and software were also discussed.

Chapter 4: Conductive Polymer Nanotube Synthesis Mechanism

This chapter has been reproduced in part with permission from: Xiao, R.; Cho, S. I.; Liu, R.; Lee, S. B., *Controlled electrochemical synthesis of conductive polymer nanotube structures*. Journal of the American Chemical Society 2007, 129, (14), 4483-4489.

4.1 Introduction

By using poly(3,4-ethylenedioxythiophene) (PEDOT) as a model compound, we have investigated the electrochemical synthetic mechanisms for synthesizing conductive polymer nanotubular structures in a porous alumina template. Three parameters—applied electropolymerization potential, monomer concentration, and base electrode shape at bottom of the template pore—were varied to obtain an electrochemical growth pattern of PEDOT nanostructures. This growth pattern which will be discussed later was understood when it was considered in two overpotential regions: low oxidation-potential region (< 1.4 V vs. Ag/AgCl) and high oxidation-potential region (> 1.4 V). The base electrode shape at the pore bottom of a template is a crucial factor for the electrochemical growth of nanotubes in the low oxidation-potential region. Monomer concentration (concentration-gradient diffusional flux in pores) and applied potential (electrochemical reaction rate) are essential in determining nanostructures in the high oxidation-potential region compared with the base electrode shape. Based on the above mechanisms, we can construct a strategy for synthesizing PEDOT nanotubes in the template pores. These mechanisms were further employed to control the nanotube dimensions of other conductive polymers such as polypyrrole and poly(3-hexylthiophene). In the electrochemical study of dimension-controlled PEDOT nanotubes, thinner wall nanotubes showed faster redox rate that is important for the development of high-performance batteries and supercapacitors compared with film structure.

Conductive polymers are indispensable materials for the development of organic electronic devices, such as electrochemical power sources,^{118, 119} flexible electronic devices,^{17, 120} and displays.^{92, 121-123} In such electronic devices poor charge-transport rate due to slow diffusion of counter-ions into/out-of the conductive polymer film during redox processes is a limitation.^{14, 15} Nanotubular conductive polymers have improved charge transport rates as well as large surface areas. Recently we have pioneered the electrochemical synthesis of poly(3,4-ethylenedioxythiophene) (PEDOT) nanotubes and used them in the development of fast electrochromic devices (< 10 ms in electrochromic color-change speed).¹⁴ The thin-walled nanotubular structure enables ions to easily diffuse into/out-of the conductive polymer, resulting in a fast color switching rate. However, detailed mechanism studies of the electrochemical synthesis of conductive polymer nanotubes^{124, 125} are very limited, despite the importance of conductive polymer nanotubes in various electronic devices.

The synthesis of conductive polymer nanotubes has been performed chemically and electrochemically with various templates.^{126, 127} Martin and coworkers pioneered the synthesis of conductive polymer nanotubes and nanofibers such as polypyrroles, polythiophenes, and polyanilines in the pores of a polycarbonate and alumina membranes.⁷¹ The Wan group introduced surfactants as templates as well as dopants to synthesize polyaniline and polypyrrole nanotubes.^{79, 80} Nanofibers of biodegradable polymers can be an alternative choice as a template: the conductive polymer is electrodeposited on the surface of electrospun nanofibers, which are removed to generate hollow conductive-polymer nanotubes.¹²⁸ In these studies, the growth of nanotubes on a template can be explained by a mechanism proposed by Martin's group based on an

interaction between the conductive polymer and the template.⁷¹ When considering this mechanism, it is difficult to explain the growth of partially-filled nanotubes that are frequently observed in electrochemical template synthesis.^{14, 15} In our previous papers,^{14, 15} we have given qualitative explanations for the formation of the partially-filled PEDOT nanotubes by identifying three deterministic experimental parameters: monomer concentration (concentration-gradient diffusional flux in pores), applied potential (electrochemical reaction rate), and base electrode shape.^{14, 15}

Here, we describe the detailed electrochemical synthetic mechanisms and structural characterizations of various conductive polymer nanotubes in a porous alumina membrane. As a function of monomer concentration and potential, electropolymerization leads either to solid nanowires or nanotubes and it is the purpose of these investigations to uncover the detailed mechanism underlying the morphological transition between nanowire and nanotube. By using PEDOT as a model compound, we have systematically investigated the effects of various experimental parameters—potential, monomer concentration, base electrode shape, electrolyte concentration, and temperature—on the nanotubular structures in the pores of the template. This mechanism was applied to the synthesis of PEDOT nanotubes in the template with smaller pore diameter and other conductive-polymer nanotubes such as polypyrrole and poly(3-hexylthiophene) (P3HT).

4.2 Practical Procedures for Conductive Polymer Electropolymerization

4.2.1 PEDOT Electropolymerization Synthesis

Electropolymerization of EDOT was performed potentiostatically at various potentials from 1.0 to 1.8 V versus Ag/AgCl reference electrode by using Pt foil (99.9 %, Alfa

Aesar, Ward Hill, MA) as a counter electrode in various concentrations of EDOT from 10 to 500 mM in acetonitrile. The experiment set-up was shown in Figure 3.19. Electrolyte solution was 0.1 M LiClO₄ in an acetonitrile solution, and reaction temperature was 25 °C, if not specified otherwise. In order to focus on the influence of monomer concentration and applied potential on PEDOT nanostructure synthesis mechanism, the electropolymerization time is fixed at 100 s.

4.2.2 Polypyrrole Electropolymerization

Polypyrrole was also synthesized potentiostatically in an aqueous solution. The choice of solvent and electrolyte is very important in the electrochemical synthesis of conductive polymers. At the oxidation potential of monomer, the solvent and electrolyte must both be very stable and provide a conductive medium for the electrochemical polymerization. For the electrochemical polymerization of pyrrole, the reaction can be conducted in an aqueous solution due to the relatively low oxidation potential of pyrrole. Because of the low solubility of pyrrole in water, sodium dodecyl sulfate (SDS) is applied to increase the solubility of pyrrole. The electrolyte is 0.1 M LiClO₄. The electrochemical polymerization is conducted at 0.7, 0.9, 1, 1.2, 1.4, 1.6 and 1.8 V for 10, 25, 50 and 100 mM pyrrole respectively. The electropolymerization time is fixed at 100 s.

4.2.3 Poly(3-hexylthiophene) (P3HT) Electropolymerization

Because the oxidation potential of 3HT is higher than that of EDOT, relatively high potentials are applied for the electropolymerization of 3HT. The electrochemical polymerization of P3HT is conducted in an acetonitrile solution for 100 mM 3HT from

1.5 to 2.0 V versus Ag/AgCl reference electrode. When the applied potential is higher than 2.0 V, the gold coating which serves as working electrode will be dissolved.

4.3 Characterization of PEDOT Nanostructures

4.3.1 Morphology of PEDOT Nanostructures

It is necessary to observe and understand the nanostructure of conductive polymer nanotubes in order to investigate their growth mechanism. The SEM images of conductive polymer nanotubes are quite different from those of metallic nanotubes because conductive polymers are not so rigid as metal. It is important to characterize three different nanostructures of conductive polymer nanotubes (nanowire, partially-filled nanotube, and complete nanotube) by using SEM and TEM. Here, we have chosen PEDOT as a model compound because of its well-known electropolymerization chemistry and electrochemical properties.^{14, 15, 129} Figure 4.1.a shows the SEM images of PEDOT nanowires which were grown in 50 mM EDOT at 1.6 V for 100 s. Due to strong surface tension at the interface between the nanowires and the solvent, PEDOT nanowires aggregated during solvent evaporation. This phenomenon has also been observed in metallic nanostructures. PEDOT nanowires have cylindrical shapes with open-ended tips. This shape indicates that tubular section may exist in the nanostructure. The TEM image (Figure 1b) revealed that the top 10 % of the nanostructure is a hollow tube.

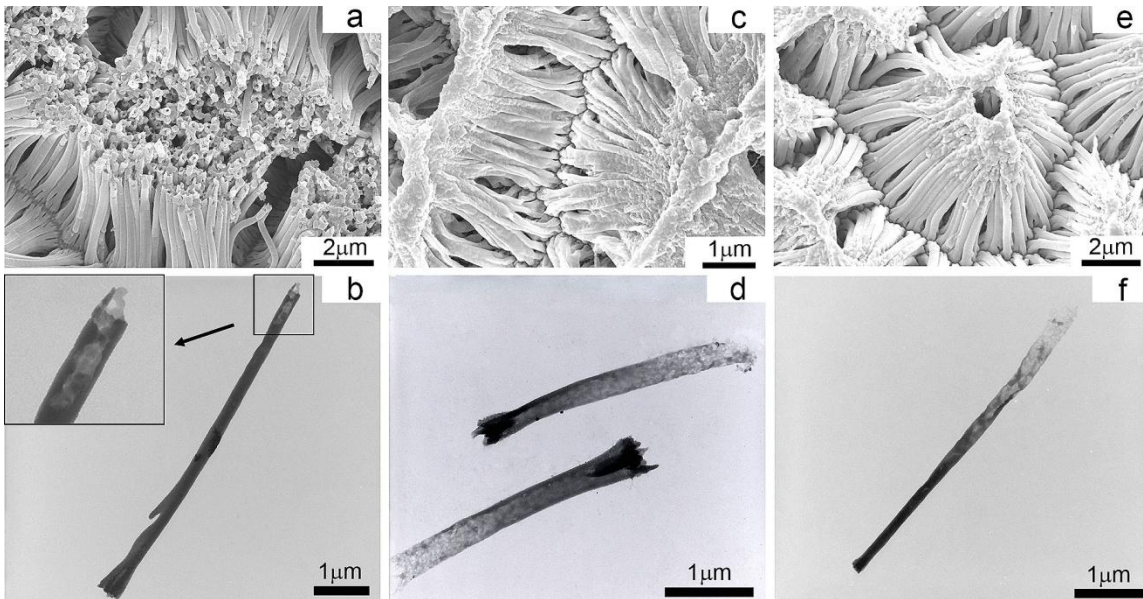


Figure 4.1. SEM and TEM images of PEDOT nanostructures synthesized potentiostatically (a,b) in 50 mM EDOT at 1.6 V, (c,d) in 50 mM EDOT at 1.2 V, and (e,f) in 25 mM EDOT at 1.5 V for 100 s. The upper (a, c, and e) and lower (b, d, and f) images were taken by SEM and TEM, respectively.

Figure 4.1.c shows the SEM image of completely hollow nanotubes which were grown in 50 mM EDOT at 1.2 V for 100 s. Unlike metallic nanotubes, no open tip structures in the SEM image of PEDOT nanotubes are observed. Instead, the top of the PEDOT nanotubes are highly-aggregated. The bottom of the nanotubes has wrinkled and collapsed structures rather than smooth cylindrical structures. This implies that the nanostructures are hollow from the bottom, and the walls of nanotubes are too thin to maintain the upright structure. While the wrinkled and collapsed structure in the SEM image can be a useful indicator for the formation of tubular structures, TEM studies are essential to observe the hollow structure of the nanotubes. The TEM image in Figure 4.1.d strongly supports that PEDOT nanostructures are completely hollow tubes with very thin walls (less than 10 nm). The outer diameter of the nanotubes (ca. 300 nm) is much larger than the pore diameter of the

alumina template (ca. 200 nm). This indicates that the cylindrical structure of the individual nanotube became flat during the TEM sampling process due to surface tension on the thin cylindrical wall.

The SEM image of partially-filled nanotubes can be considered as a combination of a nanotube and a nanowire. Figure 4.1.e shows the SEM image of partially-filled PEDOT nanotubes grown in 25 mM EDOT at 1.5 V for 100 s. As expected, the bottom of the nanostructures resembles a nanowire while its top resembles a nanotube. The TEM image (Figure 4.1.f) demonstrates that 40 % of the nanostructure is a nanowire. It also shows that the outer diameter of the tubular section increases toward the top of the nanotube because its tubular wall is very thin and can collapse easily.

It will be interesting to study further the morphologies of PEDOT nanostructures synthesized in aqueous solution. Sodium dodecyl sulfate (SDS) is applied to increase the solubility of EDOT in water because co-surfactants like (SDS) can stabilize charged species such as anionic or cationic radicals. SDS has the advantage of increasing the solubility of the thiophene derivative in water, lowering its oxidation potential and increasing the polymerization current. Electropolymerization of EDOT in aqueous solution with SDS showed that the start oxidation potential of EDOT has been lowered to about 0.8 V. Figure 4.2 shows the SEM images for PEDOT nanostructures synthesized in aqueous solution.

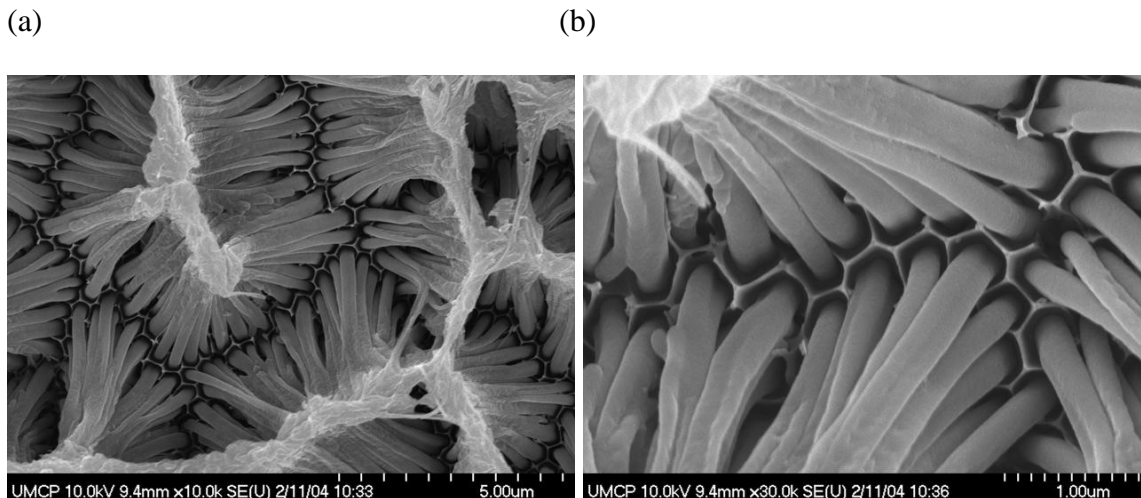


Figure 4.2. SEM images for PEDOT nanostructures synthesized in aqueous solution. Electropolymerization condition: 50 mM EDOT at 0.8 V for 100 s in water with 0.07 M SDS and 0.1 M LiClO₄.

From Figure 4.2.a it can be seen that the PEDOT nanostructures collapsed and stuck to each other. The reason is same as that for PEDOT nanotubular structures synthesized in an acetonitrile solution. Due to the high surface tension between the PEDOT thin wall and the solvent, the nanotubes of PEDOT tend to be pushed together and collapse. Figure 4.2.b shows the magnified SEM image for a. It can be seen that the PEDOT nanotubes protrude from the hexagonally patterned alumina template.

4.3.2 Control of Nanotube Length

We analyzed the dependence of nanotube length on monomer concentration and applied potential. The nanotube length was rarely affected by the monomer concentration as shown in Figure 4.3. When the monomer concentration was increased at a fixed potential, the nanotube lengths barely changed. Instead, this increase of monomer concentration

resulted in thickening of the nanotube wall. On the other hand, the nanotube length increased with the increase of applied potential. For example, the lengths of nanotubes synthesized in 50 mM EDOT and 0.1 M LiClO₄ at 1.2, 1.4, 1.6, and 1.8 V were ca. 3.4±0.2, 5.3±0.2, 7.5±0.2, and 9.3±0.3 μm, respectively (Figure 4.3). Thus, the applied potential may be a good parameter for controlling the nanotube length. Electropolymerization time is another way to adjust the nanotube length; doubling polymerization time (within the range of 200 s) increases the nanotube length by a factor of two.

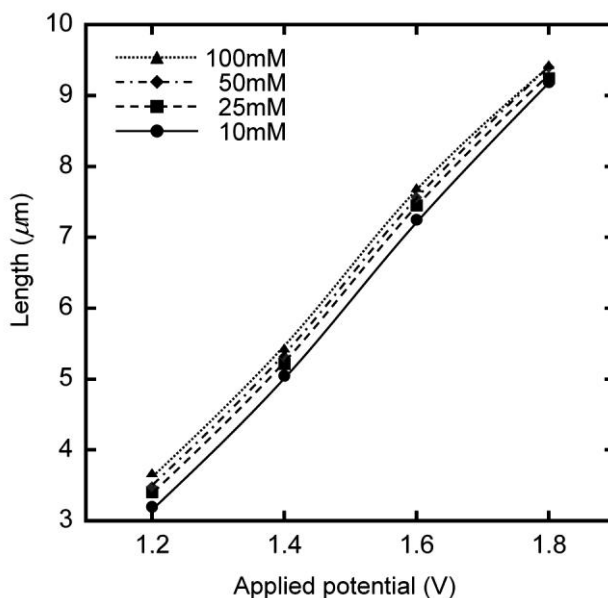


Figure 4.3. Dependence of PEDOT nanotube length on applied potential and monomer concentration at fixed 100 s polymerization time.

From Figure 4.3 it is apparent that the dependence of PEDOT nanotube length on the applied potential is almost linear. Table 4.1 shows the detailed nanotube length of each data point in Figure 4.3. The unit for nanotube length is nm. In Table 4.1, each data entry

is based on the length average of more than three PEDOT nanotubes at the same synthesis condition (same monomer concentration and applied potential).

Table 4.1 Dependence of PEDOT nanotube length on the applied potential and monomer concentration.

Concentration(mM)	10	25	50	100
potential (v)				
1.2	3.2	3.4	3.5	3.7
1.4	5.1	5.2	5.3	5.4
1.6	7.3	7.5	7.6	7.7
1.8	9.2	9.3	9.4	9.4

Note: The unit for PEDOT nanotube length is nm

4.3.3 Rigidity of PEDOT Nanotubes

In order to control the rigidity of nanotubes, we compared PEDOT nanostructures synthesized at potentials of 1.2 and 1.8 V. The low monomer concentration, 10 mM EDOT, was chosen in order to synthesize nanotubes with very thin walls (< 10 nm in thickness). Under these conditions, there is a large difference in the rigidity of nanotubes. As shown in Figure 4.4, PEDOT nanotubes synthesized at 1.2 V have a smooth, dense wall surface, while ones synthesized at 1.8 V have a rough, porous wall surface. This phenomenon is due to the fact that the diffusional monomer supply is sufficient to form

rigid wall during the polymerization reaction at the low oxidation overpotential. At low oxidation potential, the electropolymerization reaction rate is low and the growth rate of PEDOT nanotube along the template pore wall is also relatively slow. Thicker polymer nanotubes will be obtained when there is a sufficient supply of monomers from diffusion. At the high overpotential, the supply of monomer cannot meet the requirement of polymer tube growing rate which results in the formation of long and porous polymer nanotubes with thin walls.

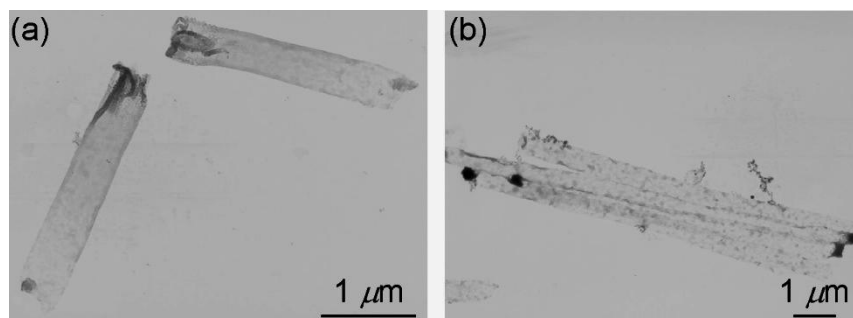


Figure 4.4. TEM images of PEDOT nanotubes synthesized at (a) 1.2 V and (b) 1.8 V for 100 s in 10 mM EDOT and 0.1 M LiClO₄.

4.4 Effects of applied potential and monomer concentration

4.4.1 General Concern

We have studied the synthesis of conductive polymer nanostructures using the electrochemical template method. We further proposed a mechanism which is widely applicable in controlling the morphologies and dimensions of one-dimensional conductive polymer nanostructures.

The growth rate and rigidity of nanostructures in electrochemical template synthesis are determined by the applied reaction potential and monomer concentration. We have proposed a growth mechanism for PEDOT nanotubes, which considers the effects of potential and concentration on nanostructures in two extreme cases (Figure 4.5).^{14, 15} One is the case for slow reaction rate and sufficient monomer supply. Nanowires formed in this condition results in the synthesis of polymer from the bottom of template pores. At the same time, due to the high monomer diffusion flux rate, monomers in bulk solution have sufficient time to diffuse into and fill the pores. The condition corresponding to this case is high monomer concentration and low applied voltage. The other extreme case is fast reaction rate and insufficient monomer supply. This results in the formation of nanotubes since fast electropolymerization generates polymer along the pore wall preferentially because of the interaction between polymer and wall surface, while at the same time the supply of monomers is limited due to the low monomer diffusion flux rate. The condition corresponding to this case is low monomer concentration and high applied voltage.

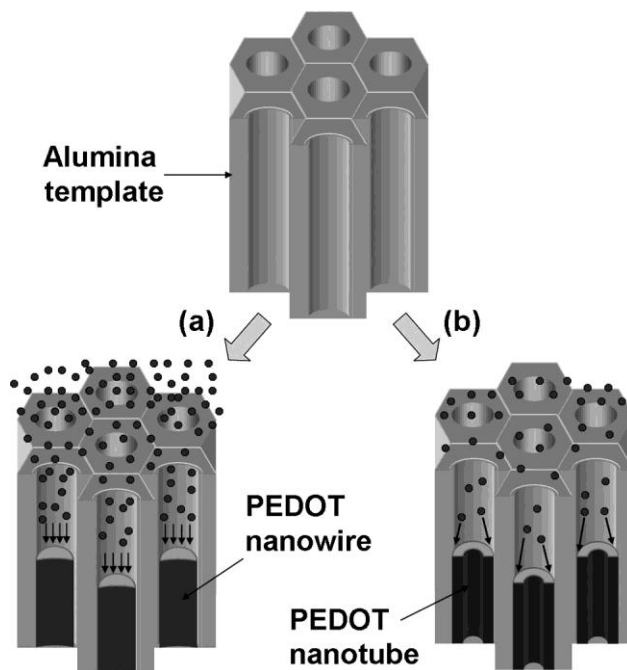


Figure 4.5. Growth mechanism of PEDOT nanostructures based on diffusion and reaction kinetics. The lower schemes represent the electropolymerization of EDOT (a) for slow reaction rate and sufficient monomer supply and (b) for fast reaction rate and insufficient monomer supply. The small black balls represent EDOT monomers.

On the basis of this mechanism, we can synthesize various PEDOT nanostructures in the pores of the alumina membrane with sputtered Au layer on one side. Tubular portion of the nanotube structure increased as we increased the applied potential from 1.4 to 1.8 V in a fixed concentration of 25 mM EDOT (Figure 4.6 a–c), while the tubular portion decreased as the monomer concentration was increased from 10 to 100 mM at a fixed potential of 1.6 V (data not shown here).

The above observation of the PEDOT nanotubular structures are consistent with the mechanism illustrated in Figure 4.5. At a fixed monomer concentration such as 25 mM,

the monomer diffusion flux rate is also fixed. When the applied potential increased from 1.4 to 1.8 V the electropolymerization reaction rate increased favoring the formation of PEDOT nanotubes along the template pore wall. On the other hand, at a fixed potential of 1.6 V the electropolymerization reaction rate is fixed. When the monomer concentration increased from 10 to 100 mM the monomer diffusion flux rate increased simultaneously. This resulted in the formation of nanowire structures with lower tubular ratios.

When we lowered the applied potential from 1.4 to 1.2 V (50 mM EDOT) expecting to have more solid nanowires, we observed a very interesting phenomenon (Figure 4.6.d–f). The tubular portion in the nanotube increased again. Further experiments showed that no matter what monomer concentration is used; well-defined PEDOT nanotubular structures will be obtained at low applied potentials like 1.2 V. This phenomenon cannot be explained with the current mechanism.

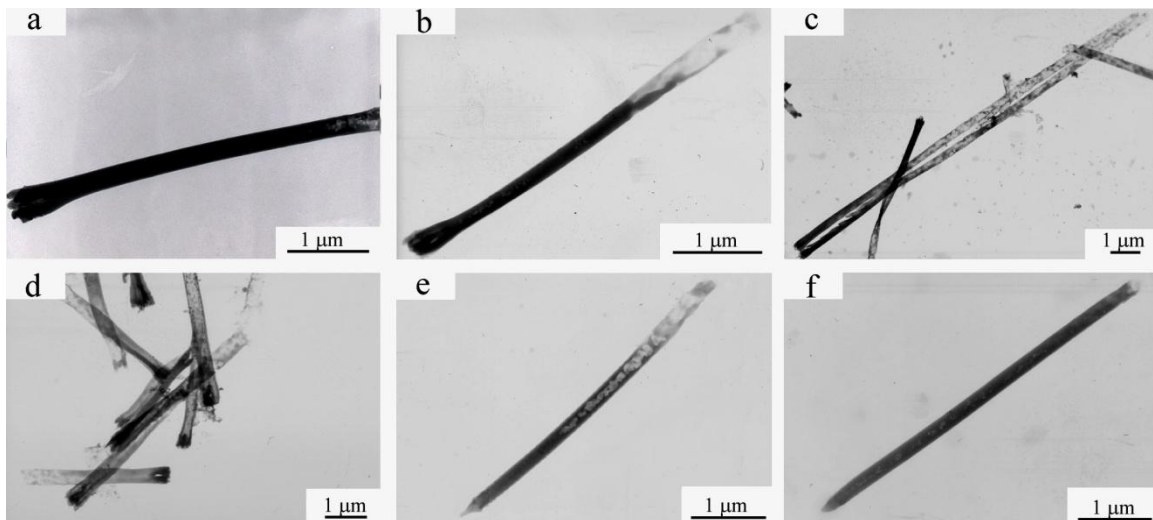


Figure 4.6. TEM images of PEDOT nanostructures in various conditions at a fixed electropolymerization time of 100 s: (a) 1.4 V, (b) 1.5 V, and (c) 1.8 V in 25 mM EDOT; (d) 1.2 V, (e) 1.3 V, and (f) 1.4 V in 50 mM EDOT.

4.4.2 Synthesis Mechanism above 1.4 V

The applied potential and monomer concentrations were varied systematically while fixing the electropolymerization time at 100 s. The resulting nanostructures were analyzed by using SEM and TEM and are summarized in Figure 4.7 by plotting the tubular ratio, R , versus applied potential. R is defined as the length of tubular section divided by total length. R is one for a complete nanotube and zero for a solid nanowire. The fixed reaction time of 100s gives a proper experimental condition that enables us to observe the electrochemical growth of PEDOT nanostructures from complete nanotube to nanowire shapes. For sufficient reaction times, all PEDOT nanostructures become partially-filled nanotubes and eventually solid nanowires.

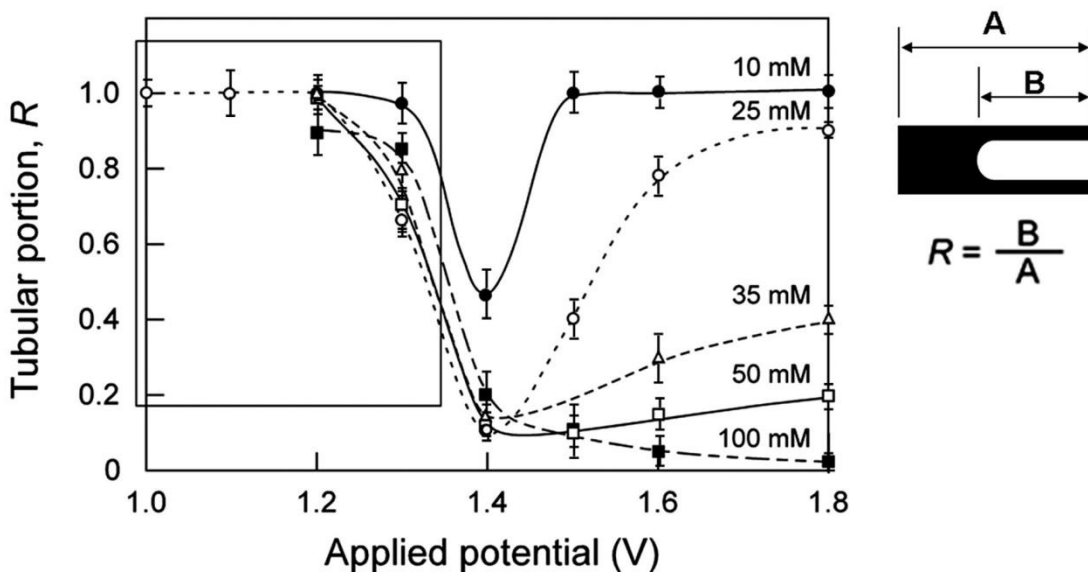


Figure 4.7. Plots of tubular portion for PEDOT nanotubes vs. applied potential. Electrochemical polymerization was performed potentiostatically with a fixed polymerization time of 100 s. The tubular portion, R , is defined as the length of the

tubular section divided by the total length. The data were obtained from TEM images. The lines were added to help guide the eye.

At first glance, the potential dependence of PEDOT nanostructures looks complicated. Dividing the curve into two regions from 1.4 V may be helpful in understanding the potential dependence of the nanostructures. The tubular portion increases along with the applied potential at potentials higher than 1.4 V. This region can be well explained by the mechanism based on the diffusion-limited reaction.¹⁴ At low monomer concentration and high electropolymerization potential (e.g., 10 mM EDOT, 1.8 V), we observed that the reaction current was continuously decaying with the increase of time. The reason lies on the limited supply of monomers by diffusion. At high monomer concentration and moderate electropolymerization potential (e.g., 100 mM EDOT, 1.4 V), the reaction current reached a plateau value instantly due to sufficient supply of monomers by diffusion. This implies that the electropolymerization of EDOT is a reaction that depends on diffusion. The polymerization reaction at high potentials proceeded for the monomer consumption to exceed the monomer supply. Polymers would grow preferentially along the pore wall to form nanotubes because of the interaction of polymer and wall surface. As the potential increased, more porous, thinner, and longer nanotubes were obtained because of fast polymer growth which has been discussed above. At low oxidation potentials which are lower than 1.4 V, however, the growth of PEDOT nanotubes deviates from our expectation significantly. The tubular portion of the nanostructure increases even though the monomer concentration increases. Our experiment showed that even at very high monomer concentration such as 500 mM, well-defined PEDOT nanotubular structures can be obtained. Furthermore, nanotubular structures are favored

nearly independent of monomer concentration at 1.2 V. These phenomena cannot be explained by using our previous mechanism based upon the diffusion and reaction kinetics.¹⁴ This implies that another mechanism is operating at low potentials, which will be discussed later.

At potentials higher than 1.4 V, monomer concentration is also an important variable to determine the PEDOT nanostructures as shown in Figure 4.7. It is expected that hollow nanotubes can be grown instead of solid nanowires when the polymerization reaction rate is fast enough to consume all the monomers diffused from the bulk solution. Decreasing monomer concentration is an alternative way to achieve faster monomer consumption than monomer supply. An approximate calculation, based upon the density of PEDOT ($\rho = 1.64 \text{ g/cm}^3$) obtained by X-ray diffraction,¹³⁰ shows that 1.3×10^{10} monomers (ca. 10 M EDOT in concentration) are required to fill a pore (ca. $2 \times 10^{-12} \text{ cm}^3$ in volume). Thus, fast diffusional supply of monomers is required for the synthesis of solid nanowires in all the conditions of current study. Because of relatively slow reaction rates, however, we could obtain full nanowires around 100 mM EDOT. Another way to increase the diffusional flux of monomers is to stir the solution or to apply a pulsed potential. This facilitated the monomer diffusion into the membrane pores, and nanowires could even be obtained in low concentrations and high voltages such as 25 mM EDOT and 1.6 V.

4.4.3 Synthesis Mechanism below 1.4 V

To electrochemically deposit nanomaterials in the template pores, a thin layer of gold was sputtered on one side of the alumina template. This gold layer serves as a working electrode in the electropolymerization process. Using field emission SEM we found that

the gold was also sputtered inside the template pore bottom and resulted in the formation of a gold base electrode with ring structure.

The base electrode shape is an important factor in nanotube growth at oxidative potentials below 1.4 V. Usually, the sputtered gold is introduced into the pores of the alumina membrane and forms annular electrodes at the bottom of pores (Figure 4.8.a). The nanotube growth at low potentials may be attributed to the annular shape of the gold electrode at the bottom of the pore. The oxidation of EDOT starts around 1.2 V to form PEDOT.¹²⁹ At this onset oxidation potential, the electrochemically active sites are critical in polymerization and dominate on top of the annular Au electrode in each pore. The high-curvature surface (sharp end) on the top of the annular Au electrode has high charge density or electric field and is electrochemically more active relative to smooth surrounding surface. This phenomenon is called 'tip' effect.¹³¹ Thus, EDOT polymerization is expected to preferentially occur on the top of the base electrode rather than on the wall surface of the base electrode.

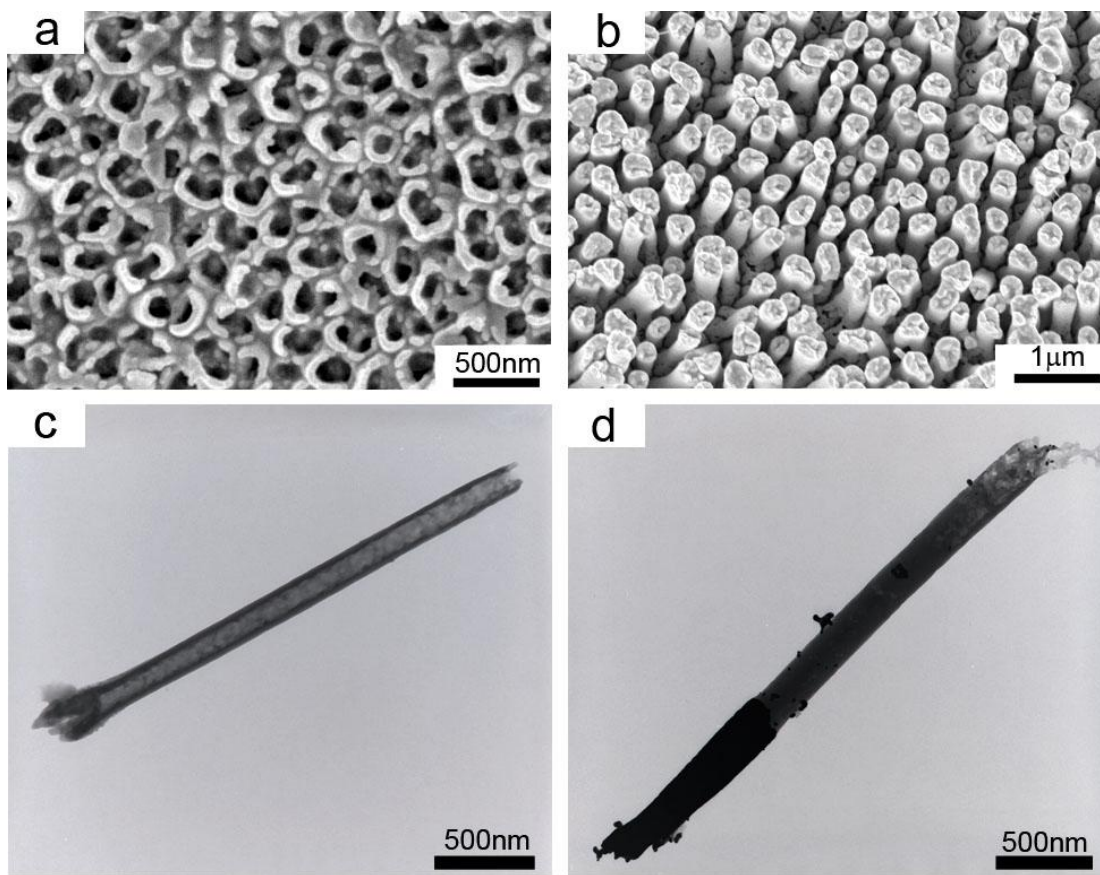


Figure 4.8. SEM images of (a) annular base electrodes (Au-sputtering only) and (b) flat-top base electrodes (Au sputtering and electrodeposition) and TEM images of PEDOT nanostructures grown at 1.2 V for 100 s (c) in 500 mM EDOT on the annular electrodes and (d) in 10 mM EDOT on the flat-top base electrodes.

Figure 4.9 shows the synthesis process of PEDOT nanotubular structures on the gold bottom electrode at potentials below 1.4 V. At electrochemically active sites on the top of the gold bottom electrode well-defined PEDOT nanotubular structures can be obtained.

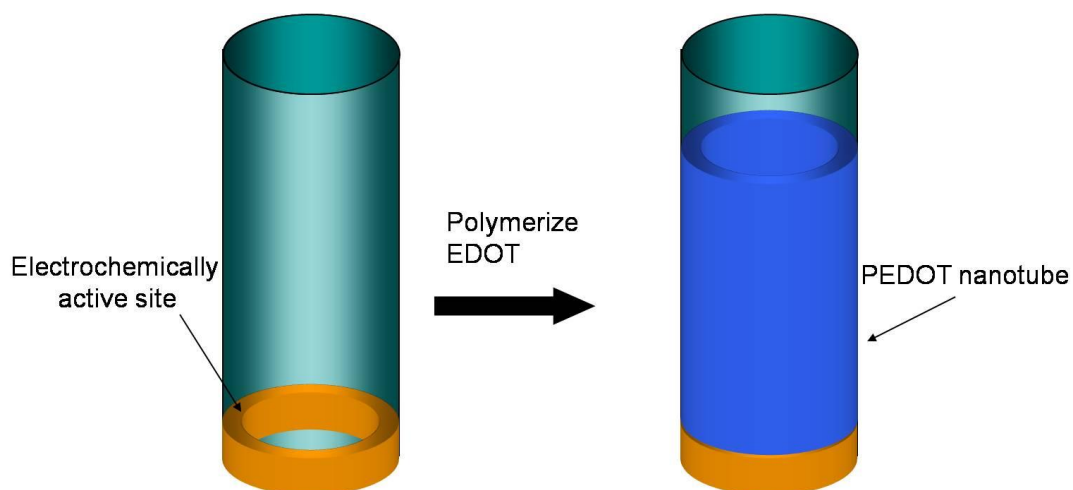


Figure 4.9. Schematic illustration of PEDOT nanotube synthesis on a gold bottom electrode at low applied potential.

To prove this hypothesis, we made flat-top base electrodes by further depositing gold electrochemically on the annular electrode. Figure 4.8.b shows the SEM image of electrodeposited flat-top electrodes after removing the alumina template. The annular or sharp edge structure was eliminated by this process, and the top surface of the base electrodes was flat. Then, we synthesized PEDOT on the flat top of these electrodes. In the TEM sampling process, we did not dissolve the base gold electrodes so PEDOT nanostructures could be clearly differentiated from the base gold electrode in TEM images. As shown in Figure 4.8.d, almost filled nanotube (nanowire) was fabricated even at 1.2 V. Indeed, while we could not make nanotubular structures at low oxidation potentials on the flat-top electrodes, we could synthesize nanotubular structures even at very high concentrations (0.5 M EDOT) on the annular gold electrodes (Figure 4.8.c). These results support very well the hypothesis that the top surfaces of the annular Au electrodes are electrochemically active for growing the nanotubular structures of PEDOT.

Figure 4.10 shows the fabrication of PEDOT nanostructures on a gold bottom electrode with flat top.

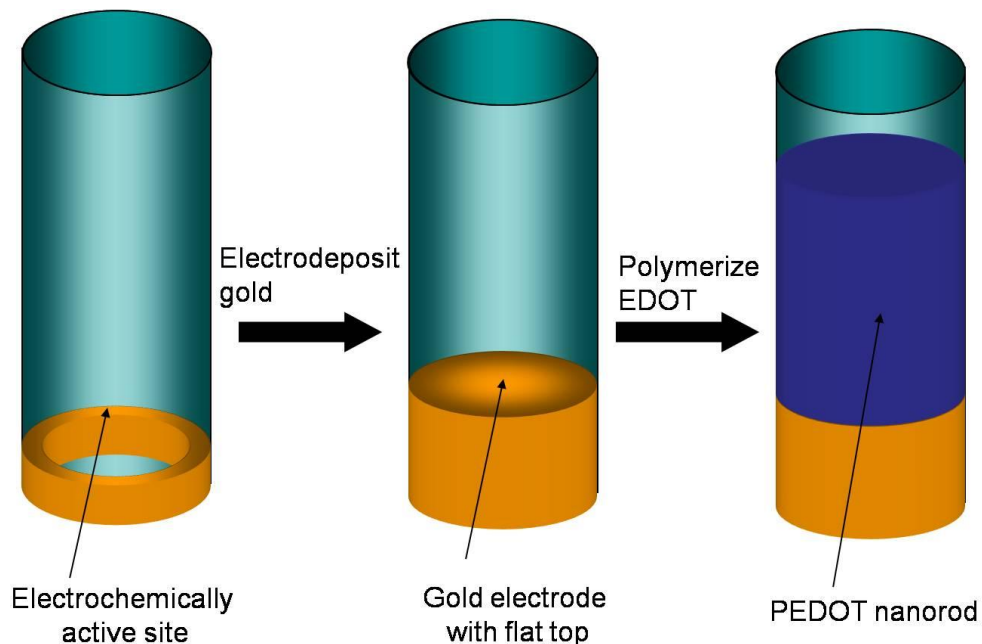


Figure 4.10. Schematic representation of PEDOT nanostructure synthesis on a gold bottom electrode with a flat top. The electrochemically active sites on the top of the gold bottom electrode with a ring structure have been blocked by further depositing gold on the bottom of the template pore.

In the case of flat-top electrodes, only the first monomer diffusion mechanism may exist, since the flat-top electrode does not have any preferential electrochemically active sites. Therefore, it is important to know whether the first mechanism still applies to the flat-top electrode. If it applies, we can obtain a higher tubular portion (R) in nanotubular structures as the reaction potential is increased. The tubular portion was plotted vs. applied potential (Figure 4.11). PEDOT was synthesized by changing applied potential

from 1.2 to 1.8 V at a fixed electropolymerization time of 100 s in 10 mM EDOT. Figure 4.11 shows exactly what we expected. The tubular portion increased as the reaction potential was increased.

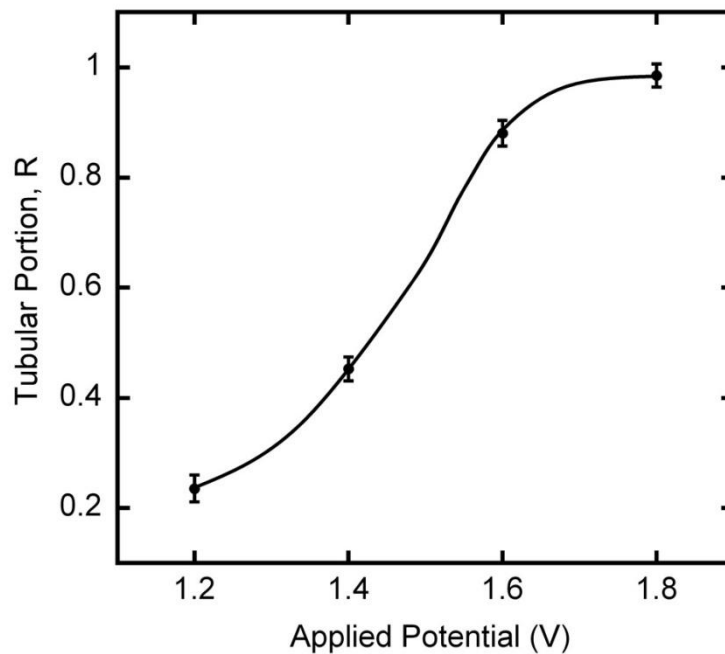


Figure 4.11. Plot of tubular portion vs. applied potential for PEDOT nanostructures grown on the flat-top Au electrodes in the pores of an alumina membrane (10 mM EDOT, 100 s in polymerization time).

We have also observed the decrease of tubular portion in nanotubular structure as we increased the monomer concentration. These results strongly support the first mechanism, which is related with the monomer diffusion flux rate and electropolymerization reaction rate, to control the structure of nanotubes on the flat-top electrodes in the template pores. At the same time, this result also proved that the existence of a gold bottom electrode

with ring structure is essential for the formation of PEDOT nanotubular structures at low applied potentials.

4.5 Influences of Electrolyte Concentration and Temperature

The flux of monomers and polymerization rates can be affected by the concentration of electrolyte (LiClO_4) and temperature. Therefore, it is necessary to study their effects on PEDOT nanostructures—the variation of the characteristic curves in Figure 4.7—in order to have universal characteristics to selectively synthesize solid nanowires and hollow nanotubes of PEDOT material. First, we investigated the LiClO_4 concentration effect by analyzing PEDOT nanostructure (tubular portion, R) synthesized with three LiClO_4 concentrations of 0.01, 0.1, and 1 M and at three selective potentials of 1.2, 1.4, and 1.8 V. We chose the 25 mM EDOT as a model monomer concentration because PEDOT nanostructures showed dramatic change over the applied potentials in this concentration. Tubular portion was plotted as a function of applied potentials in Figure 4.12.a at the LiClO_4 concentrations in 0.01, 0.1 and 1 M. The R values at the given potential were not sensitive to the change of electrolyte concentration. However, the length of nanotubes increased dramatically as the LiClO_4 concentration increased (data not shown here). For example, the lengths of nanotubes synthesized at 1.4 V with 0.01, 0.1, and 1 M LiClO_4 were 3.4, 5.2, and 6.2 μm , respectively. These results indicate that the electrolyte concentration has greater effect on polymerization rate than on the diffusion rate.¹³² It is natural that the length of nanotubes decreases with the reduction of electrolyte concentration because the dopant, ClO_4^- , plays an important role in electropolymerization

reaction rate by being incorporated into the positively-charged polymer layer as a counter ion during the oxidation.

Second, we studied the temperature effect by comparing the tubular portions of PEDOT nanostructures synthesized at 25 and 50 °C in 25 mM EDOT and 0.1 M LiClO₄. The plot of tubular portion vs. applied potential (Figure 4.12.b) shows that the nanotubes can be filled more readily at high temperature (50 °C) than at low temperature (25 °C). These results can be explained by the fact that the monomer flux in the pores increases significantly due to the increase of diffusion coefficient of EDOT monomer and convective mass transfer at the interface between the pores and bulk solution at the elevated temperature. Therefore, increasing temperature gives similar effect as increasing monomer concentration on the PEDOT nanostructures. However, the change in nanotube lengths was less than 10 % at each point and relatively insensitive to temperature change (data not shown here).

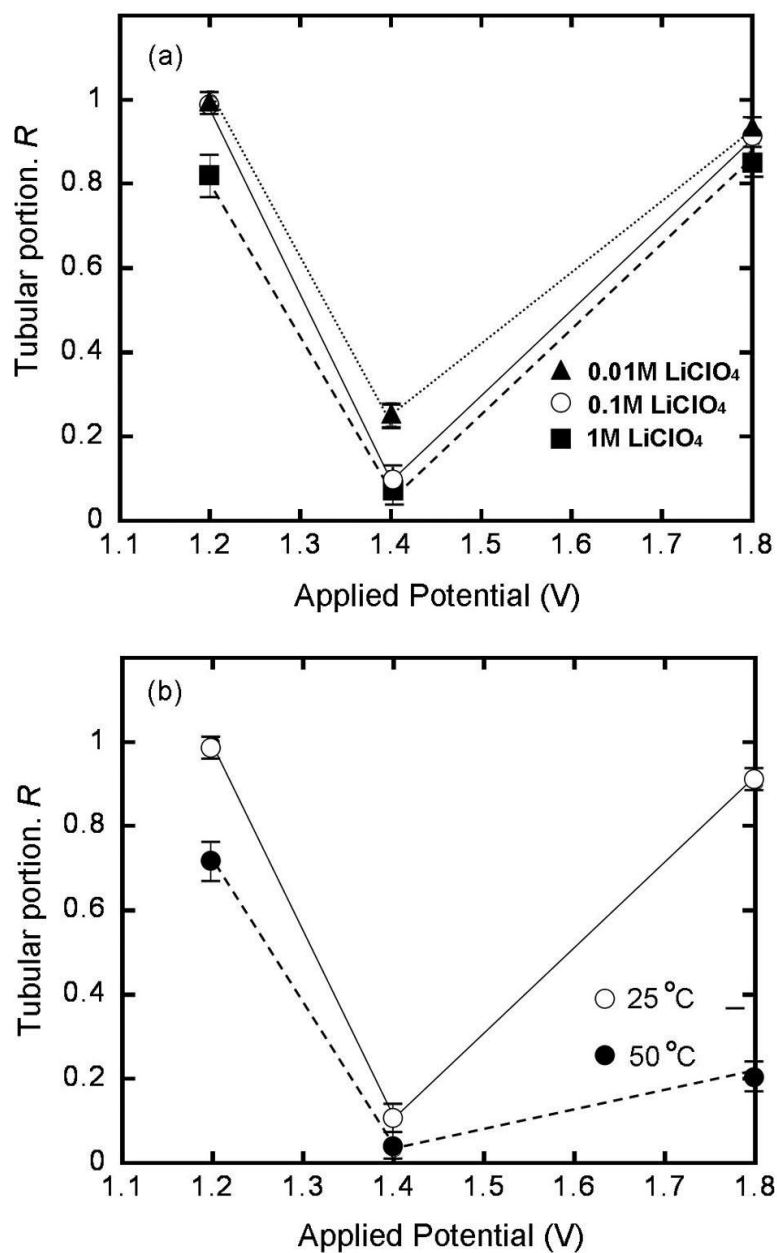


Figure 4.12. Plots of tubular portion for PEDOT nanostructures vs. applied potentials. Electropolymerizations were performed at 25 °C with the LiClO_4 concentrations of 0.01, 0.1, and 1 M for (a) while it was done in 0.1 M LiClO_4 at 25 and 50 °C for (b). EDOT concentration was 25 mM in both cases.

4.6 Synthesis of PEDOT Nanotubes in the Smaller Pores

We have fabricated PEDOT nanostructures by using commercially available alumina template (ca. 200 nm diameter) under various monomer concentrations and applied potentials. Based on the dependence of nanotube tubular ratio on the parameters like monomer concentration, electropolymerization potential, electrolyte concentration and temperature we proposed a mechanism which can guide the synthesis of PEDOT nanostructures by using electrochemical template synthesis method. It will be interesting to know the behavior of PEDOT nanostructure synthesis in alumina template with smaller pores.

It is more difficult to grow the nanotubular structures of PEDOT in the smaller pores, because the smaller pores may be filled faster with the PEDOT at a given electropolymerization time. However, we have successfully synthesized the PEDOT nanotubes in pores with 80 nm diameter by using annular Au electrodes at the bottom of the pores. Figure 4.13.a shows a SEM image of a home-made alumina template which has highly-ordered hexagonal pattern of pores and a pore diameter of 80 nm. The bottom of the template was coated with a thin layer of gold as a working electrode. Its SEM image (Figure 4.13.b) after removal of the template clearly shows the annular shape of Au electrode for each pore, which is very helpful for the growth of nanotubular structures. The PEDOT nanotubes were successfully synthesized at 1.2 V for 100 s in 10 mM EDOT as shown in Figure 4.13.c and d respectively.

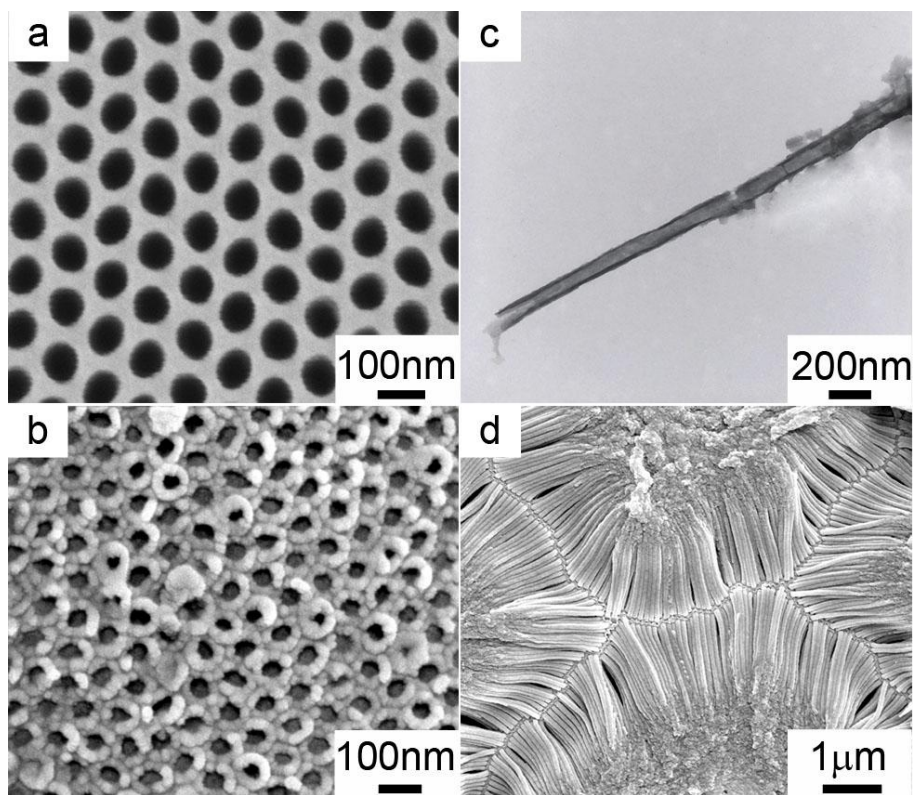


Figure 4.13. SEM images of (a) a home-made alumina template with 80-nm pores in diameter, (b) annular Au electrodes after the removal of alumina template, and (c) TEM and (d) SEM images of PEDOT nanotube synthesized at 1.2 V for 100 s in 10 mM EDOT.

From these results it is apparent that well-defined PEDOT nanotubular structures can be obtained with the aid of gold bottom electrodes even in alumina template with smaller pores. This proved that the mechanism of the electrochemically active sites on the top of the gold bottom electrode also applies for the synthesis of PEDOT nanotubular structures in alumina templates with small pore diameters.

4.7 Synthesis Mechanism for Polypyrrole

Many research groups studied the electrochemical synthesis of polypyrrole because of its potential applications to sensors and electronic devices,^{13, 133, 134} but, the polypyrrole nanostructures synthesis mechanism is still unknown.

To investigate the effect of applied potential and monomer concentration on polypyrrole nanostructures, the polypyrrole polymerization was performed potentiostatically in aqueous solutions of 10, 25, 50, and 100 mM pyrrole at various potentials for 100 s. The TEM data were analyzed to plot the tubular ratio vs. applied potential. The potential dependence of polypyrrole nanostructures has two different growth regions as shown in Figure 4.14. The result implies that the electrochemically active site mechanism applies for the growth of the nanotubular structure of polypyrrole on the annular Au electrode around potentials below 0.8 V while the diffusion and reaction kinetics mechanism applies at potentials above 1.2 V. In the potential range between 0.8 and 1.2 V, the two mechanisms seem to compete with each other. The polymerization rate of pyrrole starts to increase around 0.7 V.²³ Thus, nanotubular structures are preferentially synthesized independent of monomer concentrations around 0.7 V. On the other hand, low monomer concentration and high potential are preferred for the synthesis of nanotubes at the potentials higher than 1.2 V. These results strongly support our mechanisms for electrochemical synthesis of polypyrrole nanotubes. Figure 4.15 shows representative electron microscopic images of polypyrrole nanostructures synthesized at three different conditions.

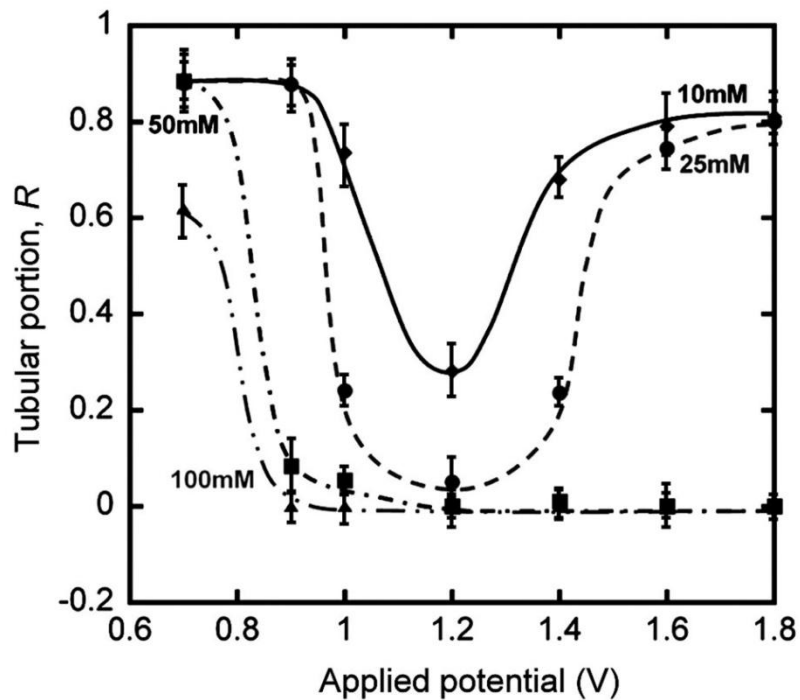


Figure 4.14. Plot of tubular portion for polypyrrole nanotubes vs. applied potential. Electrochemical polymerization was performed potentiostatically with the fixed polymerization time of 100 s. The tubular portion, R , is defined as the length of the tubular section divided by the total length. The data were obtained from the corresponding TEM images. The lines were added to help guide the eyes.

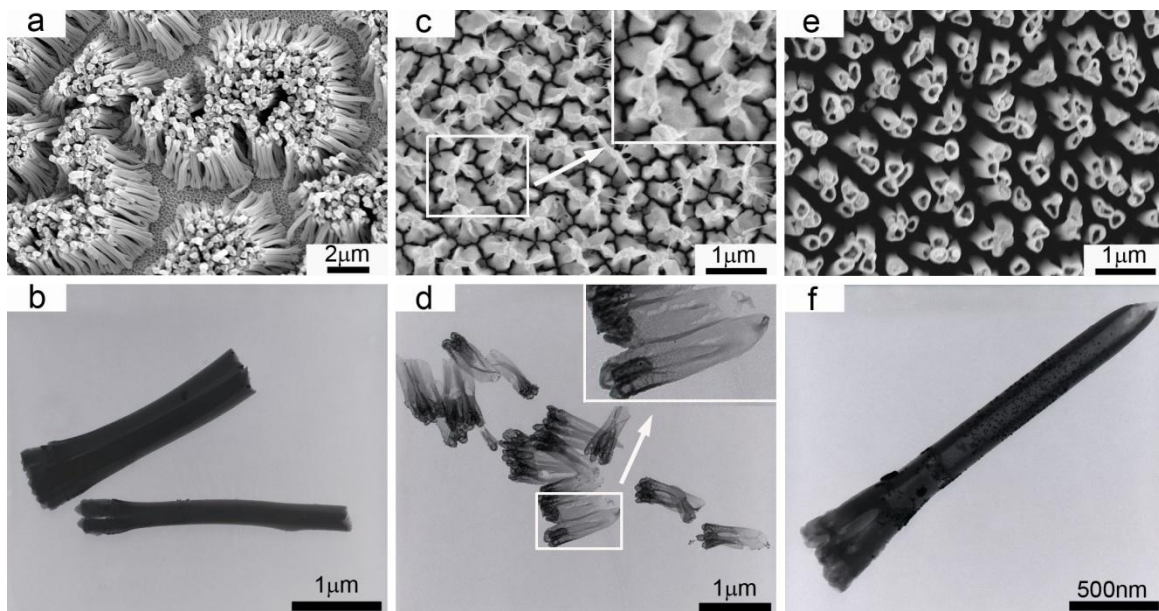


Figure 4.15. Electron micrographs of polypyrrole nanostructures synthesized potentiostatically for 100 s (a,b) in 50 mM pyrrole at 1.4 V, (c,d) in 10 mM pyrrole at 0.7 V, and (e,f) in 25 mM pyrrole at 1.8 V. The upper (a, c, and e) and lower (b, d, and f) images were taken by SEM and TEM, respectively.

From Figure 4.15 it can be seen that the gold bottom electrode has a critical role in the fabrication of polypyrrole nanotubular structures. At low applied potential like 0.7 V, polypyrrole nanotubes grow preferentially along the template pore wall on the top of the electrochemically active sites. Figure 4.16 shows two SEM images of the gold bottom electrodes for polypyrrole nanostructure synthesis.

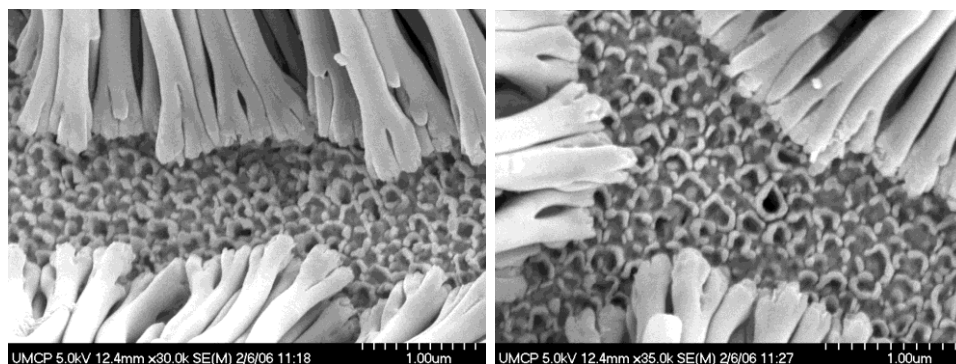
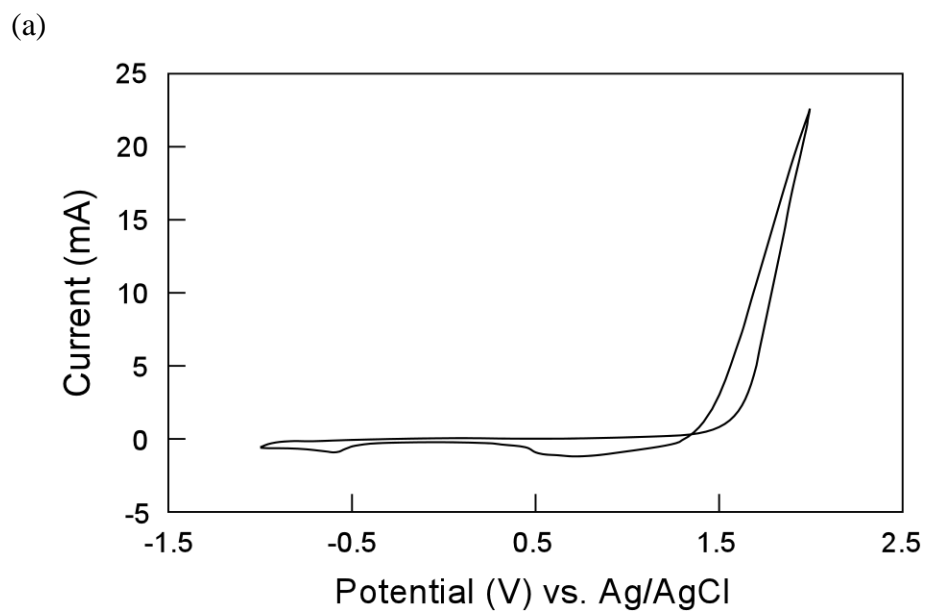


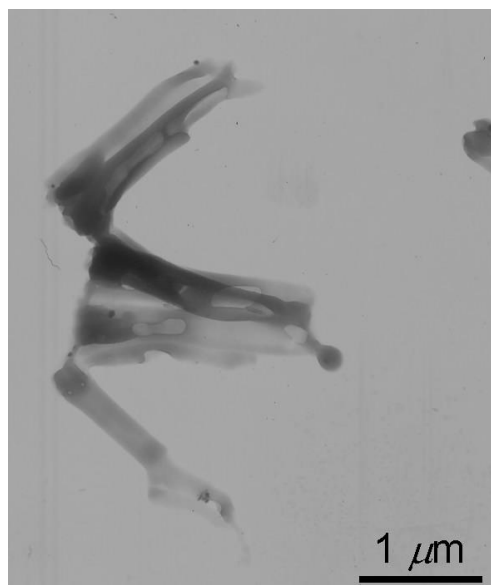
Figure 4.16. SEM images for the gold bottom electrode after removal of alumina template.

4.8 Synthesis Mechanism of poly(3-hexylthiophene)(P3HT) Nanostructures

The cyclic voltammogram for 3-hexylthiophene (3HT) was obtained at a scan rate of 0.1 V/s in an acetonitrile solution of 0.1 M 3HT and 20 mM LiClO₄ by using an indium-doped tin oxide electrode as a working electrode. The polymerization rate of 3HT starts to increase around 1.5 V as shown in Figure 4.17.a. Thus, we attempted to synthesize P3HT nanostructures at constant potentials higher than 1.5 V (vs. Ag/AgCl reference electrode) in 100 mM 3HT and 20 mM LiClO₄ in an acetonitrile solution. P3HT nanotubes could be synthesized at low oxidation potential of 1.5 V (Figure 4.17.b). Nanowires were preferred to nanotubes as the applied potential was increased to 2.0 V (Figure 4.17.c). At potentials greater than 2.0 V, the dissolution of base gold electrode prevented further electrochemical study.



(b)



(c)

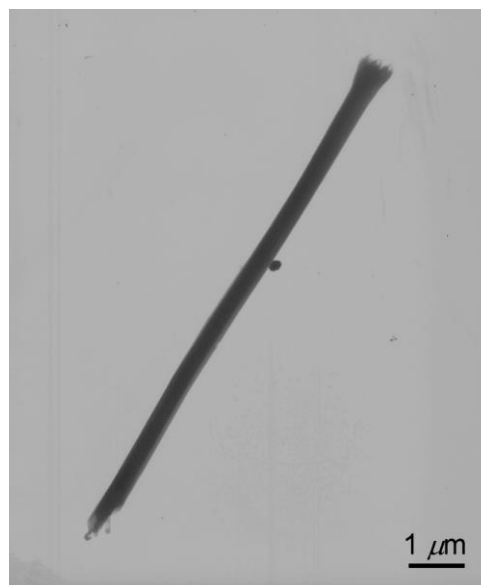


Figure 4.17. (a) Cycle voltammogram of 3-hexylthiophene (0.1 M) in an acetonitrile solution of 20 mM LiClO_4 at a scan rate of 0.1 V/s. TEM images of (b) P3HT nanotubes synthesized at 1.5 V for 400 s and (c) P3HT nanowire synthesized at 2.0 V for 200 s.

4.9 Summary

We have successfully investigated two electrochemical synthetic mechanisms of conductive polymer nanotubes in a porous alumina template using PEDOT as a model compound. The mechanism based on electrochemical active sites applies to growth of the nanotubular structure of PEDOT on the annular Au electrode at the potentials below 1.4 V, while the mechanism based on diffusion and reaction kinetics works at potentials above 1.4 V. These mechanisms were also successfully employed to control the dimensions of polypyrrole and P3HT nanostructures.

Chapter 5: Electrochromic Properties of PEDOT nanostructures

5.1 Introduction

In the first chapter we discussed the electrochromic properties of PEDOT and its derivatives. For real applications, electrochromic materials must have properties such as long-term stability, rapid redox switching and large changes in transmittance or reflectance. Before the introduction of conductive polymers, inorganic materials were used as electrochromic materials. Difficulties in fabrication, processing, and slow response time have motivated the research on other materials of higher quality and performance. Conjugated polymers, especially PEDOT are suitable for electrochromic applications due to their fast color switching, lower oxidation potentials and good stability at ambient and elevated temperatures.^{14, 15, 25} As a cathodically coloring polymer, PEDOT's color is a dark opaque blue in its reduced state and transparent pale blue in its oxidized state. Figure 5.1 shows the color change process of PEDOT.

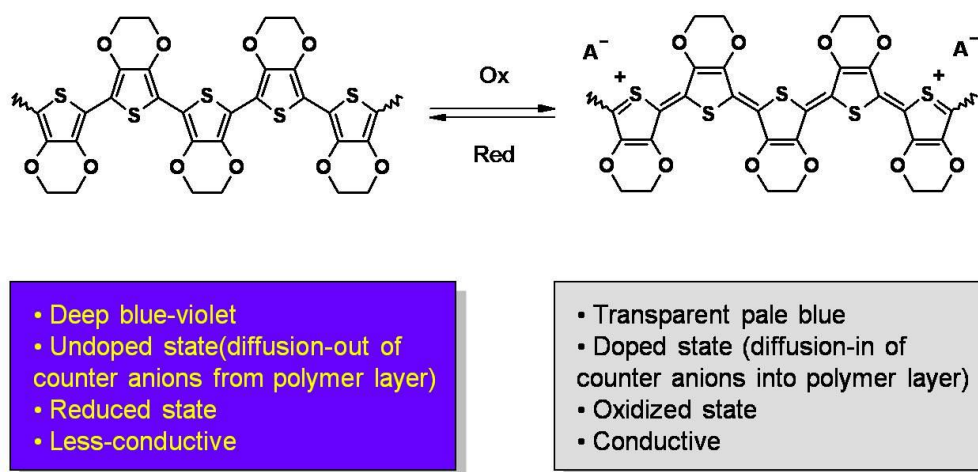


Figure 5.1. Color change process for PEDOT

5.2 Effect of Nanotube Wall Thickness on Redox Rates

5.2.1 Control of PEDOT Nanotube Wall Thickness

In order to study the relationship between PEDOT nanotube wall thickness and the redox rates, it is necessary to precisely control the nanotube wall thickness. Because of the influence of electrochemically active sites on the top of gold base electrodes, well-defined PEDOT nanotubular structures can be obtained at low applied potentials. We chose 1.2 V as the electropolymerization potential for the synthesis of PEDOT nanotubes with various wall thicknesses at different monomer concentrations from 10 to 500 mM. Figure 5.2 shows the dependence of PEDOT nanotube wall thickness upon the monomer concentration at 1.2 V.

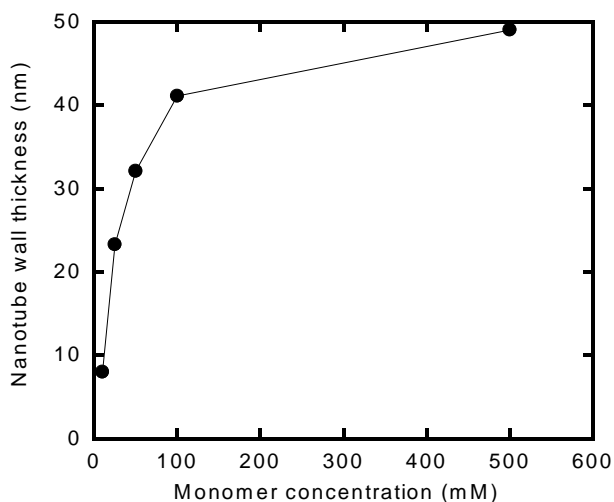


Figure 5.2. Schematic illustration of the dependence of PEDOT nanotube wall thickness on the monomer concentration.

In Figure 5.2 it can be seen that as monomer concentration increases from 10 to 500 mM, the PEDOT nanotube wall thickness also increases. But the incremental rate of the nanotube wall thickness slows with the increase in monomer concentration.

5.2.2 Relationship between Redox Rates and Nanotube Wall Thickness

Nanotube wall thickness is an important factor in achieving fast electrochemistry. Thin nanotube walls permit fast electrochemistry due to the short diffusion time of counter-ions into and out-of the polymer layer during the redox reactions of the conductive polymer nanotube. The correlation between the redox rate and nanotube wall thickness was obtained by plotting the electrochromic color-switching rate of PEDOT vs. nanotube wall thickness. The electrochemical reactions of conductive polymer include not only redox reactions but also electrical double layer charging/discharging at the interface between the electrolyte solution and the PEDOT. Electrochromic optical response does not involve charging and discharging processes, representing only redox reactions by the diffusion of counter-ions into/out-of the polymer layer. Polymerization was performed at 1.2 V on the annular Au electrodes. The monomer concentration was varied from 10 to 500 mM to adjust the wall thickness.

Figure 5.3 is a plot of response time vs. tube wall thickness. As expected, the response time increases along with wall thickness. However, the increase in 0.1 M LiClO₄ (open circle) does not agree well with theoretical trend (solid line):

$$t = \frac{\pi}{16 D} \left(\frac{\bar{C}}{C_s} \right)^2 x^2, \text{ where } t$$

represents response time, x is film thickness (here, thickness of nanotube wall), D is the diffusion coefficient of counter ions (ClO₄⁻), and \bar{C} and C_s represent average and

saturation concentration of counter ions in a polymer layer, respectively. The deviation from the theory can be understood by considering the amount of electrolytes in the pores. When the nanotube wall is thin, the counter ions in the nanotube can completely dope the oxidized polymer. A rough calculation based on the density of PEDOT showed that 0.1 M LiClO₄ electrolyte solution can completely dope a PEDOT nanotube with only 2 nm in wall thickness in a 200-nm pore while 1 M LiClO₄ electrolyte solution can dope up to 15 nm wall thickness without further diffusion of electrolytes from the bulk solution. As the wall thickness increases, the total amount of PEDOT in the nanotube becomes larger than that can be doped by 0.1 M LiClO₄ electrolyte. Therefore, the amount of electrolytes inside the nanotube is not sufficient to dope all the PEDOT. Thus more counter-ions (ClO₄⁻) should diffuse into the nanotube from the bulk solution, which results in longer response time. To support our explanation, we measured response times in a highly concentrated electrolyte, 1 M LiClO₄. As shown in Figure 5.3, the response times measured in 1 M LiClO₄ (closed circles) are shorter than those in 0.1 M LiClO₄ (open circles), and follow quite well with the theoretical values.

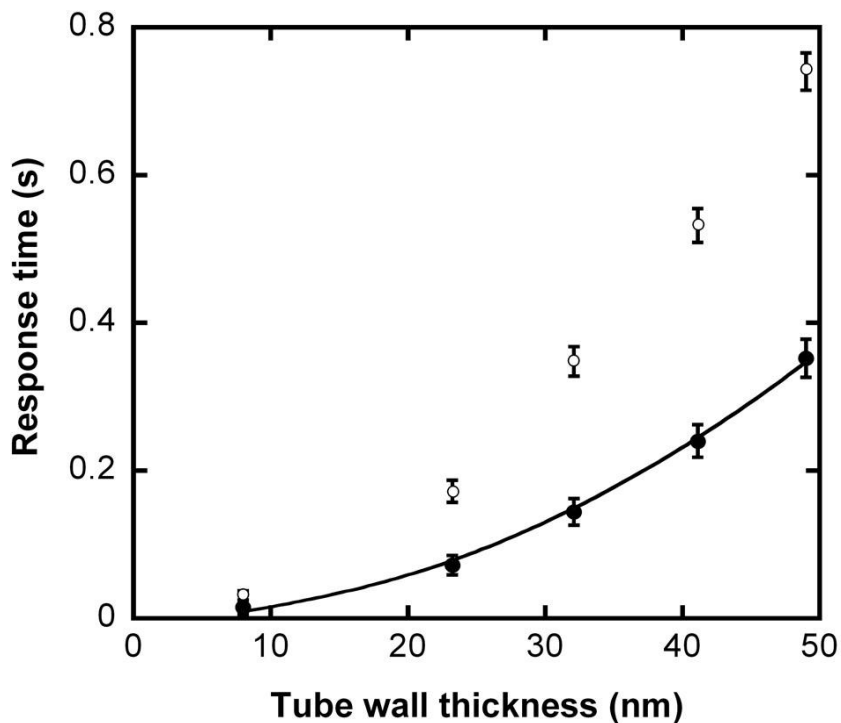


Figure 5.3. Plot of electrochromic response time vs. nanotube wall thickness. The response time was measured for the oxidation of PEDOT in the electrolyte solution of 0.1 M (open circle) or 1 M LiClO₄ (closed circle) in acetonitrile. The solid line is a theoretical fit (see text for details). The optical response rate was measured using a reflectance measurement system (Ocean optics Inc.) which contained a light source (LS-1), a standard reflection probe (R400-7), and a probe holder (RPH-1). A photodiode was used to detect the reflected light and an oscilloscope (Tektronics, TDS1012) was used to analyze the signal.

5.3 Electrochemical Response and Optical Response of PEDOT Nanotubes

In order to compare the electrochemical response and optical response of PEDOT nanotubes, we fabricated an electrochemical cell composed of Ag/AgCl reference, platinum counter, and PEDOT working electrodes. PEDOT nanotubes were synthesized

in 10 mM EDOT at 1.2 V for 100 s in an acetonitrile solution by using a commercially available alumina template. Continuous potential steps between 1.0 V and -1.0 V were applied in 0.1 M LiClO₄, in order to switch the electrochemical device from the oxidized state to reduced state. The electrochemical response data were collected by a potentiostat and the optical response was measured at 600 nm wavelength through the reflectivity of PEDOT nanotubes (Figure 5.4). It is obvious that the optical response is much faster than the electrochemical response no matter for the coloring or de-coloring process. The explanation of this observation is that, in electrochemical reaction, there always exists the electrical double layer between the electrolyte solution and the PEDOT nanotube interface. Thus, the electrochemical response of a conductive polymer includes not only redox reactions but also the charging/discharging of the electrical double layer, which leads to the delay of the electrochemical response. The optical response does not involve charging/discharging processes, resulting in a faster response compared to the electrochemical response.

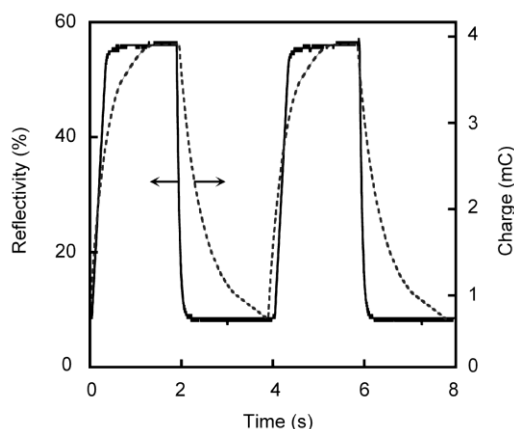


Figure 5.4. The electrochemical response versus optical response. The solid line is for the optical response and the broken line is for the electrochemical response.

5.4 Summary

From the study of electrochromic properties of PEDOT nanotubes through the dependence of optical response time on tube wall thickness, it is apparent that well-defined PEDOT nanotubular structure can achieve fast color change rate for the application of electrochromic devices. At the same time the fast charge-discharge rate for PEDOT nanotube with thin wall is also essential for the applications like supercapacitors, batteries and other energy storage devices.

Chapter 6: Electrochemical Synthesis of PEDOT nanostructures for Application of Electrochromic Window Device

6.1 Introduction

The proper choice of a porous template and a conductive-polymer nanostructure is essential for the fabrication of electrochromic devices. We have demonstrated that nanotubes of conductive polymers have electrochemical and electrochromic properties such as fast charge/discharge of counter-ions and rapid colour change between redox states by applying potentials,^{14, 15} superior to conventional films. These properties enabled us to develop fast reflection-type electrochromic devices.^{14, 15} For the application of fast window-type electrochromic device, it is necessary that the whole device have a degree of transparency. A porous anodic aluminium oxide (AAO) film that is made on a transparent indium-doped tin oxide (ITO)/glass substrate via aluminium evaporation and anodization can meet this requirement. We have showed that the annular base electrode, which is generated at the bottom of template pores during metal coating for a conductive electrode, plays an important role in synthesizing rigid nanotubes of conductive polymers.^{15, 25} For an AAO template directly anodized on the ITO/glass substrate this annular shaped bottom electrode is absent. In this chapter, we will discuss the electrochemical synthesis of conductive polymer nanotubes on flat-top nano-electrodes. Poly(3,4-ethylenedioxythiophene) (PEDOT) was used as a model compound, and a porous AAO film, which is in solid contact with a transparent ITO/glass substrate, was used as a template. We demonstrated the fast colour-switching of a window-type electrochromic device based on PEDOT nanotube arrays.

Porous AAO and track-etched polycarbonate (PC) membranes have been used as templates in the synthesis of conductive polymer nanotubes. The PC membrane provides cylindrical pores with low density (up to 10^9 pores/cm²) and pore diameters between 0.01 and 20 μ m. Because of its flexibility, this membrane is useful for synthesizing nanostructures and is a potential template for the development of a flexible nano-electrochromic device. On the other hand, the AAO membrane has highly ordered hexagonal pores with high density (ca. 10^{11} pores/cm²) and nanometre-range pore diameters. Porous AAO structures have been generated on various substrates such as silicon, metal, and glass.^{113, 115, 117, 135} For example, Crouse *et al.* developed a convenient method to fabricate porous AAO nanostructures on a silicon surface by depositing and anodizing a thin layer of aluminium.¹³⁵ Highly ordered porous AAO nanostructures on a silicon substrate were obtained in the Masuda group by patterning an aluminium layer using an imprinting technique before anodization. The patterned AAO film on the silicon substrate could be fabricated using sol-gel processing, photolithography, plasma etching, and anodization.¹³⁶ Rabin *et al.* fabricated a thick porous AAO film on a Ti-coated silicon wafer, where the Ti layer provided a strongly adhering interface.¹³⁷ Tian *et al.* constructed an AAO film on a Ti surface in order to make a free-standing AAO membrane easily.¹¹² Chu *et al.* showed that a porous AAO film could also be prepared on an ITO/glass substrate and metal nanorods could be deposited into the pores.¹¹³ The transmittance of the porous AAO film was almost comparable to that of the ITO/glass substrate. This high transparency, which the PC membrane lacks, is an important property for the development of window-type electrochromic devices. Because the bottoms of the pores are in good contact with a flat, conductive ITO layer, no further

metal deposition onto the membrane surface is required to make a conductive base electrode. However, this eliminates the possibility of introducing annular electrodes at the pore bottoms, which are required to synthesize rigid hollow nanotubes at low oxidation potential.

6.2 Template Fabrication and PEDOT Nanostructure Synthesis

6.2.1 Fabrication of Alumina Template on ITO Glass

The porous AAO film was prepared by electron-beam evaporation and subsequently anodizing this thin layer of aluminium on the ITO/glass substrate (Figure 6.1). The film was characterized using scanning electron microscopy (SEM). PEDOT nanostructures were synthesized potentiostatically in the AAO template pores and characterized using transmission electron microscopy (TEM). Finally, we investigated the electrochromic properties of the fabricated electrochromic window using a transmittance measurement system.

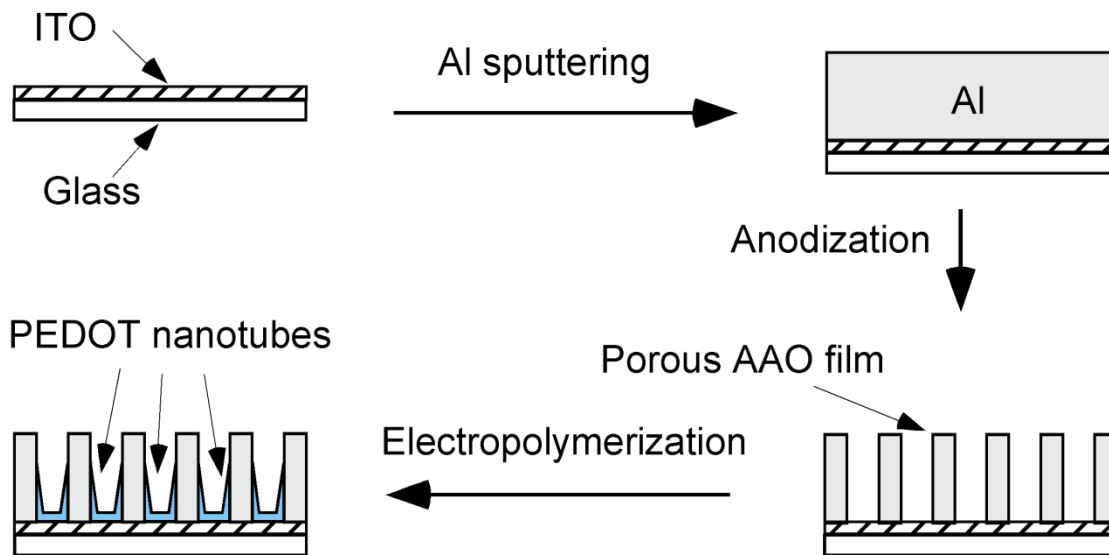


Figure 6.1 Schematic diagram of the fabrication of PEDOT nanotubes in a porous AAO film, in direct contact with a conductive, transparent ITO/glass substrate.

Figure 6.2 shows SEM images of the top and bottom of a porous AAO film. The AAO film has high pore density and good pore regularity in the pore diameter of 60–80 nm (Fig. 6.2.a) even though anodization step was performed only once. The bottom structure could be characterized after detaching the AAO film from the ITO/glass substrate with strong adhesive tape. The bottom surface looks much smoother than the top surface. This means that the AAO film was generated in good contact with the ITO surface. Usually, the bottoms of the pores are covered with a thin barrier layer after the aluminum anodization. The barrier layer at the bottom is thinner than that at the pore wall and has some defects.¹¹³ The thin alumina barrier layer could be removed (Fig. 6.2.b) by chemical etching without complete dissolution of the lateral barrier layer (pore wall) during the pore-widening process. The pore-widening process must be controlled very precisely. If the etching time is too short, the barrier layer cannot be removed. If the etching time is

too long, the top of the alumina template will be over-etched. Thus, the pore-widening should be stopped at the instant moment when the alumina barrier layer has been removed.

Pores at the bottom show more variation in diameters, compared to the top, depending on the degree of the barrier-layer etching. The exposure of the conductive ITO surface allows us to electrochemically deposit PEDOT in the pores. There is a very apparent difference between alumina templates fabricated by anodizing aluminum foil and aluminum coating on ITO glass. For the electrochemical reaction in the pores of a free-standing AAO film, one side of the template can be coated with a conductive metal layer by sputtering or evaporation. This produces annular metal electrodes at the pore bottoms. For anodic alumina templates fabricated on ITO glass, this step is missing, and thus no annular base electrodes are generated. These annular base electrodes are crucial for the synthesis of PEDOT nanotubes at low oxidation potentials. We could also fabricate porous AAO structures with highly-ordered cylindrical pores by the two-step anodization method (Figure 6.2.c) or with larger pore diameter (ca. 100 nm) at a potential of 80 V (Figure 6.2.d). As the pore diameter is increased for a fixed template thickness, monomers in the bulk solution can diffuse more easily into the pores. Large template pores inhibit the synthesis of hollow nanotubes, and thus we used a template with a small pore diameter (ca. 70 nm).

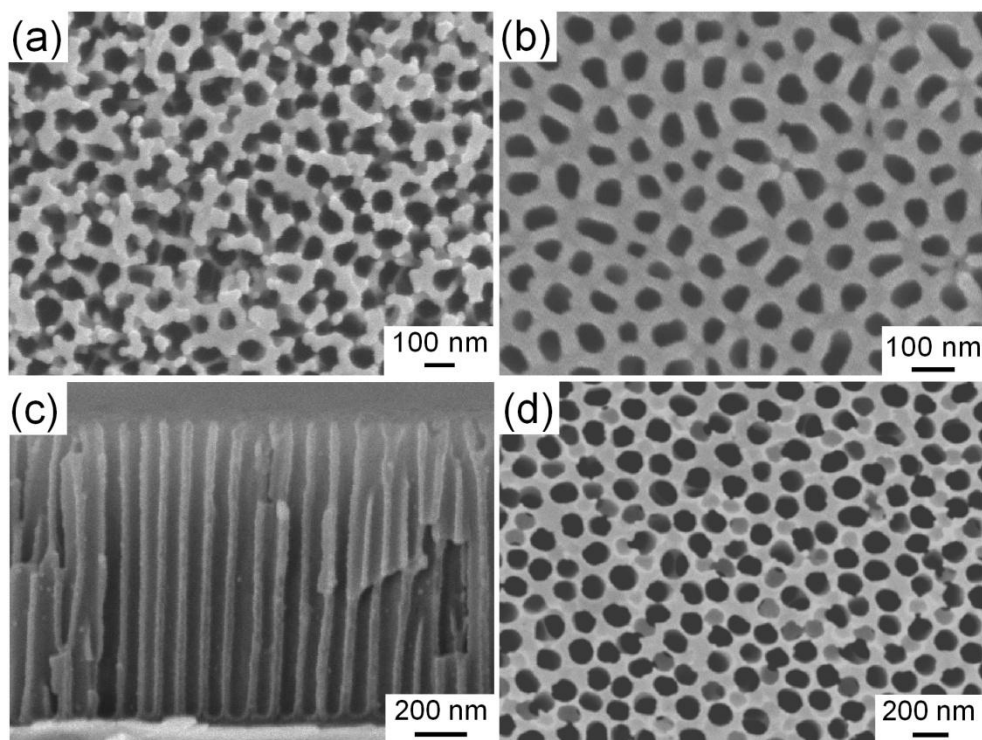


Figure 6.2. SEM images of porous AAO films viewed from (a,d) top, (b) bottom, and (c) cross section. The AAO films were synthesized at the potential of (a–c) 40 V and (d) 80 V. In the case of (c), two-step anodization method was used.

6.2.2 Electrochemical Synthesis of PEDOT in Template

The previous research revealed that the PEDOT nanotube filling at the flat-top electrodes in the template pores is mainly governed by the monomer concentration (concentration-gradient diffusional flux in pores) and applied potential (electrochemical reaction rate). In this study conditions are similar, however, the thickness of the current template is 5 % of that of commercially available templates. Thus, the facile diffusion of monomers into the pores may inhibit the synthesis of nanotubes even at high applied potentials. We studied the influence of potentials on PEDOT nanostructures synthesis at potentials of 1.2, 1.4, 1.6, and 1.8 V (vs. Ag/AgCl).

The high charge-transfer resistance at the electrode surface will have a significant effect on the PEDOT polymerization efficiency at 1.2 V, the threshold oxidation potential. This effect is manifested by the short length of solid PEDOT nanowires (data not shown here) at 1.2 V even at electropolymerization times of 150 s. We could grow solid PEDOT nanowires ca. 1 μm long at 1.4 V. As the potential increased to 1.6 V, we could synthesize partially filled nanotubes as shown in Figure 6.3.a. Further increase of the applied potential resulted in the increase of nanotubular portion (Figure 6.3.b). It should be noticed that we could not grow PEDOT nanotubes at 1.2 V. This can be attributed to the absence of the annular shape electrodes. Also the tubular portion was slightly decreased compared to the previous results obtained with commercially available templates (ca. 60 μm in thickness). For example, the previous tubular ratio at 1.6 V was approximately 0.9²⁵ while the current tubular ratio was 0.4–0.5. This is caused by the difference in the template thickness. Because the current template is 40 times thinner than the commercially available one, the bulk solution monomers can readily diffuse into the pores of the thin template. This leads to reduce the nanotube portion in the thin template.

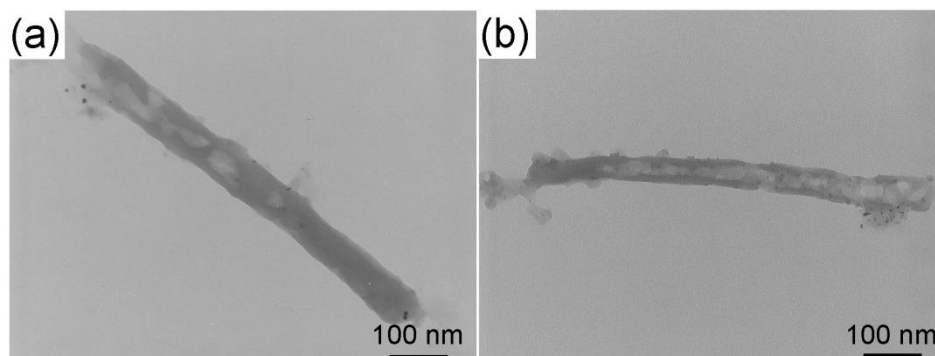


Figure 6.3. TEM images of PEDOT nanostructures synthesized at (a) 1.6 V and (b) 1.8 V for 30 s in 2.5 mM EDOT. The electrolyte was 0.1 M LiClO_4 in acetonitrile.

6.3 Study for Window-Type Electrochromic Device

Low overpotentials are preferred to the high overpotentials for the synthesis of rigid nanotubes because sufficient monomer can be supplied at the slow reaction rate. However, there is difficulty in synthesizing complete nanotubes at low oxidation potentials. On the other hand, the synthesis of complete nanotubes is possible at high overpotential. However, their electrochromic performance is poor because of highly-porous structures. Thus, we used a compromise structure, partially-filled nanotubes, for application to a window-type electrochromic device. Partially filled PEDOT nanotubes were synthesized at the moderately high potential of 1.6 V.^{14, 25} The electrochromic performance was tested using a patterned electrochromic device with four pixels as shown in Figure 6.4.a (1 cm² in total area of each pixel). Each pixel is composed of PEDOT nanotube arrays (SEM image in Figure 6.4.a). The patterning could be performed by using the following method: The pattern was defined by a thin adhesive tape as a mask or by using photolithography on an ITO/glass substrate. The patterned substrate was coated with a thin layer of aluminium by E-beam evaporation or sputtering, and then the mask was removed. The exposed ITO surface was completely oxidized during the anodization process and became electrically nonconductive.¹¹³ These processes facilitated the patterning of the ITO electrode layer with the AAO film. Each pixel was switched from an oxidized state to a reduced state by applying alternating square potentials from 1.0 to -1.0 V in 1 M LiClO₄ electrolyte solution. For experimental convenience in a proof-of-concept experiment, the adjacent pixel was used as a counter electrode.

Thus, first and third pixels were oxidized while second and fourth pixels were reduced, or vice versa. The oxidized and reduced PEDOT are transparent pale blue and deep blue, respectively, as in a conventional thin film.

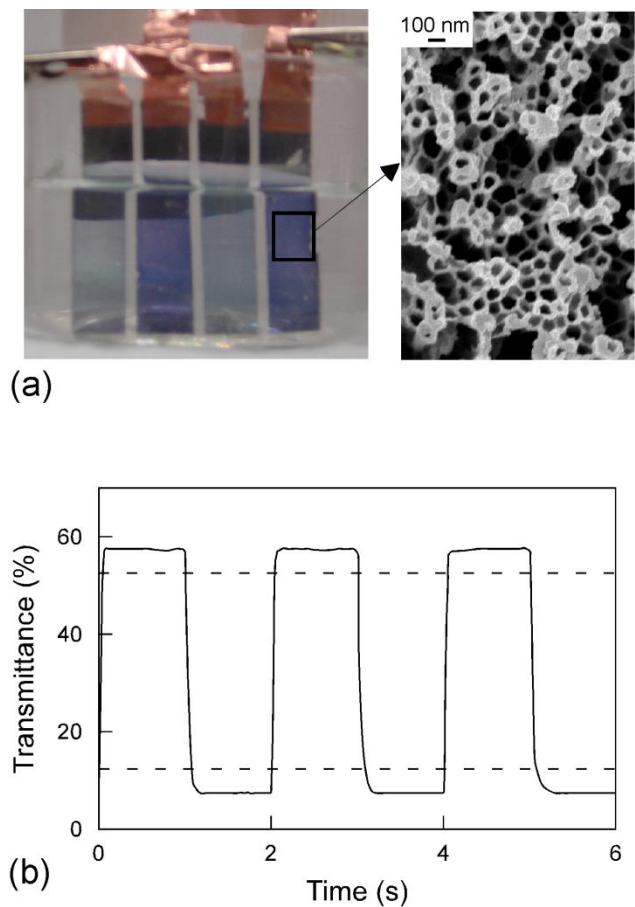


Figure 6.4. (a) Electrochromic device with four pixels. First and third pixels were oxidized (pale blue) and second and fourth ones were reduced (dark blue). The right picture is a magnified SEM image, showing PEDOT nanotubular array structures. (b) Plot of the electrochromic response at 600 nm as a function of time. The alternating square potentials from 1.0 to -1.0 V were applied to switch redox states. The dashed lines represent 90% recovery of the full response.

Figure 6.4.b shows the electrochromic responses monitored at 600 nm as a function of time for the first three potential switches (1 s in step time) at one of the pixels. The colour-switching times for de-colouring (oxidation) and colouring (reduction) processes were 50 and 70 ms, respectively. As expected, the switching time of partially-filled PEDOT nanotubes was slower than that of hollow nanotubes (20–30 ms)¹⁵ but faster than that of a conventional film (1–2 s).⁵⁶ PProDOT-Me₂ showed ten times faster electrochromic response than PEDOT.¹³⁸ Meanwhile, the current electrochromic device showed good transmittance, comparable to the value reported for a conventional film⁵⁶ because of the glass-like transparency of the AAO film directly anodized on the ITO/glass substrate. The color-switching rate of the electrochromic device was measured using a home-made transmittance measurement system, composed of a light source and two standard optical fibres. The transmitted light was detected with a photodiode and analyzed using an oscilloscope.

Figure 6.5 further demonstrated SEM images for PEDOT nanotubular structures synthesized in the above alumina template on ITO glass.

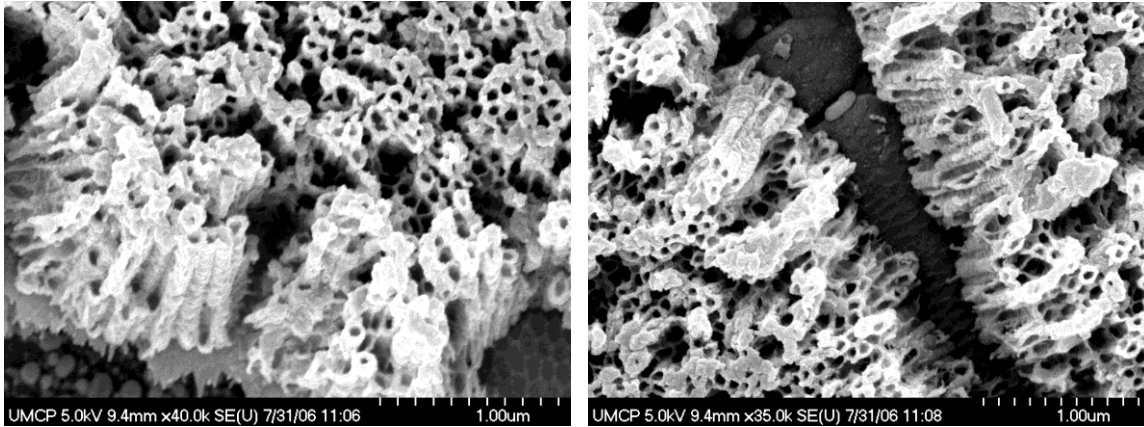


Figure 6.5. SEM images for PEDOT nanotubular structures synthesized in an alumina template on ITO glass. The conditions are 10 mM EDOT, 1.8 V, 10 s electropolymerization.

It can be seen that after removing alumina template with phosphoric acid, free-standing PEDOT nanotubular structures remain on the ITO glass substrate.

6.4 Summary

We discussed the synthesis of PEDOT nanotubes in a porous AAO film in direct contact with an ITO/glass substrate and their applicability to a window-type electrochromic device. PEDOT nanotubes could not be synthesized at 1.2 V because of the absence of annular base electrodes. For the synthesis of hollow PEDOT nanotubes at flat-top electrodes in the pores, conditions were high oxidation potential (>1.4 V) and low monomer concentration (2.5 mM). The current fabrication method is well adapted to the fabrication of pattern pixels.

Chapter 7: Conclusions

This thesis has discussed the fundamental background of conductive polymers, one-dimensional nanomaterials and the mechanism for PEDOT nanostructure synthesis for electrochromic applications. In the first chapter we introduced two synthetic methods for conductive polymers: chemical polymerization and electropolymerization. Then we discussed the structures and properties of conductive polymers such as polypyrrole, polythiophene, and poly (3, 4-ethylenedioxythiophene). Applications of conductive polymers have been discussed including electrochromic devices, electronic and photovoltaic devices, and chemical sensors and biosensors.

Chapter 2 focuses on the background and recent development of one-dimensional nanomaterials. The vapor-liquid-solid process, self-assembly and template synthesis methods were introduced. Attention has been given to the versatile template method because of the facile control of nanostructure morphology, high throughput and low cost. Among many template synthesis methods, porous materials including anodic alumina template and track-etched polycarbonate membrane with cylindrical pores have been extensively studied. The last section of this chapter extensively focused on the synthetic methods, properties and applications of various one-dimensional conductive polymer nanostructures including polypyrrole, polyaniline and polythiophene.

Chapter 3 discussed experimental methods. Details of the fabrication of alumina templates have been addressed. The AAO template on ITO glass was also studied because of its high mechanical strength and optical transparency. In chapter 3 the sample preparation, equipment hardware and software were discussed.

Chapter 4 is the most important part of the thesis. In this chapter the conductive polymer nanotube synthesis mechanisms have been studied using PEDOT, polypyrrole and P3HT. Through the detailed experiments, two mechanisms have been proposed to explain the synthesis of PEDOT nanostructures above and below 1.4 V. It has been found that the bottom gold electrode is critical for the fabrication process especially at low applied potentials. Besides the studies of monomer concentration and electropolymerization potentials, the influences of electrolyte concentration and temperature were discussed. The synthesis mechanisms for polypyrrole and P3HT have also been addresses.

Chapter 5 discussed the electrochromic properties of PEDOT nanostructures through the study of redox rates dependence on nanotube wall thickness. The electrochemical response and optical response of PEDOT nanotubes have also been compared.

The electrochemical synthesis of PEDOT nanostructures for application of electrochromic window device has been discussed in chapter 6. In this chapter we introduced the anodic alumina template synthesized on ITO glass. Because of its mechanical strength and optical transparency we deposited PEDOT nanotubular structures inside this template and demonstrated its use as an electrochromic window-type display device.

References

1. Street, G. B.; Clarke, T. C., *IBM Journal of Research and Development* **1981**, 25, (1), 51-57.
2. Walatka, V. V., Jr.; Labes, M. M.; Perlstein, J. H., *Physical Review Letters* **1973**, 31, (18), 1139-1142.
3. Greene, R. L.; Street, G. B.; Suter, L. J., *Physical Review Letters* **1975**, 34, (10), 577-579.
4. Wolmershauser, G.; Brulet, C. R.; Street, G. B., *Inorganic Chemistry* **1978**, 17, (12), 3586-3588.
5. Street, G. B.; Gill, W. D.; Geiss, R. H.; Greene, R. L.; Mayerle, J. J., *Journal of the Chemical Society, Chemical Communications* **1977**, (12), 407.
6. Akhtar, M.; Kleppinger, J.; MacDiarmid, A. G.; Milliken, J.; Moran, M. J.; Chiang, C. K.; Cohen, M. J.; Heeger, A. J.; Peebles, D. L., *Journal of the Chemical Society, Chemical Communications* **1977**, (13), 473-474.
7. Gill, W. D.; Bludau, W.; Geiss, R. H.; Grant, P. M.; Greene, R. L.; Mayerle, J. J.; Street, G. B., *Physical Review Letters* **1977**, 38, (22), 1305-1308.
8. Shirakawa, H.; Louis, E. J.; MacDiarmid, A. G.; Chiang, C. K.; Heeger, A. J., *Journal of the Chemical Society, Chemical Communications* **1977**, (16), 578-580.
9. MacDiarmid, A. G.; Heeger, A. J., *Synthetic Metals* **1980**, 1, (2), 101-118.
10. Ovchinnikov, A. A.; Belinskii, A. E.; Misurkin, I. A.; Ukrainskii, I. I., *International Journal of Quantum Chemistry* **1982**, 22, (4), 761-774.

11. Chance, R. R.; Bredas, J. L.; Silbey, R., *Physical Review B: Condensed Matter and Materials Physics* **1984**, 29, (8), 4491-4495.
12. Kuivalainen, P.; Stubb, H.; Isotalo, H.; Yli-Lahti, P.; Holmstroem, C., *Physical Review B: Condensed Matter and Materials Physics* **1985**, 31, (12), 7900-7909.
13. Van Dyke, L. S.; Martin, C. R., *Langmuir* **1990**, 6, (6), 1118-1123.
14. Cho, S. I.; Kwon, W. J.; Choi, S.-J.; Kim, P.; Park, S.-A.; Kim, J.; Son, S. J.; Xiao, R.; Kim, S.-H.; Lee, S. B., *Adv. Mater.* **2005**, 17, (2), 171-175.
15. Cho, S. I.; Choi, D. H.; Kim, S.-H.; Lee, S. B., *Chemistry of Materials* **2005**, 17, (18), 4564-4566.
16. Forzani, E. S.; Zhang, H.; Nagahara, L. A.; Amlani, I.; Tsui, R.; Tao, N., *Nano Letters* **2004**, 4, (12), 2519.
17. Facchetti, A.; Yoon, M.-H.; Marks, T. J., *Advanced Materials* **2005**, 17, (14), 1705-1725.
18. Yoshida, S.; Ono, T.; Oi, S.; Esashi, M., *Nanotechnology* **2005**, 16, (11), 2516-2520.
19. Hussain, A. M. P.; Saikia, D.; Singh, F.; Avasthi, D. K.; Kumar, A., *Nuclear Instruments & Methods in Physics Research, Section B: Beam Interactions with Materials and Atoms* **2005**, 240, (4), 834-841.
20. Huynh Wendy, U.; Dittmer Janke, J.; Alivisatos, A. P., *Science* **2002**, 295, (5564), 2425-2427.
21. Skaarup, S.; Bay, L.; West, K., *Synthetic Metals* **2007**, 157, (6-7), 323-326.
22. Sathiyarayanan, S.; Azim, S. S.; Venkatachari, G., *Electrochimica Acta* **2006**, 52, (5), 2068-2074.

23. Jang, J., *Advances in Polymer Science* **2006**, 199, (Emissive Materials: Nanomaterials), 189-259.
24. Zhang, X.; Lee, J.-S.; Lee, G. S.; Cha, D.-K.; Kim, M. J.; Yang, D. J.; Manohar, S. K., *Macromolecules* **2006**, 39, (2), 470-472.
25. Xiao, R.; Cho, S. I.; Liu, R.; Lee, S. B., *Journal of the American Chemical Society* **2007**, 129, (14), 4483-4489.
26. Kizilcan, N.; Ustamehmetoglu, B., *Journal of Applied Polymer Science* **2005**, 96, (3), 618-624.
27. Nabid, M. R.; Sedghi, R.; Entezami, A. A., *Journal of Applied Polymer Science* **2007**, 103, (6), 3724-3729.
28. Murugendrappa, M. V.; Prasad, M. V. N. A., *Journal of Applied Polymer Science* **2007**, 103, (5), 2797-2801.
29. Zhang, J.; Barker, A. L.; Mandler, D.; Unwin, P. R., *Journal of the American Chemical Society* **2003**, 125, (31), 9312-9313.
30. Li, G.; Zhang, Z., *Macromolecules* **2004**, 37, (8), 2683-2685.
31. Lin, H.-K.; Chen, S.-A., *Macromolecules* **2000**, 33, (22), 8117-8118.
32. Li, P.; Yuan, C., *Langmuir* **2000**, 16, (16), 6715-6718.
33. Zhang, X.; Manohar, S. K., *Journal of the American Chemical Society* **2004**, 126, (40), 12714-12715.
34. Wu, A.; Kolla, H.; Manohar, S. K., *Macromolecules* **2005**, 38, (19), 7873-7875.
35. Derue, G.; Coppee, S.; Gabriele, S.; Surin, M.; Geskin, V.; Monteverde, F.; Leclere, P.; Lazzaroni, R.; Damman, P., *Journal of the American Chemical Society* **2005**, 127, (22), 8018-8019.

36. van den Boogaard, M.; Bonnet, G.; Van't Hof, P.; Wang, Y.; Brochon, C.; van Hutten, P.; Lapp, A.; Hadziioannou, G., *Chemistry of Materials* **2004**, 16, (23), 4383-4385.
37. McCullough, R. D.; Ewbank, P. C.; Loewe, R. S., *Journal of the American Chemical Society* **1997**, 119, (3), 633-634.
38. Wang, F.; Kon, A. B.; Rauh, R. D., *Macromolecules* **2000**, 33, (14), 5300-5302.
39. Ji, J.; Coffer, J. L., *Journal of Physical Chemistry B* **2002**, 106, (15), 3860-3863.
40. Zhang, H.; Muellen, K.; De Feyter, S., *Journal of Physical Chemistry C* **2007**, 111, (23), 8142-8144.
41. Kimura, M.; Sato, M.; Adachi, N.; Fukawa, T.; Kanbe, E.; Shirai, H., *Chemistry of Materials* **2007**, 19, (11), 2809-2815.
42. Han, M. G.; Foulger, S. H., *Chemical Communications* **2005**, (24), 3092-3094.
43. Zhang, X.; MacDiarmid, A. G.; Manohar, S. K., *Chemical Communications* **2005**, (42), 5328-5330.
44. Jang, J.; Bae, J.; Park, E., *Advanced Materials* **2006**, 18, (3), 354-358.
45. Chen, W.; Wan, X.; Xu, N.; Xue, G., *Macromolecules* **2003**, 36, (2), 276-278.
46. Sigmund, W. M.; Weerasekera, G.; Marestin, C.; Styron, S.; Zhou, H.; Elsabee, M. Z.; Ruehe, J.; Wegner, G.; Duran, R. S., *Langmuir* **1999**, 15, (19), 6423-6427.
47. Sabouraud, G.; Sadki, S.; Brodie, N., *Chemical Society Reviews* **2000**, 29, (5), 283-293.
48. Somani, P.; Radhakrishnan, S., *Chemical Physics Letters* **1998**, 292, (1,2), 218-222.

49. Chen, X. B.; Issi, J. P.; Devaux, J.; Billaud, D., *Journal of Materials Science* **1997**, 32, (6), 1515-1518.
50. Wang, J.; Chen, J.; Wang, C. Y.; Zhou, D.; Too, C. O.; Wallace, G. G., *Synthetic Metals* **2005**, 153, (1-3), 117-120.
51. Xu, Z.; Horowitz, G.; Garnier, F., *Journal of Electroanalytical Chemistry and Interfacial Electrochemistry* **1988**, 246, (2), 467-472.
52. Groenendaal, L. B.; Jonas, F.; Freitag, D.; Pielartzik, H.; Reynolds, J. R., *Advanced Materials* **2000**, 12, (7), 481-494.
53. Kumar, A.; Reynolds, J. R., *Macromolecules* **1996**, 29, (23), 7629-7630.
54. Chen, X.; Xing, K.-Z.; Inganaes, O., *Chemistry of Materials* **1996**, 8, (10), 2439-2443.
55. Chandrasekhar, P.; Zay, B. J.; Birur, G. C.; Rawal, S.; Pierson, E. A.; Kauder, L.; Swanson, T., *Advanced Functional Materials* **2002**, 12, (2), 95-103.
56. Kumar, A.; Welsh, D. M.; Morvant, M. C.; Piroux, F.; Abboud, K. A.; Reynolds, J. R., *Chemistry of Materials* **1998**, 10, (3), 896-902.
57. Van Dyke, L. S.; Martin, C. R. *Electrochemical investigations of electronically conductive polymers. 4. By controlling the supermolecular structure, charge transport rates can be enhanced*; Dep. Chem., Texas A and M Univ., College Station, TX, USA.: 1990; p 36 pp.
58. Horowitz, G.; Hajlaoui, R.; Fichou, D.; El Kassmi, A., *Journal of Applied Physics* **1999**, 85, (6), 3202-3206.
59. Yu, J.-B.; Byun, H.-G.; So, M.-S.; Huh, J.-S., *Sensors and Actuators, B: Chemical* **2005**, B108, (1-2), 305-308.

60. Gerard, M.; Chaubey, A.; Malhotra, B. D., *Biosensors & Bioelectronics* **2002**, 17, (5), 345-359.
61. Cosnier, S.; Ionescu, R. E.; Herrmann, S.; Bouffier, L.; Demeunynck, M.; Marks, R. S., *Analytical Chemistry* **2006**, 78, (19), 7054-7057.
62. Jang, J.; Chang, M.; Yoon, H., *Advanced Materials* **2005**, 17, (13), 1616-1620.
63. Nishizawa, M.; Mukai, K.; Kuwabata, S.; Martin, C. R.; Yoneyama, H., *Journal of the Electrochemical Society* **1997**, 144, (6), 1923-1927.
64. Xia, Y.; Yang, P.; Sun, Y.; Wu, Y.; Mayers, B.; Gates, B.; Yin, Y.; Kim, F.; Yan, H., *Advanced Materials* **2003**, 15, (5), 353-389.
65. Che, G.; Jirage, K. B.; Fisher, E. R.; Martin, C. R., *Journal of the Electrochemical Society* **1997**, 144, (12), 4296-4302.
66. Li, N.; Martin, C. R.; Scrosati, B., *Electrochemical and Solid-State Letters* **2000**, 3, (7), 316-318.
67. Trofin, L.; Lee, S. B.; Mitchell, D. T.; Martin, C. R., *Journal of Nanoscience and Nanotechnology* **2004**, 4, (3), 239-244.
68. Sides, C. R.; Martin, C. R., *Modern Aspects of Electrochemistry* **2007**, 40, 75-126.
69. Goldberger, J.; He, R.; Zhang, Y.; Lee, S.; Yan, H.; Choi, H.-J.; Yang, P., *Nature* **2003**, 422, (6932), 599-602.
70. Yin, L.-W.; Bando, Y.; Zhan, J.-H.; Li, M.-S.; Golberg, D., *Advanced Materials* **2005**, 17, (16), 1972-1977.
71. Martin, C. R., *Science* **1994**, 266, (5193), 1961-1966.
72. Brumlik, C. J.; Martin, C. R., *Journal of the American Chemical Society* **1991**, 113, (8), 3174-3175.

73. Johnson, S. A.; Ollivier, P. J.; Mallouk, T. E., *Science* **1999**, 283, (5404), 963-965.
74. Penner, R. M.; Martin, C. R., *Journal of the Electrochemical Society* **1986**, 133, (10), 2206-2207.
75. Klein, J. D.; Herrick, R. D., II; Palmer, D.; Sailor, M. J.; Brumlik, C. J.; Martin, C. R., *Chemistry of Materials* **1993**, 5, (7), 902-904.
76. Possin, G. E., *Physica* **1971**, 55, 339-343.
77. Wagner, R. S.; Ellis, W. C., *Applied Physics Letters* **1964**, 4, (5), 89-90.
78. Jorritsma, J.; Gijs, M. A. M.; Kerkhof, J. M.; Stienen, J. G. H., *Nanotechnology* **1996**, 7, (3), 263-265.
79. Zhang, Z.; Wei, Z.; Wan, M., *Macromolecules* **2002**, 35, (15), 5937-5942.
80. Shen, Y.; Wan, M., *Journal of Polymer Science, Part A: Polymer Chemistry* **1999**, 37, (10), 1443-1449.
81. Kuang, Q.; Lin, Z.-W.; Lian, W.; Jiang, Z.-Y.; Xie, Z.-X.; Huang, R.-B.; Zheng, L.-S., *Journal of Solid State Chemistry* **2007**, 180, (4), 1236-1242.
82. Son, S. J.; Reichel, J.; He, B.; Schuchman, M.; Lee, S. B., *Journal of the American Chemical Society* **2005**, 127, (20), 7316-7317.
83. Masuda, H.; Fukuda, K., *Science* **1995**, 268, (5216), 1466-1468.
84. He, B.; Son, S. J.; Lee, S. B., *Langmuir* **2006**, 22, (20), 8263-8265.
85. Walther, M.; Kapon, E.; Christen, J.; Hwang, D. M.; Bhat, R., *Applied Physics Letters* **1992**, 60, (5), 521-523.

86. Muller, T.; Heinig, K. H.; Schmidt, B., *Nuclear Instruments & Methods in Physics Research, Section B: Beam Interactions with Materials and Atoms* **2001**, 175-177, 468-473.
87. Fasol, G., *Science* **1998**, 280, (5363), 545-546.
88. Penner, R. M., *Journal of Physical Chemistry B* **2002**, 106, (13), 3339-3353.
89. He, R.; Law, M.; Fan, R.; Kim, F.; Yang, P., *Nano Letters* **2002**, 2, (10), 1109-1112.
90. Moeller, S.; Perlov, C.; Jackson, W.; Taussig, C.; Forrest, S. R., *Nature* **2003**, 426, (6963), 166-169.
91. Friend, R. H.; Gymer, R. W.; Holmes, A. B.; Burroughes, J. H.; Marks, R. N.; Taliani, C.; Bradley, D. D. C.; Dos Santos, D. A.; Bredas, J. L.; Logdlund, M.; Salaneck, W. R., *Nature* **1999**, 397, (6715), 121-128.
92. Andersson, P.; Nilsson, D.; Svensson, P.-O.; Chen, M.; Malmstrom, A.; Remonen, T.; Kugler, T.; Berggren, M., *Advanced Materials* **2002**, 14, (20), 1460-1464.
93. Karasz, F. E.; Chien, J. C. W.; Galkiewicz, R.; Wnek, G. E.; Heeger, A. J.; MacDiarmid, A. G., *Nature* **1979**, 282, (5736), 286-288.
94. Chien, J. C. W.; Schlenoff, J. B., *Nature* **1984**, 311, (5984), 362-363.
95. Penner, R. M.; Martin, C. R. *Electronically conductive composite polymer membranes*; Dep. Chem., Texas A and M Univ., College Station, TX, USA.: 1985; p 31 pp.
96. Cai, Z.; Martin, C. R., *Journal of the American Chemical Society* **1989**, 111, (11), 4138-4139.

97. Martin, C. R.; Van Dyke, L. S.; Cai, Z.; Liang, W. *Template synthesis of organic microtubules*; Dep. Chem., Colorado State Univ., Fort Collins, CO, USA.: 1990; p 13 pp.
98. Duvail, J. L.; Retho, P.; Garreau, S.; Louarn, G.; Godon, C.; Demoustier-Champagne, S., *Synthetic Metals* **2002**, 131, (1-3), 123-128.
99. Guernion, N.; Ewen, R. J.; Pihlainen, K.; Ratcliffe, N. M.; Teare, G. C., *Synthetic Metals* **2002**, 126, (2-3), 301-310.
100. Cheng, G.; Zhao, J.; Tu, Y.; He, P.; Fang, Y., *Analytica Chimica Acta* **2005**, 533, (1), 11-16.
101. Park, J. W.; Lee, J. Y.; Kho, S. I.; Lee, H. S.; Kim, T. W., *Synthetic Metals* **2001**, 117, (1-3), 119-122.
102. Demoustier-Champagne, S.; Ferain, E.; Jerome, C.; Jerome, R.; Legras, R., *European Polymer Journal* **1998**, 34, (12), 1767-1774.
103. Demoustier-Champagne, S.; Stavaux, P.-Y., *Chemistry of Materials* **1999**, 11, (3), 829-834.
104. Zhang, X.; Zhang, J.; Liu, Z.; Robinson, C., *Chemical Communications* **2004**, (16), 1852-1853.
105. Delvaux, M.; Duchet, J.; Stavaux, P. Y.; Legras, R.; Demoustier-Champagne, S., *Synthetic Metals* **2000**, 113, (3), 275-280.
106. Pan, L.; Pu, L.; Shi, Y.; Song, S.; Xu, Z.; Zhang, R.; Zheng, Y., *Advanced Materials* **2007**, 19, (3), 461-464.
107. Huang, J.; Kaner, R. B., *Journal of the American Chemical Society* **2004**, 126, (3), 851-855.

108. Zhang, X.; Goux, W. J.; Manohar, S. K., *Journal of the American Chemical Society* **2004**, 126, (14), 4502-4503.
109. Duvail, J. L.; Retho, P.; Fernandez, V.; Louarn, G.; Molinie, P.; Chauvet, O., *Journal of Physical Chemistry B* **2004**, 108, (48), 18552-18556.
110. Xu, T. T.; Fisher, F. T.; Brinson, L. C.; Ruoff, R. S., *Nano Letters* **2003**, 3, (8), 1135-1139.
111. Thamida, S. K.; Chang, H.-C., *Chaos* **2002**, 12, (1), 240-251.
112. Tian, M.; Xu, S.; Wang, J.; Kumar, N.; Wertz, E.; Li, Q.; Campbell, P. M.; Chan, M. H. W.; Mallouk, T. E., *Nano Letters* **2005**, 5, (4), 697-703.
113. Chu, S.-Z.; Wada, K.; Inoue, S.; Todoroki, S.-i.; Takahashi, Y. K.; Hono, K., *Chemistry of Materials* **2002**, 14, (11), 4595-4602.
114. Parkhutik, V. P.; Shershul'skii, V. I., *Journal of Physics D: Applied Physics* **1992**, 25, (8), 1258-1263.
115. Chu, S.-Z.; Inoue, S.; Wada, K.; Kurashima, K., *Journal of Physical Chemistry B* **2004**, 108, (18), 5582-5587.
116. Nielsch, K.; Muller, F.; Li, A.-P.; Gosele, U., *Advanced Materials* **2000**, 12, (8), 582-586.
117. Chu, S.-Z.; Wada, K.; Inoue, S.; Isogai, M.; Yasumori, A., *Advanced Materials* **2005**, 17, (17), 2115-2119.
118. Song, H.-K.; Palmore, G. T. R., *Advanced Materials* **2006**, 18, (13), 1764-1768.
119. Wang, J.; Yang, J.; Xie, J.; Xu, N., *Advanced Materials* **2002**, 14, (13-14), 963-965.

120. Sirringhaus, H.; Kawase, T.; Friend, R. H.; Shimoda, T.; Inbasekaran, M.; Wu, W.; Woo, E. P., *Science* **2000**, 290, (5499), 2123-2126.
121. Gaupp, C. L.; Welsh, D. M.; Rauh, R. D.; Reynolds, J. R., *Chemistry of Materials* **2002**, 14, (9), 3964-3970.
122. Argun, A. A.; Aubert, P.-H.; Thompson, B. C.; Schwendeman, I.; Gaupp, C. L.; Hwang, J.; Pinto, N. J.; Tanner, D. B.; MacDiarmid, A. G.; Reynolds, J. R., *Chemistry of Materials* **2004**, 16, (23), 4401-4412.
123. Heuer, H. W.; Wehrmann, R.; Kirchmeyer, S., *Advanced Functional Materials* **2002**, 12, (2), 89-94.
124. Szklarczyk, M.; Strawski, M.; Donten, M. L.; Donten, M., *Electrochemistry Communications* **2004**, 6, (9), 880-886.
125. Kim, B. H.; Park, D. H.; Joo, J.; Yu, S. G.; Lee, S. H., *Synthetic Metals* **2005**, 150, (3), 279-284.
126. Bognitzki, M.; Hou, H.; Ishaque, M.; Frese, T.; Hellwig, M.; Schwarte, C.; Schaper, A.; Wendorff, J. H.; Greiner, A., *Advanced Materials* **2000**, 12, (9), 637-640.
127. Jang, J.; Yoon, H., *Advanced Materials* **2003**, 15, (24), 2088-2091.
128. Dong, H.; Prasad, S.; Nyame, V.; Jones, W. E., Jr., *Chemistry of Materials* **2004**, 16, (3), 371-373.
129. Groenendaal, L. B.; Zotti, G.; Aubert, P.-H.; Waybright, S. M.; Reynolds, J. R., *Advanced Materials* **2003**, 15, (11), 855-879.
130. Aasmundtveit, K. E.; Samuelsen, E. J.; Pettersson, L. A. A.; Inganas, O.; Johansson, T.; Feidenhans, R., *Synthetic Metals* **1999**, 101, (1-3), 561-564.

131. Enze, L., *Journal of Physics D: Applied Physics* **1986**, 19, (1), 1-6.
132. Van den Schoor, R. C. G. M.; Van de Leur, R. H. M.; De Wit, J. H. W., *Synthetic Metals* **1999**, 99, (1), 17-20.
133. Aquino-Binag, C. N.; Kumar, N.; Lamb, R. N.; Pigram, P. J., *Chemistry of Materials* **1996**, 8, (11), 2579-2585.
134. Liu, X.; Ly, J.; Han, S.; Zhang, D.; Requicha, A.; Thompson, M. E.; Zhou, C., *Advanced Materials* **2005**, 17, (22), 2727-2732.
135. Crouse, D.; Lo, Y.-H.; Miller, A. E.; Crouse, M., *Applied Physics Letters* **2000**, 76, (1), 49-51.
136. Brevnov, D. A.; Barela, M.; Piyasena, M. E.; Lopez, G. P.; Atanassov, P. B., *Chemistry of Materials* **2004**, 16, (4), 682-687.
137. Rabin, O.; Herz, P. R.; Lin, Y.-M.; Akinwande, A. I.; Cronin, S. B.; Dresselhaus, M. S., *Advanced Functional Materials* **2003**, 13, (8), 631-638.
138. Aubert, P.-H.; Argun, A. A.; Cirpan, A.; Tanner, D. B.; Reynolds, J. R., *Chemistry of Materials* **2004**, 16, (12), 2386-2393.